UNIVERSITY OF CALIFORNIA, SAN DIEGO

M13 Bacteriophage Based Protein Sensors

A dissertation submitted in partial satisfaction of the

requirements for the degree Doctor of Philosophy

in

Materials Science and Engineering

by

Ju Hun Lee

Committee in Charge:

Professor Jennifer N. Cha, Chair
Professor Sadik C. Esener
Professor Xiaohua Huang
Professor Sungho Jin
Professor Donald J. Sirbuly

2013

The dissertation of Ju Hun Lee is approved, and it is acceptable in quality and form for publication on microfilm:

_____

_____

_____

_____

_____

Chair

University of California, San Diego

2013

DEDICATION

Dedicated to my loving Mom and Dad

who have always shown unfailing love and support

TABLE OF CONTENTS

LIST OF FIGURES

LIST OF TABLES

ACKNOWLEDGEMENTS

During my graduate studies at University of California at San Diego, I have been blessed to meet so many talented people. Firstly, I cannot thank my advisor enough for being my mentor; I would like to express my sincerest gratitude to Professor Jennifer Cha for giving me a wonderful opportunity to be part of the greatest journey that I have experienced thus far. Her heartfelt encouragement, guidance, and passion for science always inspire me to joyfully follow my own trail and do my best without any hesitation.

I sincerely appreciate Prof. Sungho Jin for all the kinds of kind considerations, valuable suggestion and supportive encouragements as a director of my program as well as my committee member. And I would like to also thank my committee members, Prof. Donald J. Sirbuly, Prof. Sadik C. Esener, Prof. Xiaohua Huang for helpful discussions and suggestions on my dissertation.

I am indebted to all my former and present members of the Jennifer group who are my colleagues as well as good friends of mine. In particular, I am truly grateful to Dr. Dylan W. Domaille for being a dependable friend and many helpful discussions, valuable suggestions. I also would like to acknowledge all of my labmates: Dr. Albert Hung, Hyunwoo Noh, Lauren Forbes, Matt Nakatsuka, Phyllis Xu, Taeseok Oh, Michael Brasino, and Ke Ma. Without their helps and friendships, I would not have been able to succeed.

I am also thankful to my colleagues: prof. Markus Raschke, Dr. Joanna Atkin for helping me to set up and measure Raman spectroscopy.

I would like to recognize and thank Charlotte Lauve for the administrative paperwork, invaluable advice, and numerous informative notices.

I would truly like to thank my wonderful friends who are like family and made this incredible journey possible: Namseok Park, Kimoon Um, Kangmu Lee, Chunsong Kwon, Byoungwook Kim, Jinseok Yang, Hyunsoo Kim, Sungyen Hwang, Ji Hoon Kim, Kanguk Kim, Kyungtae Kim, Kyoungrok Lee, Eunho Noh, Jongkil Park, Dr. Donghyup Shin, Dr. Yonghak Park, Hyongman Cho, Seokheon Cho, Heemin Kang, Dr. Sanyong Kim, Dr. Ilsun Woon, Sunsin Kwon, Daehoe Lee, Jun Lee, Dr. Kunbae Noh, Dr. Woorim Shin, Dr. Yongsung Hwang, Yeseok Song, Sunyoung Noh, Dr. Young Oh, Jaeyoon Moon, Yoontae Hwang, Dr. Chulmin Choi, Dr. Sunghwan Cho, Dr. Tae Jung choi, Dr. Youngpyo Hong, Sungkyu Han, Sunghee Woo, Jun ho Kim, Jun Hong Park, Seokhyeong Kang, Joowook Kim, Woongju Mun, Hyunwoo Lim, Benjamin Park for their prayer and friendship.

Lastly, I would like to express my deepest gratitude to parents: my mom and dad for their unfailing love, support, and prayer.

Chapter 2, in full, is a reprint of the material as it appears in *Anal. Chem.*, *Ju Hun Lee*, *Jennifer N. Cha*, Vol. 83, page 3516-3519, **2011**. The dissertation author was the primary investigator and author of this paper.

Chapater 3, in full, is a reprint of the material as it appears in ACS Nano, Ju Hun Lee, Dylan W. Domaille, Jennifer N. Cha, Vol. 6, page 5621-5626, 2012. The dissertation author was the primary investigator and author of this paper.

Chapter 4, in part, is a reprint of the material as it appears in Adv. Func. Materials, Ju Hun Lee, Phyllis F. Xu, Dylan W. Domaille, Chulmin Choi, Sungho Jin, Jennifer N. Cha, *Submitted.* The dissertation author was the primary investigator and author of this paper.

Ju Hun Lee

La Jolla, September 2013

VITA

2006	Bachelor of Science in Materials Science and Engineering, Korea University, Korea
2008	Master of Science in Materials Science and Engineering, Korea University, Korea
2013	Doctor of Philosophy in Materials Science and Engineering, University of California, San Diego, U. S. A.

LIST OF PUBLICATIONS

[1] H. Noh, A. Hung, C. M. Choi, **J. H. Lee**, J. Y. Kim, S. H. Jin, J. N. Cha, 50 nm DNA Nanoarrays Generated from Uniform Oligonucleotide Films, ***ACS Nano***, 2009, 3, 2376.

[2] **J. H. Lee**, J. N. Cha, Amplified Protein Detection through Visible Plasmon Shifts in Gold Nanocrystal Solutions from Bacteriophage Platforms, ***Anal. Chem.***, 2011, 83, 3516.

[3] P. Xu, H. Noh, **J. H. Lee**, J. N. Cha, DNA Mediated Assembly of Single Walled Carbon Nanotubes: Role of DNA Linkers and Annealing, ***Phys. Chem. Chem. Phys.***, 2011, 13, 10004.

[4] **J. H. Lee**, D. W. Domaille, J. N. Cha, Amplified Protein Detection and Identification through DNA-Conjugated M13 Bacteriophage, ***ACS Nano***, 2012, 6, 5621.

[5] D. W. Domaille, **J. H. Lee**, J. N. Cha, High Density DNA Loading on M13 bacteriophage Provides Access to Colorimetic and Fluorescent Protein Microarray Biosensors, ***Chem. Comm.***, 2013, 49, 1759.

[6] P. F. Xu, H. Noh, **J. H. Lee**, D. W. Domaille, M. A. Nakatsuka, A. P. Goodwin, J. N. Cha, Imparting the Unique Properties of DNA into Complex Material Architecture and Function, ***Mater. Today***, *In Press* (review paper).

[7] **J. H. Lee**, P. F. Xu, D. W. Domaille, C. M. Choi, S. Jin, J. N. Cha, M13 Bacteriophage as Materials for Amplified Surface Enhanced Raman Scattering Protein Sensing, ***Adv. Func. Mater.***, *Submitted*.

[8] P. F. Xu, **J. H. Lee**, K. Ma, C. Choi, S. Jin, J. Wang, J. N. Cha, Enhanced Raman Signals from Switchable Nanoparticle Probes, ***Chem. Comm.***, *Submitted*

[9] **J. H. Lee**, D. W. Domaille, T. Oh, H. Noh, C. Choi, S. Jin, J. N. Cha, High Yielding Facile Approach for Covalent Attachment of DNA and Proteins on Micropatterned Surfaces. *(manuscript in preparation)*

[10] **J. H. Lee**, D. W. Domaille, M. D. Brasino, J. N. Cha, Quantitative Multiplexed protein sensing with alternative affinity amplifiable M13 bacteriophage biosensing platform. *(manuscript in preparation)*

ABSTRACT OF THE DISSERTATION

M13 Bacteriophage Based Protein Sensors

by

Ju Hun Lee

Doctor of Philosophy in Materials Science and Engineering

University of California, San Diego, 2013

Professor Jennifer N. Cha, Chair

Despite significant progress in biotechnology and biosensing, early detection and disease diagnosis remains a critical issue for improving patient survival rates and well-being. Many of the typical detection schemes currently used possess issues such as low sensitivity and accuracy and are also time consuming to run and expensive. In addition, multiplexed detection remains difficult to achieve. Therefore, developing advanced approaches for reliable, simple, quantitative analysis of multiple markers in solution that also are highly sensitive are still in demand. In recent years, much of the research has primarily focused on improving two key components of biosensors: the bio-recognition agent (bio-receptor) and the transducer. Particular bio-receptors that have been used

include antibodies, aptamers, molecular imprinted polymers, and small affinity peptides. In terms of transducing agents, nanomaterials have been considered as attractive candidates due to their inherent nanoscale size, durability and unique chemical and physical properties. The key focus of this thesis is the design of a protein detection and identification system that is based on chemically engineered M13 bacteriophage coupled with nanomaterials. The first chapter provides an introduction of biosensors and M13 bacteriophage in general, where the advantages of each are provided. In chapter 2, an efficient and enzyme-free sensor is demonstrated from modified M13 bacteriophage to generate highly sensitive colorimetric signals from gold nanocrystals. In chapter 3, DNA conjugated M13 were used to enable facile and rapid detection of antigens in solution that also provides modalities for identification. Lastly, high DNA loadings per phage was achieved via hydrozone chemistry and these were applied in conjunction with Raman active DNA-gold/silver core/shell nanoparticles toward highly sensitive SERS sensing.

CHAPTER 1: Introduction of biosensor and M13 bacteriophage

"The greatest sin that only the young can commit is to become ordinary."

- Martha Graham

1.1 Introduction of Biosensors

After developing the first diagnostic, known as "enzyme electrodes",[1] the term "biosensor" was introduced in the late 1970's.[2] During the past three decades, new biosensor designs have continued to be developed for various applications (*i.e.* early-stage diagnosis, monitoring therapeutic response, and determining the efficacy of the treatment), detecting pollutants and pesticides in the environment, food-borne pathogens in the food supply, and biological warfare agents.[3] Since 1989, two Divisions of the International Union of Pure and Applied Chemistry (IUPAC), namely Physical Chemistry (Commission I.7 on Biophysical Chemistry formerly Steering Committee on Biophysical Chemistry) and Analytical Chemistry (Commission V.5 on Electroanalytical Chemistry) have prepared recommendations on the definition, classification and nomenclature related to electrochemical biosensors; these recommendations can also be extended to other types of biosensors.[4, 5] According to IUPAC document, as shown in Figure 1.1, a biosensor is defined as the following:

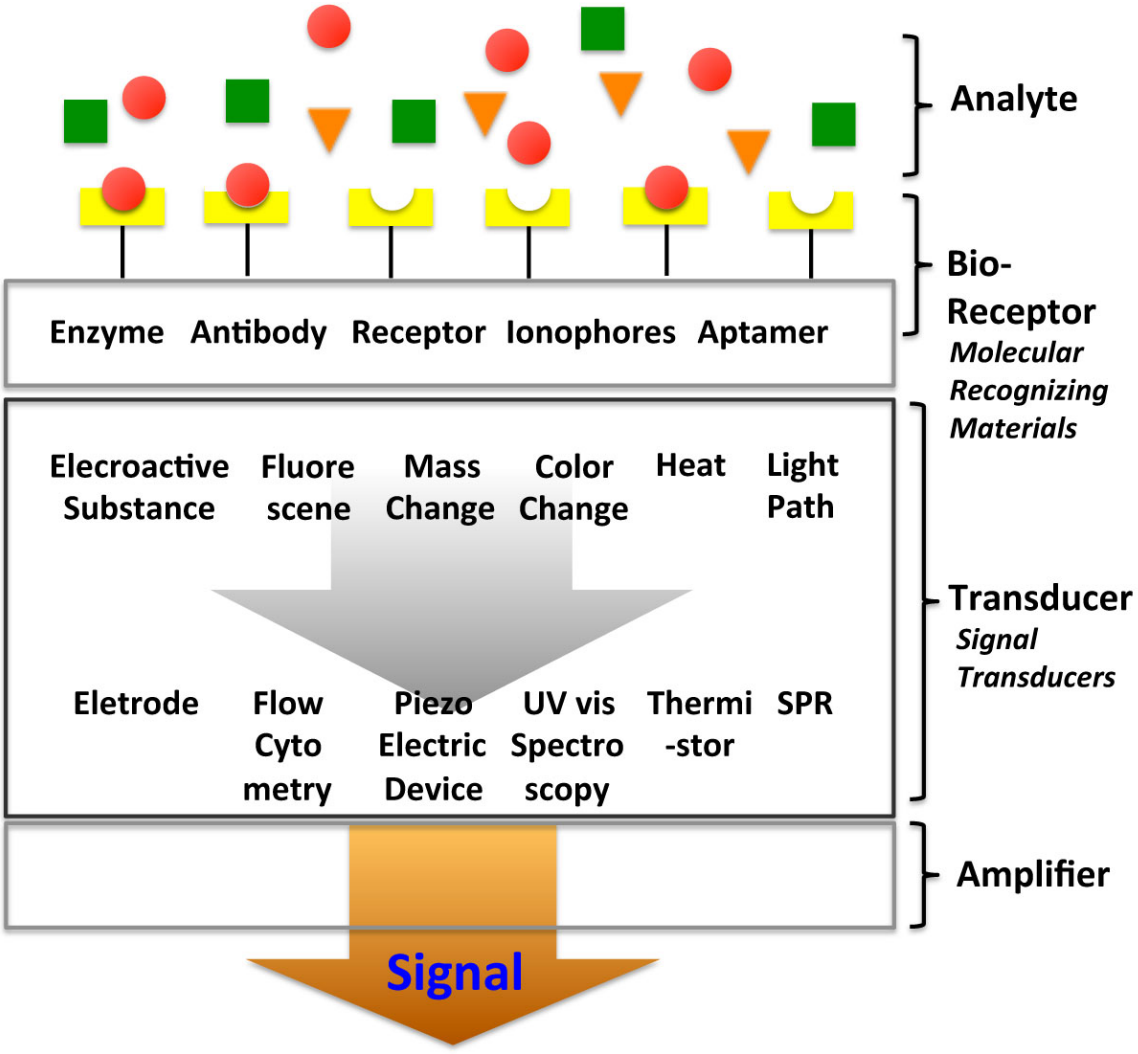

Figure 1.1 General model for chemical and biological sensors. Biosensor is mainly consisted of bioreceptor and transducer. *Note: SPR represented Surface Plasmonic Resonance.

"A chemical/biological sensor is a device that transforms chemical/biological information, ranging from the concentration of a specific sample component to total composition analysis, into an analytically useful signal. Chemical/biological sensors contain usually two basic components connected in series: a chemical (molecular) recognition system (receptor) and a physico-chemical transducer. Biosensors are chemical sensors in which the recognition system utilizes a biochemical mechanism"[5]

1.1.1 The Biological Recognition System

The recognition component of a biosensor is to capture or anchor certain analytes on defined surfaces or substrates with a high degree of selectivity and specificity.[5] Selectivity is a term directly related to specificity.[6] Selectivity is when an incorrect species generates the same type of signal, *e.g.*, with the same wavelength, working potential, and any other measuring parameter but with an intensity different from that of the target analyte.[6] Specificity, on the other hand, occurs when the bioreceptor responds only to a specific target substrate to produce a unique signal.[6] In order to design optimal biosensors, it is key that they respond to a substrate with high specificity by generating a unique signal or signal change.[6] Most biosensors are classified by the bioreceptors and biodetection schemes used.[5] The earliest example of a biosensor, shown by Clark et al, used the enzyme glucose oxidase to measure glucose concentrations. Glucose oxidase was entrapped in a low molecular weight cutoff

membrane of a P_{O2} (potential) electrode. In the presence of glucose, the enzyme oxidizes glucose, and the oxygen potential decreases; this decrease can be used to quantify the amount of glucose present. However, this strategy cannot be used as a general approach, as it requires that an enzyme exists for the target analyte. In order to detect other biomolecules (*e.g.* proteins, nucleic acids, etc), biocomplexing or bioaffinity recognition element based biosensor were developed. In this approach, one component, typically an antibody or antagonist/agonist receptor, is used to bind a target, and a second component provides a detectable signal, such as an enzyme that produces a color change. Among these, the most developed and successful biosensors are based on immunochemical reactions where the binding of an antigen (Ag) to a specific antibody (Ab) generates an enzymatic reaction and examples include ELISA (Enzyme-Linked ImmunoSorbent Assay) or Western blotting. While to date antibodies have been heavily used as recognition agents, due to their complex 3-dimensional structure and susceptibility to degradation, aggregation, modification (e.g. oxidation or deamidation) and denaturation,[7] alternative binding agents such as nucleic acids (aptamers), polypeptides (engineered binding proteins) and inorganic matrices (molecular imprinted polymers) have been developed and studied. For example, the molecularly imprinted polymers (MIPs) are semi-synthetic receptors where polymers that contain tailor-made recognition sites are synthesized and used.[3, 8-10] This particular technology has attracted attention as alternatives to antibodies because of their inherent stability while retaining specificity and affinity for the target. However, in order to synthesize and design different specific ligands chemically, additional techniques such as computational chemistry, combinatorial chemistry, molecular imprinting and self-assembly are needed, none of which is trivial.

The most successful strategy thus far for imprinting protein targets involves the use of small linear portion epitopes of the target protein.[10] For example, aptamers are oligonucleotide ligands that are selected for high affinity binding to molecular targets.[7] Both RNA- and ssDNA (single-stranded DNA)-based aptamers, generally 15–60 nucleotides long have been designed and used. Aptamers can have affinities in the nanomolar range, which is comparable with that of monoclonal antibodies. Target-binding aptamers are generally selected using a SELEX (systematic evolution of ligands by exponential enrichment) procedure.[11, 12] Despite the versatility of aptamers, the SELEX process often involves labor intensive processes that need to be optimized for each analyte (e.g. selection buffer, number of selection rounds).[13]

In addition to nucleic acids, antibody mimics by use of short peptides has shown promise for biosensing.[7] A key aspect for successful design and engineering of an analyte binding scaffold is to start with a large library and apply combinatorial screening and analysis. For this, a powerful high-throughput technology for evolution-driven engineering is molecular display: the generation of large and diversity (poly)peptide libraries and subsequent selection for variants with desired biological and physicochemical properties. One particular panning technique that has been heavily used is phage display where peptides that bind specific targets of interest can be isolated. While some of these short peptides have been further used for sensing applications, because the peptides are initially attached to a large virus scaffold and are only composed of a few amino acids, these screening techniques typically yield binding motifs that show much lower affinities and specificity than the original phage.[15] To address all of the aforementioned challenges with biosensors, we show here the design, synthesis and

testing of modified M13 bacteriophage with nanomaterials for sensing. The merits of M13 bacteriophage platforms will be discussed in later section (Section 1.2.4).

1.1.2 Detection or Measurement mode: Transducer

The transducer part is the other main component of the sensor which converts that binding of a specific analyte from solution into a measurable and quantifiable signal.[5, 16] In a sensor, the act of binding to an antigen can cause the production of ions, electrons, gases, heat, mass or light which are converted into signals by the transducers, often amplified and displayed in a suitable form.[16] Different classes of transducer modes are amperometric, potentiometric, voltammetric, impedimetric, conducto-metric, thermometry, calorimetric, colorimetric, polarimetric, mass change, ion charge, field effect, evanescent filed detection, and surface plasmon resonance (SPR).[2, 5, 6, 16] Recently, nanotechnology has also been used to generate a broad spectrum of highly innovative approaches for overcoming some of the traditional challenges of biosensors.[17] Nanotechnology based sensing systems will be discussed in Section 1.3.

1.2 Introduction of M13 Bacteriophage

1.2.1 Structural Properties of M13 bacteriophage

The filamentous bacteriophage is approximately 6.5 nm in diameter and ~1 μm in length.[18-21] The average molecular weight of the phage is approximately 1.64×10^7 Da[19] and each bacteriophage consists of 5 different capsid proteins (Table 1.1). Within each phage is a circular, single-stranded DNA that is encapsulated by the approximately 2700 copies of the major coated protein p8 and capped with 5 copies of four different

minor coat proteins (p9, p7, p6, and p3).[19] Among these structural proteins, p3 and p8 capsid proteins are important for our study in biosensor applications. The p3 protein is the one of minor capsid proteins, composed three different domains parts such as N1 (1~68), N2 (87~217), and CT (257~406).[22] The crystal structure of the N1 domain has been determined from complexes with a domain from the bacterial co-receptor TolA.[23] In this case, the amino terminus of N1 extends into solution such that a peptide or protein can be added without interfering with the p3 function. These properties and structures provide an explanation as to why the amino terminus of p3 is able to accept peptide or protein fusions which are critical for phage display to function.[22] The major capsid p8 proteins form a tube around the viral single stranded DNA in an overlapping helical array. They are oriented such that the N-terminus is located at the outside of the coat and the C-terminus interacts with the DNA at the inside of the coat (Figure 1.2b). The p8 proteins are responsible only for the structural arrangement of bacteriophage [24] and are not involved in any biological recognition.

Table 1.1 Structural proteins of M13 bacteriophage.[18]

Protein	Function	No. of amino Acids	Protein MW
p3	Minor capsid protein	406	42,522
p6	Minor capsid protein	112	12,342
p7	Minor capsid protein	33	3,599
p8	Major capsid protein	50	5,235
p9	Minor capsid protein	32	3,650

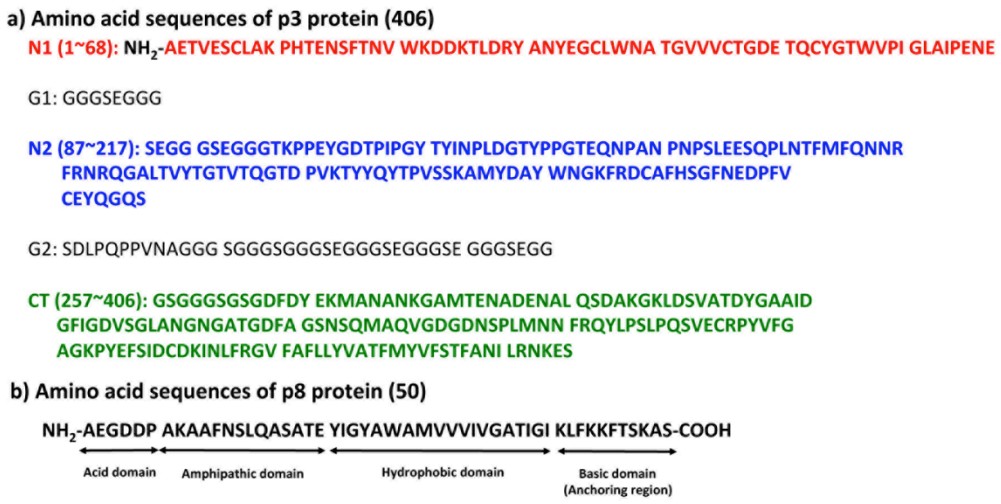

Figure 1.2 a) Amino acid sequences of minor capsid p3 protein (406 amino acids). b) Amino acid sequences of major capsid p8 protein (50 amino acids).

1.2.2 Phage Display

Phage display is powerful and well-established technology that allows expression of exogenous polypeptides on the surface of bacteriophage.[18, 25-28] The concept is simple in principle: a library of phage particles expressing a wide diversity of peptides is used to select those that bind the desired target. The filamentous M13 phage is the most commonly used vector to create random peptide display libraries. As discussed in previous section 1.2.1., small peptide or protein variants (<50 residues) can be expressed on the N-terminus of p3 without affecting the virus' infectivity. For phage display panning, the phage library (2×10^9 different peptides) is first allowed to bind to a target. The non-bound phage are then washed away, and the bound ones are eluted, and amplified through E. coli bacterial host infection. This evolutionary approach to choose the strongest binding peptide sequence is repeated several times to enrich the phage with the best affinity binder for the target. Finally the dominant binding peptides are identified by DNA analysis of the phage genome.[28] This technique has been widely employed to design and identify protein epitopes, small antibodies, and study protein interaction. Three key advantages of phage display technology are:[27]

(i) The peptide or protein displayed is physically linked to the genetic information that encodes it by virtue of its linkage to the viral coat encasing the genome.

(ii) Successive rounds of selection, called "biopanning" hone in on target-specific protein interactions by competitive screening in the presence of other potential binders.

(iii) Phage libraries are flexible platforms to genetically engineer to allow the display of either small random peptides or lengthy naturally occurring proteins with complex structures.[27]

1.2.3 Biological Application of M13 Bacteriophage

As shown in Figure 1.3, in the biological and bio-medical field, M13 has been widely used as a drug delivery carrier,[29-31] media for manipulation and separation of biomolecules and cells,[32] has served as an imaging scaffold for visualizing in vitro cancer cells and in vivo tumors, [19, 33-35] and has been used as a biosensing platform.[36-39]

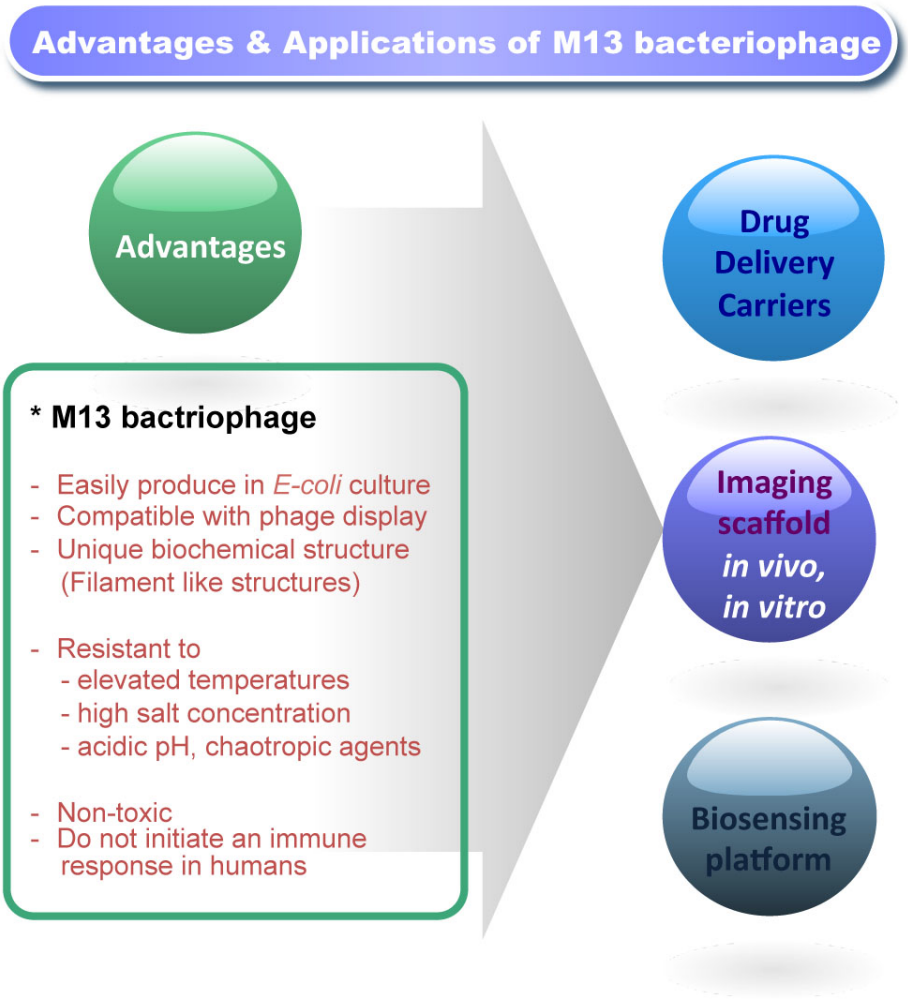

Figure 1.3 Advantages and Application of M13 Bacteriophage in Bio-medical Field

1.2.4 Advantages of M13 Bacteriopahge as Biosensing Platform

As described in Section 1.2.3., M13 bacteriophage have been used as biomaterials for various biological and biomedical applications. Becauase M13 bacteriophage can be applied toward combinatorial screening, viruses that express peptide epitopes with strong binding against target molecules is possible to isolate. Furthermore, since the antigen binding domain is only expressed on the five copies of p3 proteins, the remaining major capsid p8 proteins (~2700 copies in single phage) which is only responsible for the virus' structure can be easily modified to generate signal. As shown in Figure 1.4, 1.5, and 1.6, the high surface area of a M13 bacteriophage (18700 nm^2) over that of an antibody (IgG): (~125 nm^2) can lead to distinct advantages for signal transduction.[14, 32, 40] In addition to these key characteristics, M13 bacteriophage is thermally robust, resistant to high salt concentration, acidic pH, and chaotropic agents,[33, 38] is non-toxic, and does not initiate an immune response in humans.[41] Additionally, phage can be easily produced in high quantities in E.coli and can be easily modified chemically or through genetic engineering.[18, 22, 25]

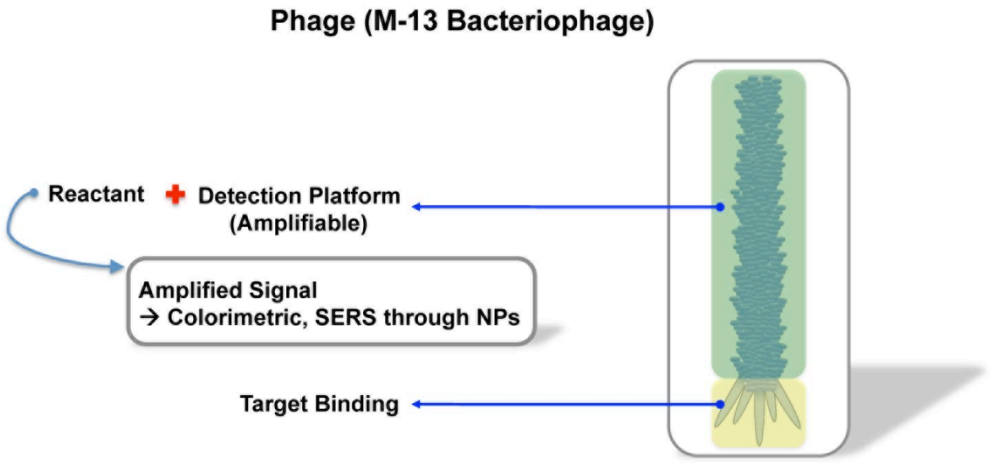

Figure 1.4 Schematic of M13 bacteriophage amplifiable platforms for biosensing.

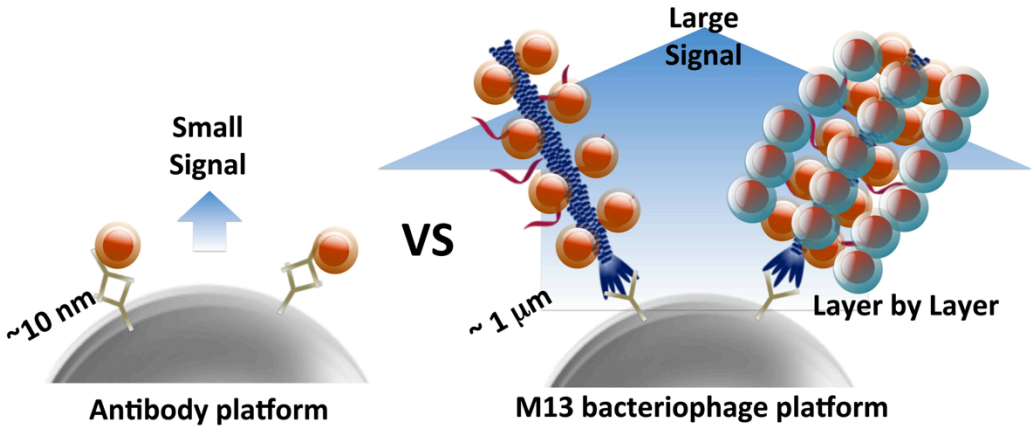

Figure 1.5 Schematic comparing antibody versus M13 bacteriophage amplifiable for SERS biosensing.

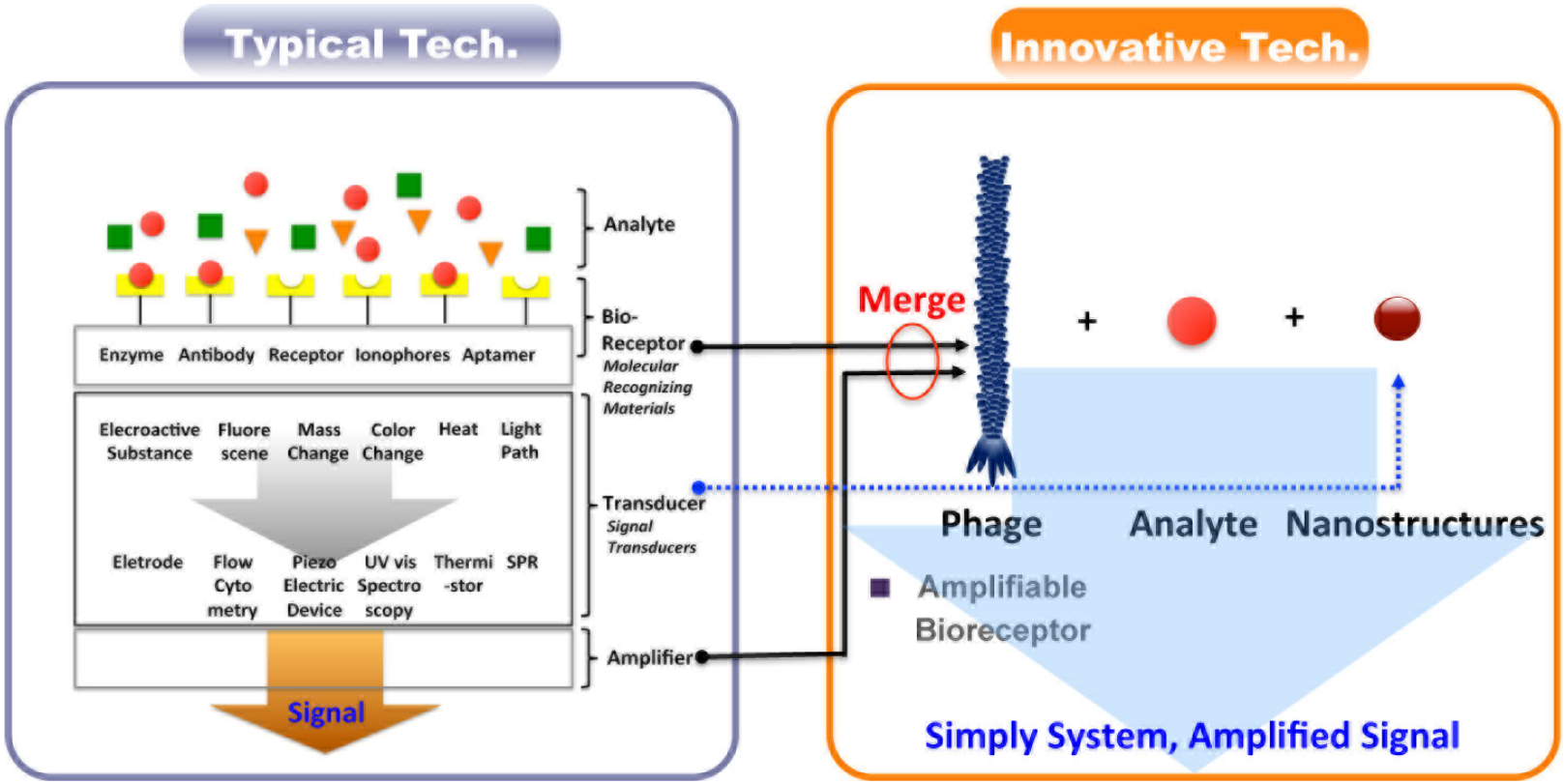

Figure 1.6 Schematic comparing typical biosensing technology and proposed M13 based nanostructure biosensor.

1.3 Nanostructure Based Sensor System

As discussed in section 1.1.2, various transducers and different technologies have been studies and developed for sensing biomolecules. Despite these great advancements in developing tools for detection and identification of different analytes in solution, there are still great challenges in developing diagnostics that demonstrate extremely high sensitivities with minimal error, low background and are both cost-effective and easy to use.[42] Early detection is critically needed for many life-threatening infections and diseases since treatment in the beginning stages has the greatest probability of success in patient survival and well-being.[17] One of the most widely used sensing modality is ELISA where detection antibodies are coupled to enzymes for signal production. However, in most cases only one biomarker is used as an indicator of the disease, which sometimes leads to false verification, and causes incorrect diagnosis. Immnoassays also can be time consuming and expensive. In addition to this some ELISA tests are not sufficiently sensitive for the detection of low level marker concentrations which exist in the early stages of the disease.[43] To date, there are no contemporary approaches for the reliable, quantitative detection of multiple low abundance protein markers that exist in a complex pool of other biomolecules in a patient's sample.[17] Moreover, proteins cannot be "amplified" as nucleic acids can by PCR and proteins are very sensitive to ambient environment such as temperature, salt concentration and pH. Nanomaterials are attractive probe candidates for biosensing applications because of their small size (1-100 nm), large surface-to-volume ratio, chemically tailorable physical properties and overall structural robustness.[44-48] The size of a nanomaterial can be an advantage over a bulk structure, simply because a target binding event that involves the use of a nanomaterial can have a

significant effect on its physical and chemical properties, thereby providing a mode of signal transduction not necessarily available with a bulk structure made of the same material. Each of these capabilities allows researchers to design materials that can potentially be implemented into new assays having improved modes of signal transduction that can compete favorably with the molecular fluorophore-dominated methods of PCR and ELISA.[44]

1.4 Overview of the Dissertation

Chapter 1 provides a brief introduction of biosensors, M13 bacteriophage and advantages of M13 bacteriophage as alternative affinity bioreceptor in biosensing systems.

Chapter 2 describes chemically modified thiolated M13 Phage via EDC chemistry and plasmonic shift based sensor by aggregation of nanoparticles through thiolated phage network

Chapter 3 describes chemically modified DNA-Phage via SPDP/s-SMCC and plasmonic sensor with DNA-gold nanoparticles

Chapter 4 describes chemically modified DNA-Phage via aldehyde/ hydrazine and surface enhanced Raman spectroscopy sensor with Raman active gold silver core shell nanoparticles

Chapter 5 describes potential future directions.

1.5 References

1. Clark, L. C.; Lyons, C. Electrode systems for continuous Monitoring in cardiovascular surgery. *Ann. N. Y. Acad. Sci.* **1962,** *102*, 29-45.

2. D'Orazio, P. Biosensors in Clinical Chemistry. *Clin. Chim. Acta* **2003,** *334*, 41-69.

3. Turner, A. P. F. Biosensors-Sense and Sensitivity. *Science* **2000**, 290, 3.

4. Hulanicki, A.; Glab, S.; Ingman, F., *IUPAC Discussion Paper* **1989,** *Commission V.1.*

5. Thévenot, D. R.; Toth, K.; Durst, R. A.; Wilson, G. S. Electrochemical biosensors: Recommended Definitions and Classification. *Biosens. Bioelectro.* **2001,** *16*, 121-131.

6. Spichiger-Keller, U. E., *Chemical sensors and biosensors for medical and biological applications*. Weiley-VCH: Weinheim, 1998.

7. Ruigrok, V. J. B.; Levisson, M.; Eppink, M. H. M.; Smidt, H.; van der Oost, J. Alternative Affinity Tools: More Attractive than Antibodies? *Biochem. J.* **2011,** *436*, 1-13.

8. Kröger, S.; Turner, A. P. F.; Mosbach, K.; Haupt, K. Imprinted Polymer-Based Sensor System for Herbicides Using Differential-Pulse Voltammetry on Screen-Printed Electrodes. *Anal. Chem.* **1999,** *71*, 3698-3702.

9. Subrahmanyam, S.; Piletsky, S. A.; Piletska, E. V.; Chen, B.; Day, R.; Turner, A. P. F. "Bite-and-Switch" Approach to Creatine Recognition by Use of Molecularly Imprinted Polymers. *Adv. Mat.* **2000,** *12*, 722-724.

10. Whitcombe, M. J.; Chianella, I.; Larcombe, L.; Piletsky, S. A.; Noble, J.; Porter, R.; Horgan, A. The rational Development of Molecularly Imprinted Polymer-Based Sensors for Protein Detection. *Chem. Soc. Rev.* **2011,** *40*, 1547-1571.

11. Tuerk, C.; Gold, L. Systematic Evolution of Ligands by Exponential Enrichment: RNA Ligands to Bacteriophage T4 DNA Polymerase. *Science* **1990,** *249*, 505-510.

12. Bock, L. C.; Griffin, L. C.; Latham, J. A.; Vermaas, E. H.; Toole, J. J. Selection of Single-Stranded DNA Molecules that Bind and Inhibit Human. *Nature* **1992,** *355*, 3.

13. Stoltenburg, R.; Reinemann, C.; Strehlitz, B. SELEX- A (r)evolutionary method to generate high-affinity nucleic acid ligands. *Biomol. Eng.* **2007,** *24*, 381-403.

14. Elgert, K. D., *Immunology: Understanding the Immune System*. John Wiley and Sons, Inc.: New York, 1998; p 58-78.

15. Bastings, M. M. C.; Helms, B. A.; van Baal, I.; Hackeng, T. M.; Merkx, M.; Meijer, E. W. From Phage Display to Dendrimer Display: Insights into Multivalent Binding. *J. Am. Chem. Soc.* **2011,** *133*, 6636-6641.

16. Sethi, R. S., Transducer aspects of biosensors. *Biosens. Bioelectron.* **1994,** *9*, 243-264.

17. Cheng, M. M.-C.; Cuda, G.; Bunimovich, Y. L.; Gaspari, M.; Heath, J. R.; Hill, H. D.; Mirkin, C. A.; Nijdam, A. J.; Terracciano, R.; Thundat, T.; Ferrari, M. Nanotechnologies for Biomolecular Detection and Medical Diagnostics. *Curr. Opin. Chem. Biol.* **2006,** *10*, 11-19.

18. Barbas III, C. F.; Burton, D. R.; Scott, J. K.; Silverman, G. J. *Phage Display: A Laboratory Manual*. Cold spring Harbor Laboratory Press, Cold Spring Harbor: New York, 2001.

19. Li, K.; Chen, Y.; Li, S.; Nguyen, H. G.; Niu, Z.; You, S.; Mello, C. M.; Lu, X.; Wang, Q. Chemical Modification of M13 Bacteriophage and Its Application in Cancer Cell Imaging. *Bioconjugate Chem.* **2010,** *21*, 1369-1377.

20. Wang, Y. A.; Yu, X.; Overman, S.; Tsuboi, M.; Thomas Jr, G. J.; Egelman, E. H., The Structure of a Filamentous Bacteriophage. *J. Mol. Biol.* **2006,** *361*, 209-215.

21. Sidhu, S. S. Engineering M13 for Phage Display. *Biomol. Eng.* **2001,** *18*, 57-63.

22. Kehoe, J. W.; Kay, B. K. Filamentous Phage Display in the New Millennium. *Chem. Rev.* **2005,** *105*, 4056-4072.

23. Riechmann, L.; Holliger, P., The C-Terminal Domain of TolA Is the Coreceptor for Filamentous Phage Infection of E. coli. *Cell* **1997,** *90*, 351-360.

24. Hemminga, M.; Vos, W.; Nazarov, P.; Koehorst, R. M.; Wolfs, C. A. M.; Spruijt, R.; Stopar, D. Viruses: Incredible Nanomachines. New Advances with Filamentous Phages. *Eur. Biophys. J.* **2010,** *39* (4), 541-550.

25. Smith, G. P.; Petrenko, V. A. Phage Display. *Chem. Rev.* **1997,** *97*, 20.

26. Pande, J.; Szewczyk, M. M.; Grover, A. K. Phage Display: Concept, Innovations, Applications and Future. *Biotechnol. Adv.* **2010,** *28*, 849-858.

27. Smothers, J. F.; Henikoff, S.; Carter, P. Affinity Selection from Biological Libraries. *Science* **2002,** *298*, 621-622.

28. Merzlyak, A.; Lee, S.-W. Phage as Templates for Hybrid Materials and Mediators for Nanomaterial Synthesis. *Curr. Opin. Chem. Biol.* **2006,** *10*, 246-252.

29. Yacoby, I.; Bar, H.; Benhar, I. Targeted Drug-Carrying Bacteriophages as Antibacterial Nanomedicines. *Antimicrob. Agents Chemother.* **2007,** *51*, 2156-2163.

30. Ngweniform, P.; Abbineni, G.; Cao, B.; Mao, C. Self-Assembly of Drug-Loaded Liposomes on Genetically Engineered Target-Recognizing M13 Phage: A Novel Nanocarrier for Targeted Drug Delivery. *Small* **2009,** *5*, 1963-1969.

31. Suthiwangcharoen, N.; Li, T.; Li, K.; Thompson, P.; You, S.; Wang, Q., M13 Bacteriophage-Polymer Nanoassemblies as Drug Delivery Vehicles. *Nano Res.* **2011,** *4*, 483-493.

32. Muzard, J.; Platt, M.; Lee, G. U., M13 Bacteriophage-Activated Superparamagnetic Beads for Affinity Separation. *Small* **2012,** *8*, 2403-2411.

33. Souza, G. R.; Christianson, D. R.; Staquicini, F. I.; Ozawa, M. G.; Snyder, E. Y.; Sidman, R. L.; Miller, J. H.; Arap, W.; Pasqualini, R. Networks of Gold Nanoparticles and Bacteriophage as Biological Sensors and Cell-Targeting Agents. *Proc. Nat. Acad. Sci. U. S. A.* **2006,** *103*, 1215-1220.

34. Carrico, Z. M.; Farkas, M. E.; Zhou, Y.; Hsiao, S. C.; Marks, J. D.; Chokhawala, H.; Clark, D. S.; Francis, M. B. N-Terminal Labeling of Filamentous Phage To Create Cancer Marker Imaging Agents. *ACS Nano* **2012,** *6*, 6675-6680.

35. Yi, H.; Ghosh, D.; Ham, M.-H.; Qi, J.; Barone, P. W.; Strano, M. S.; Belcher, A. M. M13 Phage-Functionalized Single-Walled Carbon Nanotubes As Nanoprobes for Second Near-Infrared Window Fluorescence Imaging of Targeted Tumors. *Nano Lett.* **2012,** *12*, 1176-1183.

36. Goldman, E. R.; Pazirandeh, M. P.; Mauro, J. M.; King, K. D.; Frey, J. C.; Anderson, G. P. Phage-Displayed Peptides as Biosensor Reagents. *J. Mol. Recognit.* **2000,** *13*, 382-387.

37. Petrenko, V. A.; Vodyanoy, V. J. Phage Display for Detection of Biological Threat Agents. *J. Microbiol. Methods* **2003,** *53*, 253-262.

38. Mao, C.; Liu, A.; Cao, B. Virus-Based Chemical and Biological Sensing. *Angew. Chem. Int. Ed.* **2009,** *48*, 6790-6810.

39. Arter, J. A.; Taggart, D. K.; McIntire, T. M.; Penner, R. M.; Weiss, G. A. Virus-PEDOT Nanowires for Biosensing. *Nano Lett.* **2010,** *10*, 4858-4862.

40. Pease, L. F.; Elliott, J. T.; Tsai, D.-H.; Zachariah, M. R.; Tarlov, M. J. Determination of Protein Aggregation with Differential Mobility Analysis: Application to IgG Antibody. *Biotechnol. Bioeng.* **2008,** *101*, 1214-1222.

41. Krag, D. N.; Shukla, G. S.; Shen, G.-P.; Pero, S.; Ashikaga, T.; Fuller, S.; Weaver, D. L.; Burdette-Radoux, S.; Thomas, C. Selection of Tumor-binding Ligands in Cancer Patients with Phage Display Libraries. *Cancer Res.* **2006,** *66*, 7724-7733.

42. Zhang, Y.; Guo, Y.; Xianyu, Y.; Chen, W.; Zhao, Y.; Jiang, X. Nanomaterials for Ultrasensitive Protein Detection. *Adv. Mat.* **2013**, Early view, DOI: 10.1002/adma.201301334

43. Tothill, I. E. Biosensors for Cancer Markers Diagnosis. *Semin. Cell Dev. Biol.* **2009,** *20*, 55-62.

44. Rosi, N. L.; Mirkin, C. A., Nanostructures in Biodiagnostics. *Che. Rev.* **2005,** *105*, 1547-1562.

45. Nam, J.-M.; Thaxton, C. S.; Mirkin, C. A. Nanoparticle-Based Bio-Bar Codes for the Ultrasensitive Detection of Proteins. *Science* **2003,** *301*, 1884-1886.

46. Ferrari, M. Cancer Nanotechnology: Opportunities and Challenges. *Nat. Rev. Cancer* **2005,** *5*, 11.

47. Alivisatos, P. The Use of Nanocrystals in Biological Detection. *Nature Biotechnol.* **2004,** *22*, 6.

48. Nie, S.; Xing, Y.; Kim, G. J.; Simons, J. W. Nanotechnology Applications in Cancer. *Ann. Rev. Biomed. Eng.* **2007,** *9*, 12.

CHAPTER 2: Chemically Modified Thiolated Phage via EDC chemistry and Plasmonic Shift Based Sensor by Aggregation of Nanoparticles through Thiolated Phage Network

"If we had no winter, the spring would not be so pleasant:

if we did not sometimes taste of adversity, prosperity would not be so welcome."

- Anne Bradstreet

2.1 Introduction

High sensitivity solution-based sensors for specific antigens, including cancer biomarkers such as prostate specific antigen (PSA) or lactate dehydrogenase for malaria detection are in high demand for medical diagnostics and biological assays worldwide.[1-15] These sensors must be cost-effective, require minimal additional instrumentation, minimize handling of unstable proteins such as enzymes, and produce a strong, detectable signal. We demonstrate here the engineering and implementation of M13 bacteriophage as sensing platforms that generate an amplified and immediate visible color change to a solution of gold nanoparticles in response to highly-specific antigen binding. Through the implementation of engineered phage, we show the creation of rapid, extremely sensitive, solution-based antigen-specific sensors with femto- and picomole detection limits. In past years, extensive methods have been developed to both sense and identify different proteins in solution through "sandwich" assays, in which an antigen is captured

by a surface-bound antibody and signal is generated after the addition of a different antibody bearing an agent capable of generating amplified signals. Usually this agent is an enzyme such as horseradish peroxidase (HRP), which catalyzes a colorimetric reaction, although other research groups have used electrodeposition onto metal nanoparticles to provide an optical signal as well.[11, 12] However, thermally unstable enzymes or specialized detection apparati such as microscopes or spectrophotometers have little utility in regions of the world with limited equipment and cold storage facilities,[14-20] and amplifying the signal directly from the antigen with minimal synthesis or engineering of new materials would be a more efficient and therefore more cost-effective process.[17-20] We demonstrate here an efficient and enzyme-free process in which a chemically modified M13 bacteriophage virus can both bind an antigen with excellent specificity and generate a massive, optically-detectable change to a solution of gold nanocrystals (Figure 2.1). The five pIII coat proteins located at one end of the filamentous phage bind the antigen, while the ~2700 pVIII coat proteins along the length of the phage are modified with 100-1000 pendant groups to induce the aggregation of gold nanocrystals.[21-26] Therefore while each single virus may only interact with a few antigen molecules, the numerous binding groups can amplify the aggregation of large numbers of gold nanocrystals to the point that the resultant plasmon shifts or nanoparticle flocculation can be observed by the naked eye.

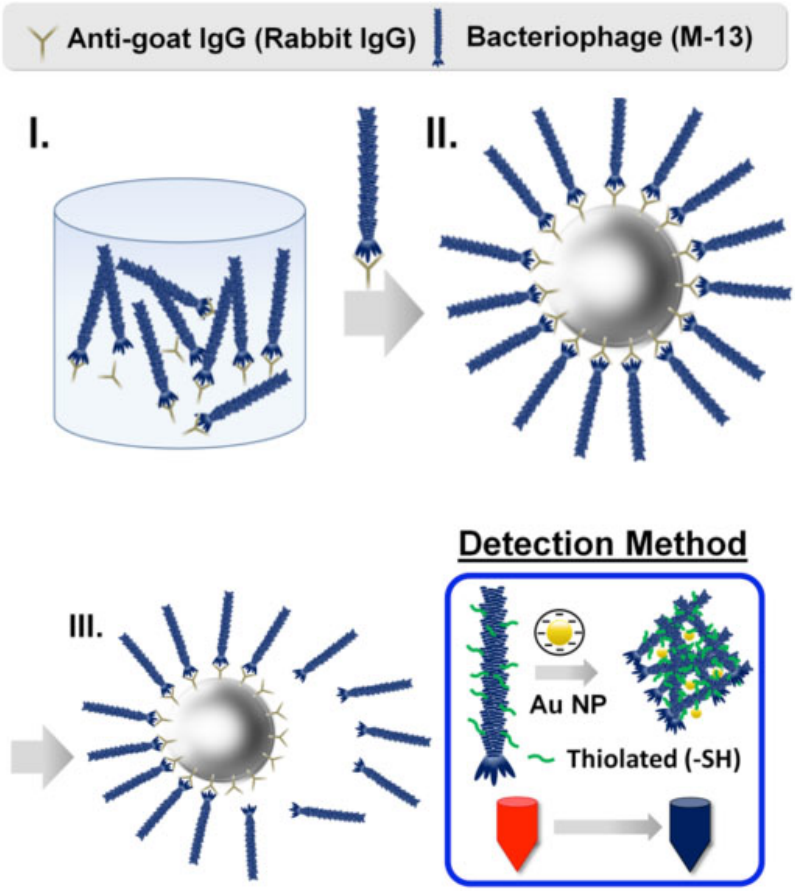

Figure 2.1 Schematic of sensor detection mechanism. (i) Antigens reacted with engineered phage are captured with magnetic beads. (ii) The modified phage are eluted into solution with pH 2 buffer (iii), neutralized, and mixed with gold nanoparticles to induce aggregation, which causes a significant color change associated with plasmon shift.

2.2 Chemical Strategy to Modification of M13 Bacteriophage

The phage were appended with excess thiol groups by reacting the phage with 1.33mM 1-ethyl-3-(3-dimethylaminopropyl)carbodiimide (EDC) and cysteamine to functionalize the accessible glutamic or aspartic acid groups of the pVIII proteins with free thiol groups (Figure 2.2). After removal of excess reagents by extensive dialysis, FITC-maleimide was reacted with modified and unmodified phage to roughly quantify the number of appended cysteamine groups per bacteriophage. Using calibration curves of FITC-maleimide and FITC reacted non-cysteamine modified phage, the relative number of cysteamine groups per phage were determined to be approximately 106 and 136 for 1.33mM and 2.67 mM EDC/cysteamine reacted phage respectively (Figure 2.3, Table 2.1). Next, varying concentrations of thiol modified phage were incubated with 20 nm phosphine-stabilized gold nanocrystals. The addition of increasing amounts of thiol modified bacteriophage caused a rapid and dramatic shift in the plasmon resonance from red to blue, indicating gold clustering or aggregation (Figure 2.4). No gold nanocrystal aggregation was observed at any concentration of unmodified phage. Obvious changes in color and plasmon resonance were observed with as little as 30 femtomoles of thiolated phage (Figure 2.4).

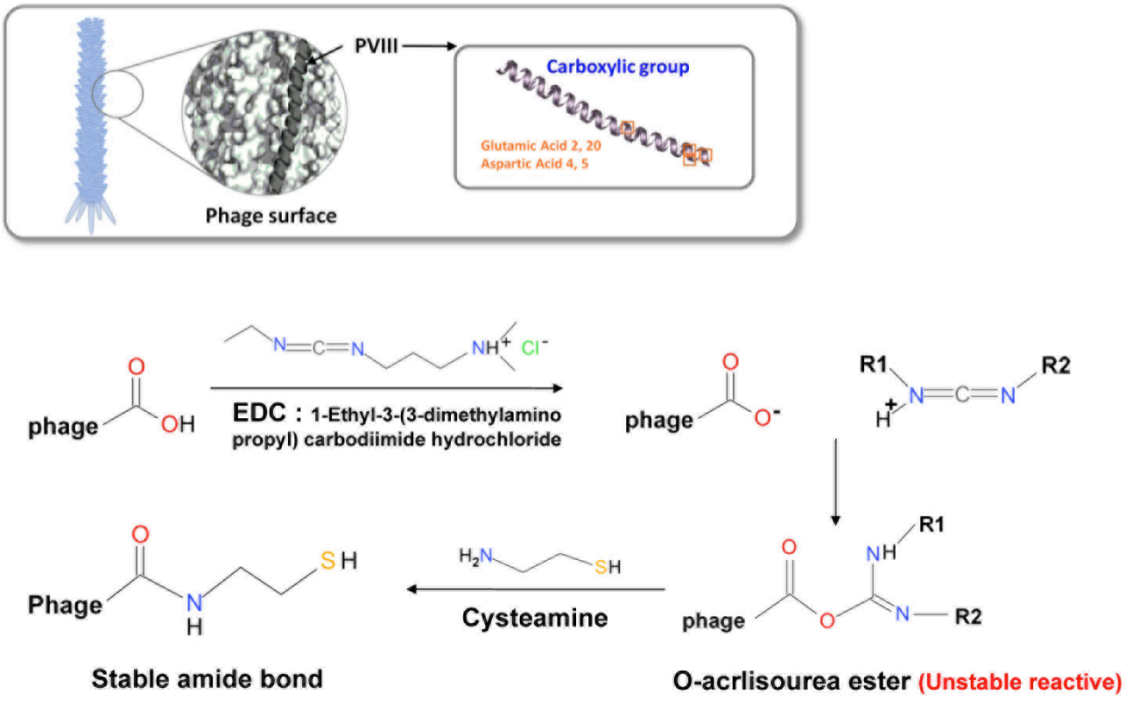

Figure 2.2 Schematic of chemical modification of phage with EDC/Cysteamine.

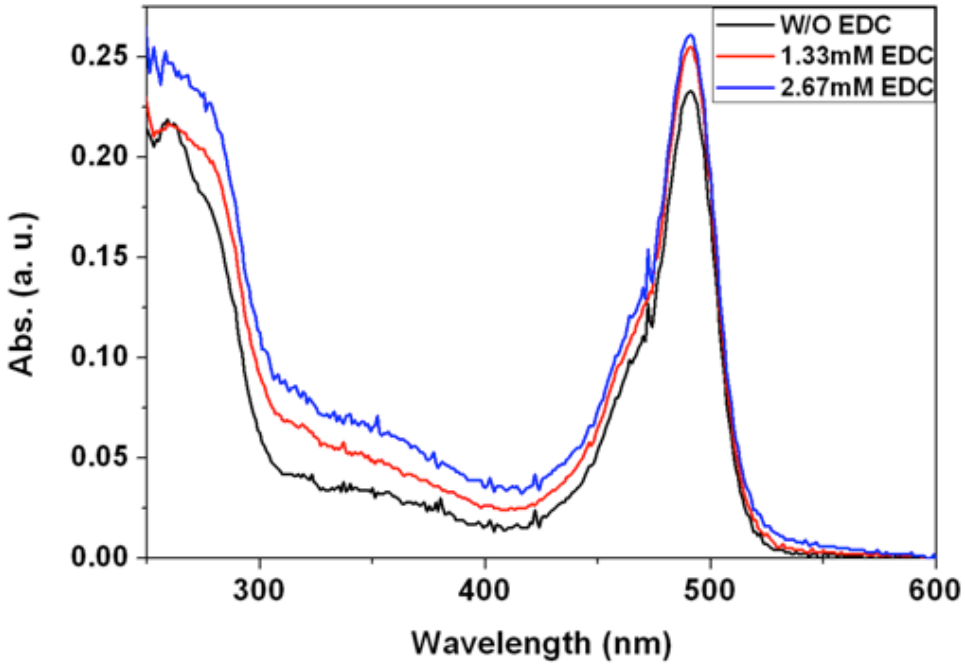

Figure 2.3 UV-vis spectra of phage, and thiolated phage with different amounts of EDC

Table 2.1 The absorbance value of phage, and thiolated phage with different amounts of EDC, and calculated modified thiol moieties per phage as shown in Figure 2.3.

	Net Abs.	Number of Dye per phage
Unmodified	0	0
1.33 mM EDC	0.022	107.0
2.67 mM EDC	0.028	136.2

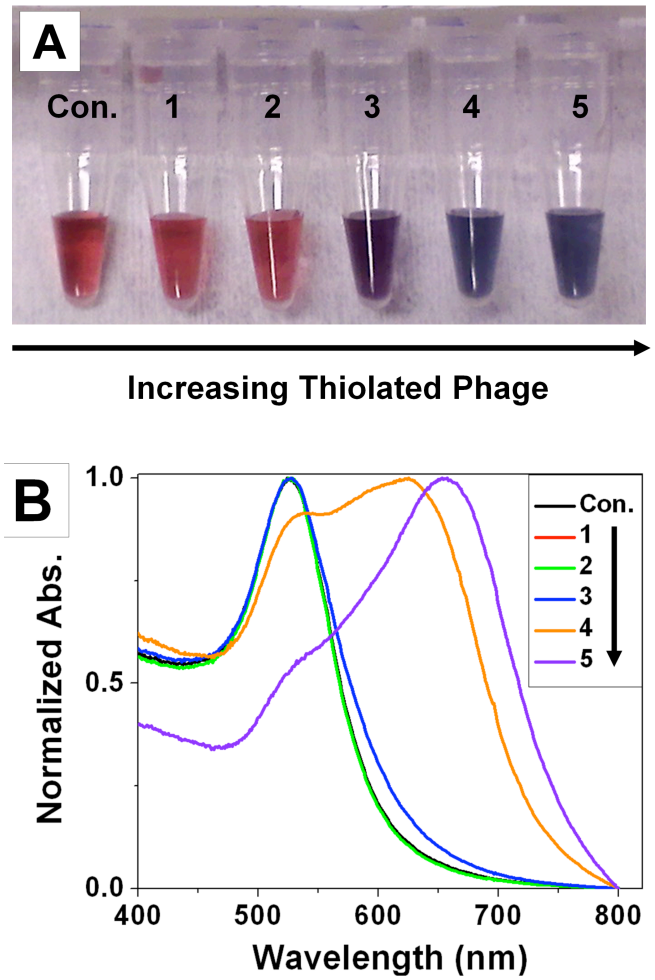

Figure 2.4 (A) Red to blue color changes due to 20nm gold nanoparticle aggregation with increasing moles of thiolated phage (0, 4, 20, 30, 40, 117 femtomoles) (B) UV-Vis spectra of showing clear red shifts in surface plasmon resonance.

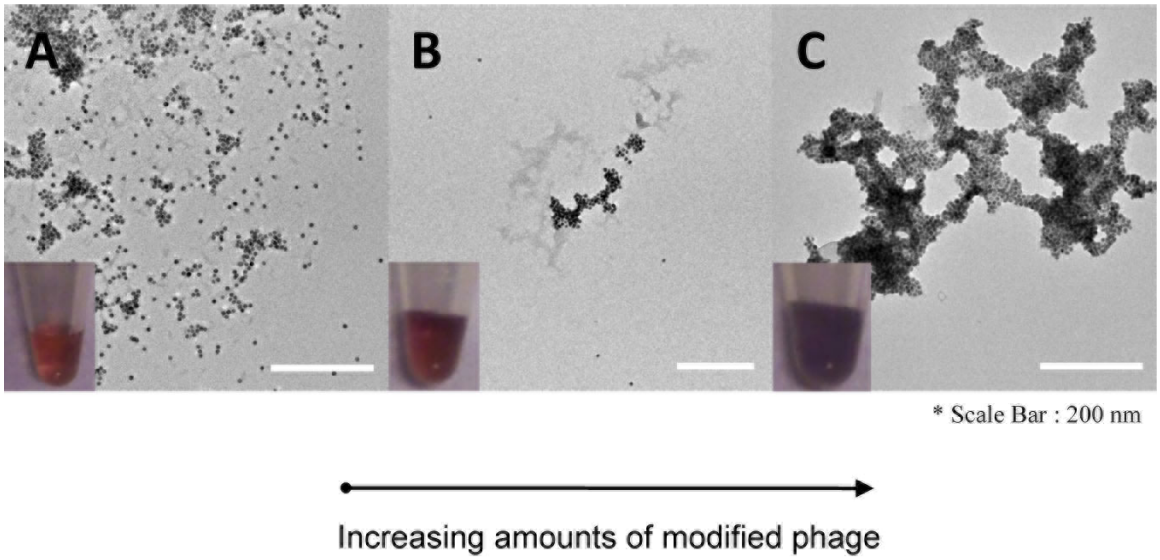

Figure 2.5 TEM images of aggregation of gold nanoparticles caused by phage networking. With increasing amounts of thiolated phage, the phage were covered by gold nanoparticles lead to more blue-shift color by naked eyes.

2.3 Phage Display

Next, phage display was run to isolate viruses that bound specifically to rabbit anti-goat IgG, a model antigen. Three rounds of screening against biotinylated rabbit anti-goat IgG bound to streptavidin conjugated magnetic microspheres (Dynabeads, Invitrogen) resulted in the isolation of a serine-rich consensus sequence (Figure 2.6). ELISAs of specific phage expressing the consensus sequence and using HRP-conjugated anti-M13 antibody, 2,2'-azino-bis(3-ethylbenzthiazoline-6-sulphonic acid) (ABTS) and H_2O_2 showed very strong binding to the anti-goat IgG (Figure 2.7, row 3). Control ELISAs with either a non-consensus sequence phage (Figure 2.7, row 2) or the consensus sequence phage against streptavidin coated plates alone (Figure 2.7, row 1) showed respectively weaker and negative binding, demonstrating the high specificity of the isolated phage for anti-goat IgG. The phage expressing the consensus sequence were next modified using EDC and cysteamine. To ensure that the modification did not affect the binding capabilities of the phage, ELISAs of the thiol-modified phage were also run against anti-goat IgG. Known concentrations of the thiol-modified phage were reacted with the model antigen, biotinylated rabbit anti-goat IgG bound to either streptavidin coated plates or magnetic beads (Dynabeads), rinsed thoroughly to remove excess phage, incubated with HRP-conjugated anti-M13 antibody and reacted with ABTS and H_2O_2. As shown in Figure 2.8 (well B), the thiolated phage bound anti-goat IgG with similar binding affinities as the non-thiolated phage, whereas control runs against the streptavidin coated surfaces showed that the thiolated phage maintained its specificity for the correct antigen (Figure 2.8, well A).

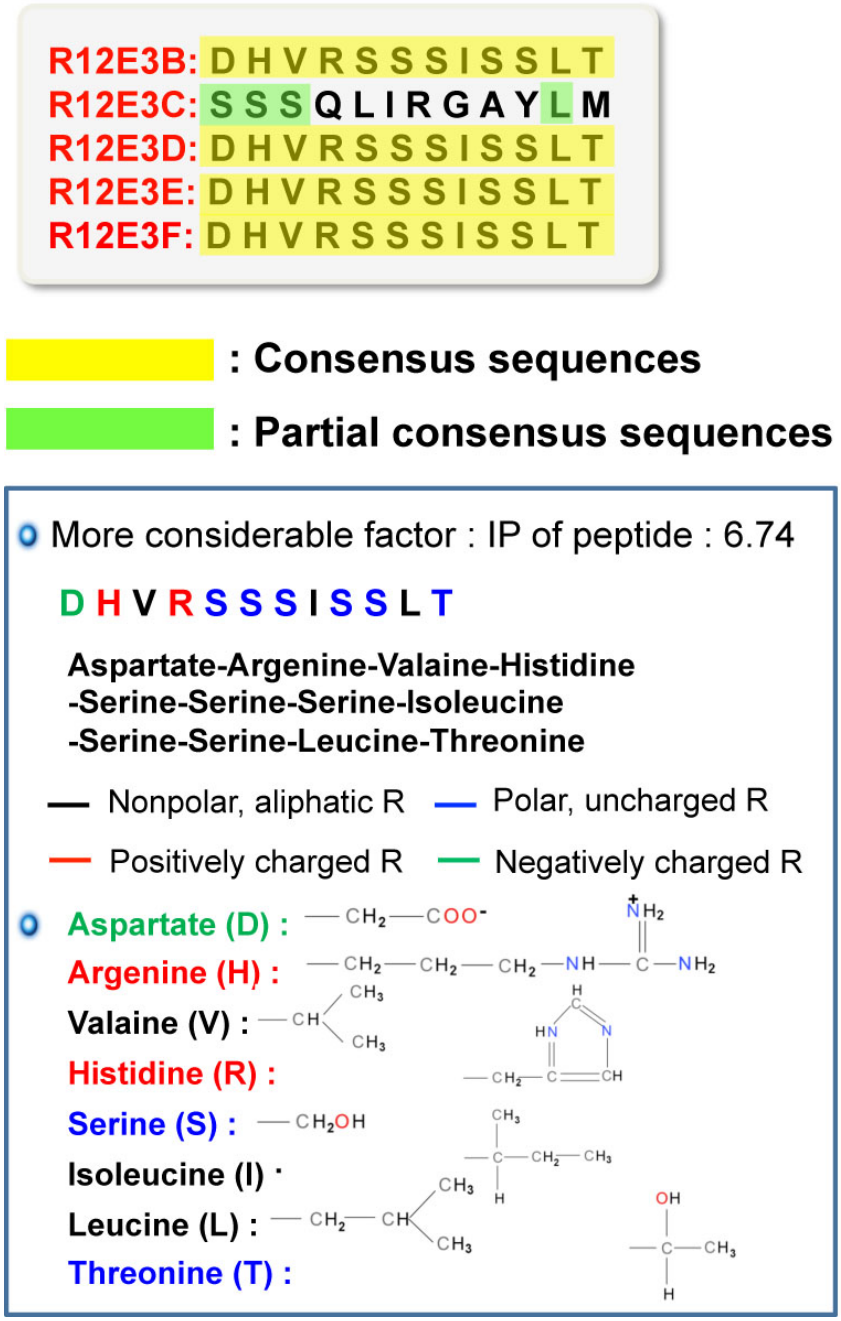

Figure 2.6 Sequence of phage isolated by screening against rabbit anti-goat IgG. Phage A, C, D, and E show a clear consensus sequence.

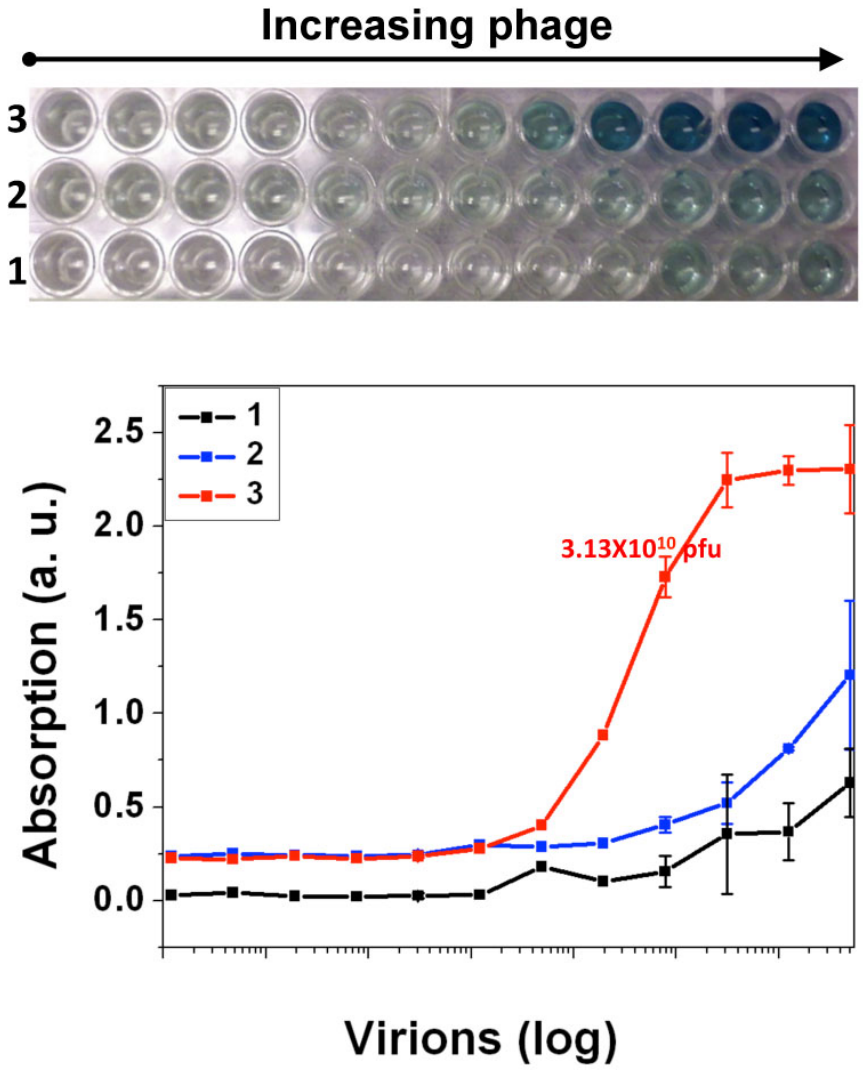

Figure 2.7 ELISA against streptavidin plates alone (row 1), rabbit anti-goat IgG using phage E3B (row 2) and rabbit anti-goat IgG using consensus phage E3A (row 3).

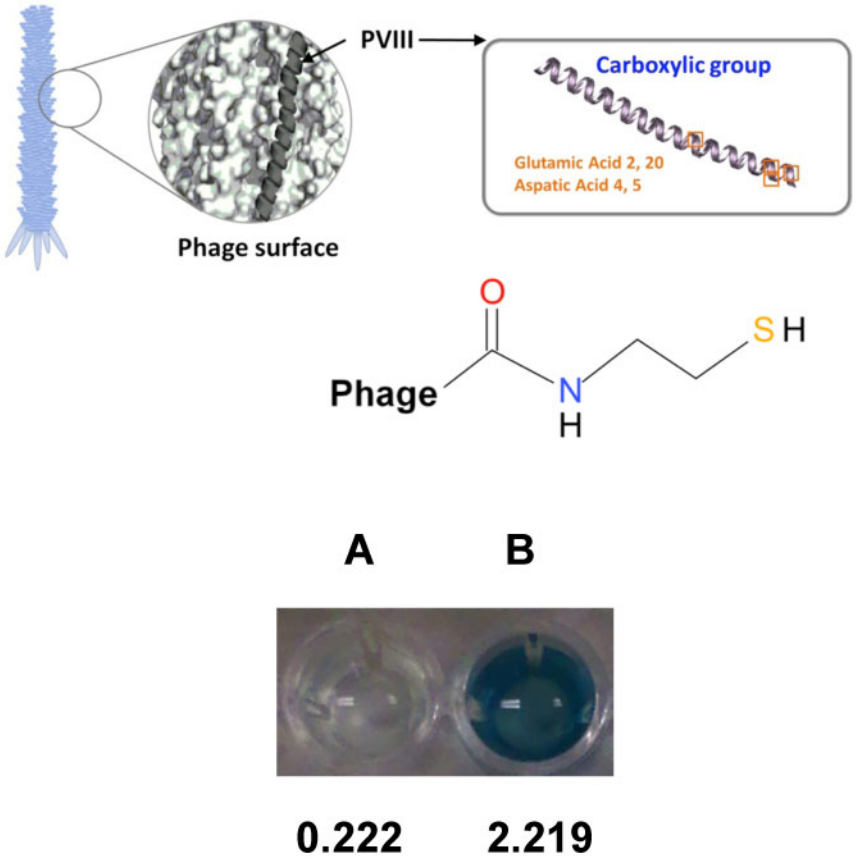

Figure 2.8 ELISA of thiolated phage for binding rabbit anti-goat IgG. Wells A and B show results for binding to streptavidin alone and anti-goat IgG respectively. The numeric values denoted below each well correspond to adsorbance units collected at 410 nm.

2.4 Diagnostic Results

Having successfully shown that thiol modification of the phage that express the consensus sequence did not prevent specific binding to anti-goat IgG, the thiolated phage were next implemented as test diagnostics for sensing the model antigen, anti-goat IgG. First, 530 fmol of the thiolated phage were mixed with different amounts of biotinylated anti-goat IgG ranging from 7 pmol to 100 fmol and captured with 250μg streptavidin-coated magnetic Dynabeads. Here, biotinylated anti-goat IgG were used as model antigens to allow capture by strepatvidin coated surfaces; in real assays, unmodified antigens would be captured by surfaces modified with known secondary antibodies. After thorough washing with Phosphate Buffer Saline with 0.1% Tween (PBST), 500μl of pH 2 glycine buffer was added to elute any bound thiolated phage, which were then collected and neutralized with Tris base (Figure 2.1). After removing the excess salts by microcentrifuge filtration and concentrating to a final volume of 25μL , 115 fmoles of 20nm gold nanocrystals was added. As shown in Figure Figure 2.9, only samples containing the correct anti-goat IgG antigen led to distinct red to blue color shifts (Figure 2.9, tubes 4-6). As expected, UV-Vis measurements showed both a dramatic broadening in the plasmon resonance peak and, at higher antigen concentrations, a significant red shift in maximum absorbance. The phage based gold nanocrystal sensors were also extremely sensitive, showing distinct color changes with as few as 100 femtomoles of antigen (Figure 2.9, tube 4). In contrast to these, eluants collected from sensing reactions that had either no anti-goat IgG (tube 1), no phage (tube 2) or the negative control antigen, biotinylated bovine serum albumin (tube 3), did not produce any visible shift in

plasmon resonance and UV-Vis spectra were identical to 20nm gold alone (Figure 2.9. 4B, #). Because the entire detection platform was run in solution, these sensors could not only detect antigens with extremely high sensitivities but was also able to perform with very high throughput and without spectroscopic equipment.

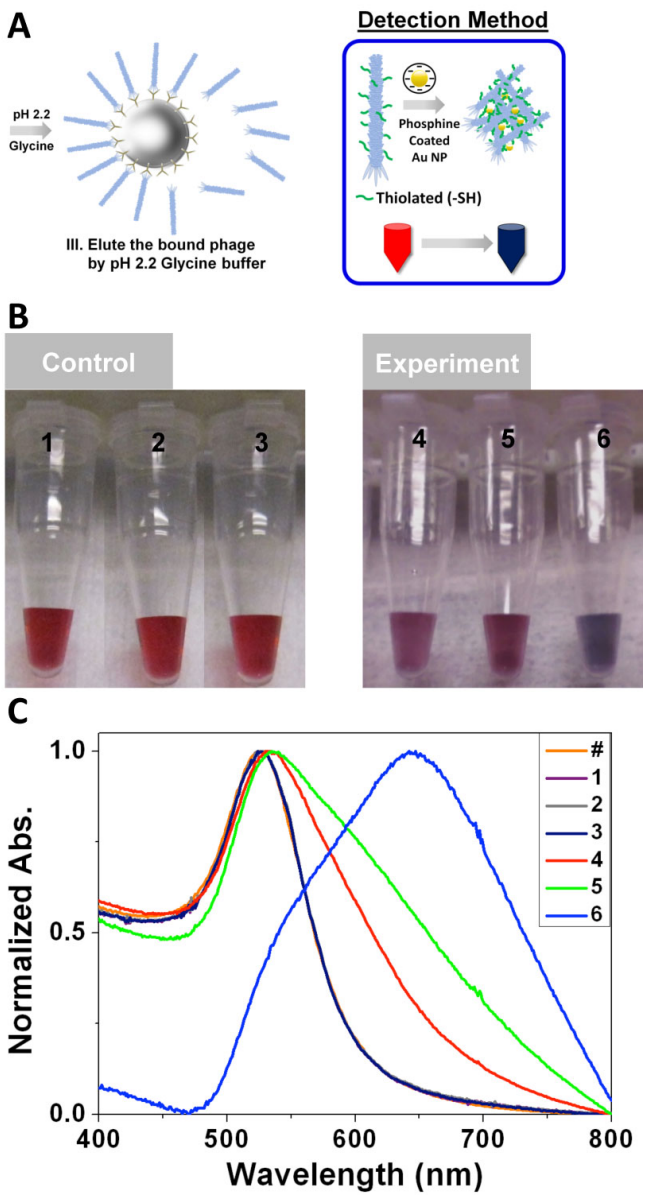

Figure 2.9 Sensing assay for rabbit anti-goat IgG with thiolated phage. (A) Schematics of forming aggregation of gold nanoparticles through thiolated phage network. (B) In samples 4-6, 100 femtomoles [4], 1.62 picomoles [5], and 6.5 picomoles [6] of anti-goat IgG were mixed with 530 femtomoles of thiolated phage and captured using magnetic beads. Following elution at pH 2, the eluants were mixed with 20nm gold. Control asays without anti-goat IgG [1], without phage [2] or with the control antigen biotinylated BSA [3] showed no color change. (C) UV Vis spectra gold nanocrystal aggregation showing distinct red shifts and broadening of the surface plasmon resonances in samples 4-6.

2.5 Materials and Experimental Sections

2.5.1 Phage Display

Phage libraries were reacted in solution with 10 pmoles biotinylated rabbit IgG. The phage-rabbit IgG complexes were incubated with pre-blocked streptavidin coated magnetic Dynabeads (Invitrogen) for 15 min and unbound phage were removed by washing with TBS and Tween-20. Bound phage were next eluted using pH 2.2 0.2 M Glycine-HCl buffer. Eluted solutions were neutralized with pH 9.1 1 M Tri buffer. This process was repeated for a total of three runs.

2.5.2 EDC/Cysteamine chemistry

Thiolated phage were synthesized by reacting phage with 1.33 mM EDC and 1.33 mM cysteamine in sterile PBS, pH 7.4.[22] Subsequent additions of 1.33 mM EDC were added at 30 min and 1 h, and the entire 1ml reactions were run for 2 h. The thiolated phage were then purified by dialysis through a 3.5K MWCO regenerated cellulose dialysis tubing (Fisher) against distilled water. Thiolated phage were stored in 20 mM pH 7.0 sodium phosphate solution.

2.5.3 Dynabead Protein Sensing

530 fmol of the thiolated phage were reacted with varying molar amounts (indicated in the text) of biotinylated rabbit anti-goat IgG in solution, captured against pre-blocked streptavidin coated Dynabeads, and washed with PBS and Tween-20. The bound phage were next eluted with pH 2.2 0.2 M Glycine-HCl buffer and the eluants

were neutralized with pH 9.1 1 M Tri buffer. The eluted solutions were filtered through 30K MWCO microcentrifuge filters and 20 nm phosphine coated gold nanoparticles (Ted Pella) were added to the filtrates for detection.

2.6 Conclusion

The work shown here demonstrates the power of modified phage-protein interactions to engineer highly-sensitive, unique, solution-based protein diagnostics that are easy to use, rapid to run, and possible to read without any spectroscopic or microscopic analysis. Because secondary antibodies and enzymes are not required for these diagnostics and M13 bacteriophage are stable biomaterials,[26] these sensing platforms should be functional in locations with limited access to equipment and facilities. The current sensitivites of these protein sensors are currently in the 100 femtomole range; efforts are underway to enhance their sensitivity further through optimization of the functionalization of the phage coat proteins, as well as developing subsequent methods for protein identification from a complex mixture.

2.7 Acknowledgements

This chapter, in full, is a reprinted with permission from *Anal. Chem.*, *Ju Hun Lee*, *Jennifer N. Cha*, Vol. 83, page 3516-3519, **2011**. Copyright ©2011 American Chemical Society. The dissertation author was the primary investigator and author of this paper.

2.8 References

1. Cui, Y.; Wei, Q.; Park, H.; Lieber, C. M. Nanowire Nanosensors for Highly Sensitive and Selective Detection of Biological and Chemical Species. *Science* **2001**, 293, 1289-1292.

2. McAlpine, M.C.; Ahmad, H.; Wang, D.; Heath, J.R. Highly ordered nanowire arrays on plastic substrates for ultrasensitive flexible chemical sensors. *Nat. Mater.* **2007**, *6*, 379-384.

3. Ferrari, M. Cancer nanotechnology: opportunities and challenges. *Nature Rev. Cancer* **2005**, *5*, 161-171.

4. Elghanian, R.; Storhoff, J.J.; Mucic, R.C.; Letsinger, R.L.; Mirkin, C.A. *Science* **1997**, *277*, 1078-1081.

5. Hahm, J.; Lieber, C. M. Direct Ultrasensitive Electrical Detection of DNA and DNA Sequence Variations Using Nanowire Nanosensors. *Nano Lett.* 2004, 4, 51-54.

6. Wang, X.; Ozkan, C. S. Multisegment Nanowire Sensors for the Detection of DNA Molecules *Nano Lett*. **2008**, *8*, 398-404.

7. Medintz, I. L.; Clapp, A. R.; Mattoussi, H.; Goldman, E. R.; Fisher, B.; Mauro, J. M. Self-Assembled Nanoscale Biosensors Based on Quantum Dot FRET Donors. *Nat. Mater.* **2003**, 2, 630-638.

8. Zhang, J.; Allen, M.D. FRET-based biosensors for protein kinases: illuminating the kinome*Mol. Biosyst*. **2007**, *3*, 759-765.

9. Borisov, S.M.; Wolfbeis, O.S. Optical Biosensors. *Chem. Rev.* **2008,** *108*, 423-461.

10. Xiang, Y.; Xie, M.; Bash, R.; Chen, J. J. L.; Wang, J. Ultrasensitive label-free aptamer-based electronic detection. *Angew. Chem. Int. Ed.* **2007,** *46*, 9054-9056.

11. Stoeva, S. I.; Lee, J.; Smith, J. E.; Rosen, S. T.; Mirkin, C. A. Multiplexed Detection of Protein Cancer Markers with Biobarcoded Nanoparticle Probes. *J. Am. Chem. Soc.* **2006**, 128, 8378-8379.

12. Kim, D.; Daniel, W.L.; Mirkin, C.A. Microarray-based multiplexed scanometric immunoassay for protein cancer markers using gold nanoparticle probes. *Anal. Chem.* **2009,** *81*, 9183-9187.

13. Martinez, A.W.; Phillips, S.T.; Whitesides, G.M.; Carrilho, E. Diagnostics for the developing world: microfluidic paper-based analytical devices. *Anal. Chem.* **2010,** *82,* 3-10.

14. Martinez, A.W.; Phillips, S.T.; Butte, M.J.; Whitesides, G.M. Patterned Paper as a Platform for Inexpensive, Low-Volume, Portable Bioassays. *Angew. Chem. Int. Ed.*, **2007,** *46*, 1318-1320.

15. Peeling, R.W.; Holmes, K.K.; Mabey, D.; Ronald, A. Rapid tests for sexually transmitted infections (STIs): the way forward. *Sex. Transm. Infect.* **2006,** *82, v*1-v6.

16. Xia, F.; Zuo, X.; Yang, R.; Xia, Y.; Kang, D.; Vallée-Bélisle, A.; Gong, X.; Yuen, J.D.; Hsu, B.B.Y.; Heeger, A.J.; Plaxco, K.W. Colorimetric detection of DNA, small molecules, proteins, and ions using unmodified gold nanoparticles and conjugated polyelectrolytes. *Proc. Natl. Acad. Sci.* **2010,** *107,* 10837-10841.

17. Heeger, P.S.; Heeger, A.J. Making sense of polymer-based biosensors. *Proc. Natl. Acad. Sci.* **1999,** *96*, 12219-12221.

18. You, C.-C.; Miranda, O.R.; Gider, B.; Ghosh, P.S.; Kim, I.-B.; Erdogan, B.; Krovi, S.A.; Bunz, U.H.F.; Rotello, V.M. Detection and identification of proteins using nanoparticle–fluorescent polymer 'chemical nose' sensors. *Nature Nano.* **2007,** *2,* 318-323.

19. Li, K.; Liu, B. Water-soluble conjugated polymers as the platform for protein sensors. *Polymer Chemistry* **2010,** *1*, 252-259.

20. Dwight, S.J.; Gaylord, B.S.; Hong, J.W.; Bazan, G.C. Perturbation of Fluorescence by Nonspecific Interactions between Anionic Poly(phenylene-vinylene)s and Proteins: Implications for Biosensors. *J. Am. Chem. Soc.* **2004,** *126*, 16850-16859.

21. Kehoe, J. W.; Kay, B. K. Filamentous Phage Display in the New Millennium. *Chem. Rev.* **2005**, 105, 4056-4072.

22. Yacoby, I.; Bar, H.; Benhar, I. Targeted Drug-Carrying Bacteriophages as Antibacterial Nanomedicines. *Agents and Chemother.* **2007**, 51, 2156-2163.

23. Zhenpeng, L.; Kock, H.; Dübel, S. Mutations in the N-terminus of the major coat protein (pVIII, gp8) of filamentous bacteriophage affect infectivity. *J. Mol. Microbiol. Biotechn.* **2003**, *6*, 57-66.

24. Souza, G.R.; Yonel-Gumruk, E.; Fan, D.; Easley, J.; Rangel, R.; Guzman-Rojas, L.; Miller, J.H.; Arap, W.; Pasqualini, R. Bottom-up assembly of hydrogels from bacteriophage and Au nanoparticles: the effect of cis- and trans-acting factors. *PLoS ONE* **2008,** *3*, 1-5.

25. Souza, G. R.; Christianson, D. R.; Staquicini, F. I.; Ozawa, M. G.; Snyder, E. Y.; Sidman, R. L.; Miller, J .H.; Arap, W.; Pasqualini, R. Networks of Gold Nanoparticles and Bacteriophage as Biological Sensors and Cell-Targeting Agents. *Proc. Natl. Acad. Sci. U. S. A.* **2006**, 103, 1215-1220.

26. Olofsson, L.; Ankarloo, J.; Andersson, P.O.; Nicholls, I.A. Filamentous bacteriophage stability in non-aqueous media. *Chem. Biol.*, **2001,** *8*, 661-671.

CHAPTER 3: Chemically Modified DNA Phage via SPDP/s-SMCC and Plasmonic Sensor with DNA-gold Nanoparticles

"One resolution I have made, and try always to keep, is this:

'To rise above little things'."

- John Burroughs

3.1 Introduction

Many diseases, including prostate and breast cancer, continue to be a global public health problem.[1, 2] In order to improve patient survival rates, advanced biomarker detection systems are necessary for early-stage diagnosis, monitoring therapeutic response, and determining the efficacy of the treatment. [3-13] However, to obtain global applicability, these biomolecule detection systems must not only be sensitive but must also be easy to use, reliable, high-throughput, and inexpensive to manufacture. Within the biomedical community, chemically engineered viruses and virus-like particles (VLPs) have generated interest due to their potential for a variety of medical applications,[14, 15] including drug delivery,[16-18] serving as in vitro imaging scaffolds,[19-21] and platforms for biosensing.[22, 23] One particular advantage for using viruses as scaffolds for imaging and detection is that they occur naturally and are readily produced by E. coli, which enables the generation of many virus copies without intensive fabrication. Furthermore, viruses are thermally and chemically robust [17] and

their coat protein composition can easily be modified synthetically or genetically, providing an inherent capacity for multivalent and orthogonal display.[21]

M13 bacteriophage is a particularly promising virus scaffold due to its well-established role in phage display technologies to identify particular peptide sequences that bind to specific targets.[24] M13 bacteriophage is a rod-like virus [25, 26] in which the five minor capsid pIII proteins located at one end of the virus are involved in biological recognition, and the remaining major capsid pVIII proteins (~2700 copies per phage) are responsible only for the structural arrangement of bacteriophage.[27] Thus, the structure of the virus allows for the major capsid proteins to be chemically modified without disrupting its ability to bind a particular antigen. This approach was recently used to produce thiol-modified M13 bacteriophage that could cause Au nanoparticle aggregation, and the resulting plasmon resonance shifts acted as optical indicators of antigens in solution.[22] In addition to detecting a single type of antigen, multiplexed protein assays are also needed as they provide a means to identify and measure multiple biomarkers in solution and thereby increase diagnostic accuracy.[2, 28-30] In this chapter, we describe the synthesis of DNA-conjugated M13 bacteriophage and demonstrate its dual applicability for rapidly detecting and identifying antigens in solution with high sensitivity and accuracy.

3.2 Theoretical background of Surface Plasmonic Resonance

Noble metal nanoparticles strongly absorb in the UV and visible range which does not occur with bulk metal. This phenomenon of absorption of light from metal nanostructures is known as localized surface plasmon resonance (LSPR). To encounter incident photons to the novel metal nanostructures induce to excite surface plasmons by resonance with coherent electron oscillations on the surface. [31-32] LSPR excitation results in wavelength selective absorption with extremely large molar extinction coefficients.[31] It occurs when light interacts with particles much smaller than the incident wavelength (radius/wavelength of light $\leq$ 0.05, Rayleigh limit), as shown in Figure 3.1. For surface plasmon resonance, materials should have a negative real and small positive imaginary dielectric constant such as Au, Ag, and Cu.[32]

If shperical nanoparticles of radius "a" is irradiated by z-polarized light of wavelength λ (where a is much smaller than the wavelength of light λ), the magnitude of the electric field appears static around the nanoparticles, allowing Maxwell's equations to be solved by using a quasi-static approximation. The resulting solution for the electromagnetic (EM) field outside the particles is given by [32]

$$E_{out}(x,y,z) = E_0\hat{Z} - \left[\frac{\varepsilon_{in} - \varepsilon_{out}}{(\varepsilon_{in} + 2\varepsilon_{out})}\right] a^3 E_0 \left[\frac{\hat{z}}{r^3} - \frac{3z}{r^5}(x\hat{x} + y\hat{y} + z\hat{z})\right].$$

ε_{in}: dielectric constant of metal nanoparticles
ε_{out}: dielectric constant of external environment (3.1)

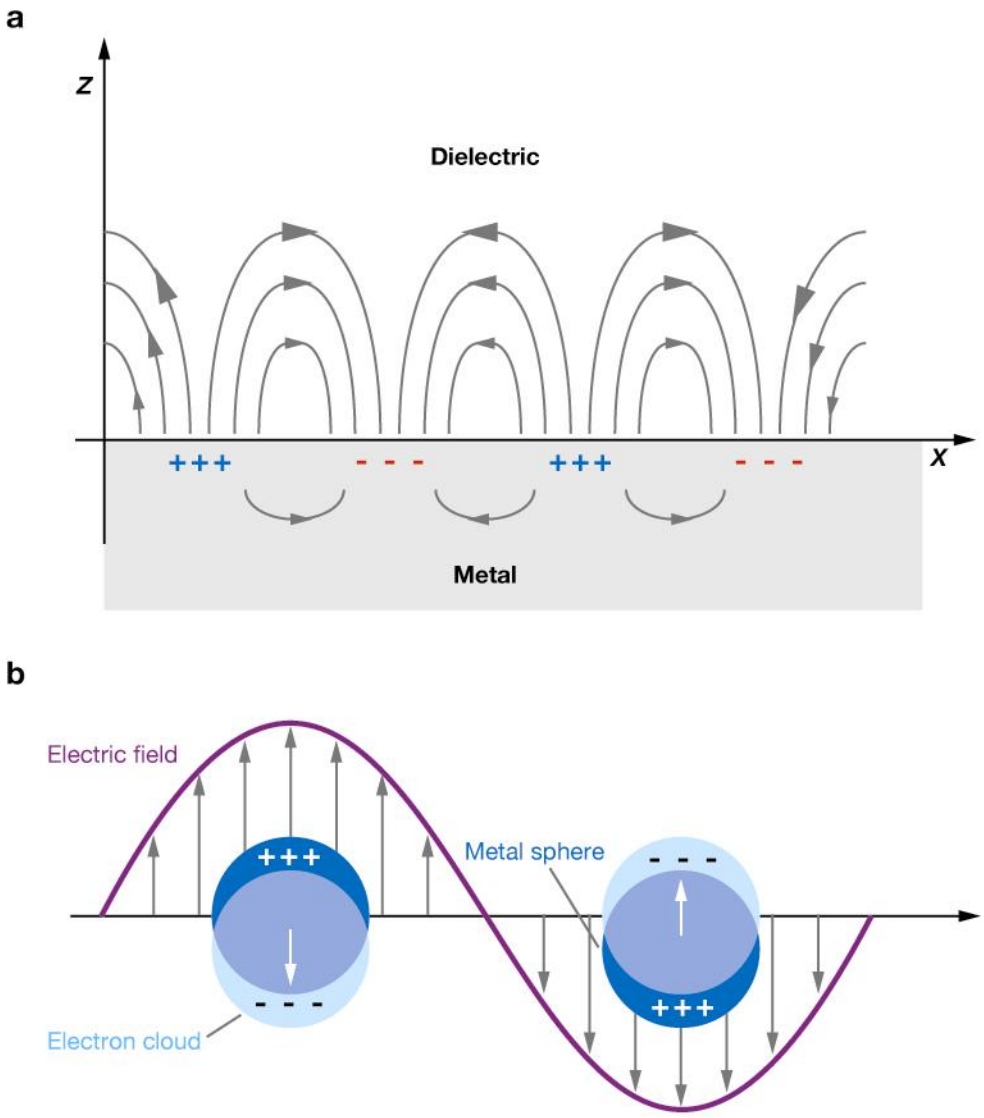

Figure. 3.1 Schematic diagrams illustrating (a) a surface plasmon polariton (or propagating plasmon) and (b). Reproduced with permission from ref 31.

Due to strong dependency of ε_{in} to the wavelength, the first term in square brackets determines the dielectric resonance condition for the particles. When the dielectric constant of the metal is roughly equal to "$-2\varepsilon_{out}$", the EM field is enhanced with respect to the incident EM field. In the case of silver and gold, this condition is met in the visible region of the spectrum. The size (a) of the nanoparticles and external dielectric constant (ε_{out}) are also key factors for determining the EM field outside the particles and these are consistent with experimental results.[32]

The calculated simplest theoretical extinction spectrum of the metal sphere as followed [31]:

$$E(\lambda) = \frac{24\pi^2 N a^3 e_{out}^{\frac{3}{2}}}{\lambda \ln(10)} \left[\frac{\varepsilon_i(\lambda)}{(\varepsilon_r(\lambda) + \chi\varepsilon_{out})^2 + \varepsilon_i(\lambda)^2} \right] \quad (3.2)$$

ε_r: real component of the metal dielectric function
ε_i: imaginary components of the metal dielectric function

Here, the "χ" that appears in front of ε_{out} is the geometric factor which is related to the aspect ratio of the nanostructure. The value of χ is 2 for the case of a sphere, but in the case of nanorod shape, the value can be as large as 20. And the "N" value corresponds to the number of finite polarizable elements (areal density of nanoparticles), each of which can interact with the applied electric field.[31, 32]

3.3 Chemical Strategy to Modification of DNA-M13 Bacteriophage

M13 bacteriophage that recognize the model antigen anti-goat rabbit immunoglobulin (IgG) were isolated through phage display.[22] Enzyme-linked immunosorbent assays (ELISAs) demonstrated that the viruses bound strongly and with high specificity to the target protein.[22] The phage did not bind to streptavidin or to surfaces conjugated with the incorrect antigen.[22] Next, the anti-goat IgG binding phage were modified with multiple copies of A_{30} DNA. In order to install thiol nucleophiles on the phage coat, thiol groups were first incorporated onto the phage coat by reacting the phage with N-succinimidyl 3-[2-pyridyldithio]-propionate (SPDP) (Figure 3.2) so that we could effectively conjugate the maleimide-derivatized DNA to the phage coat. The majority of the phage coat consists of 2700 copies of the same 50-amino acid peptide, which do not have any cysteine or disulfide bonds. While some disulfide bonds are buried in the minor capsid proteins of phage, the solvent-accessible SPDP groups would be much more accessible to tris(2-carboxyethyl)phosphine hydrochloride (TCEP-HCl) to be easily reduced in the presence of a stoichiometric amount of TCEP (relative to SPDP groups) and release pyridine 2-thione and expose free thiol groups on the phage. Finally, maleimide-bearing oligonucleotides (A_{30}), produced from amine-terminated A_{30} and sulfosuccinimidyl 4-[N-maleimidomethyl] cyclohexane-1-carboxylate (s-SMCC), were coupled with the thiol groups on the phage. While it is plausible that the amines on the phage could react with the maleimide-derivatized DNA, since the coupling is carried out at pH 7 chemoselectivity is enhanced for the introduced thiol groups. In addition, the reaction rate of sulfhydryls with maleimides is 1000-fold faster than the reaction rate with amines[33];

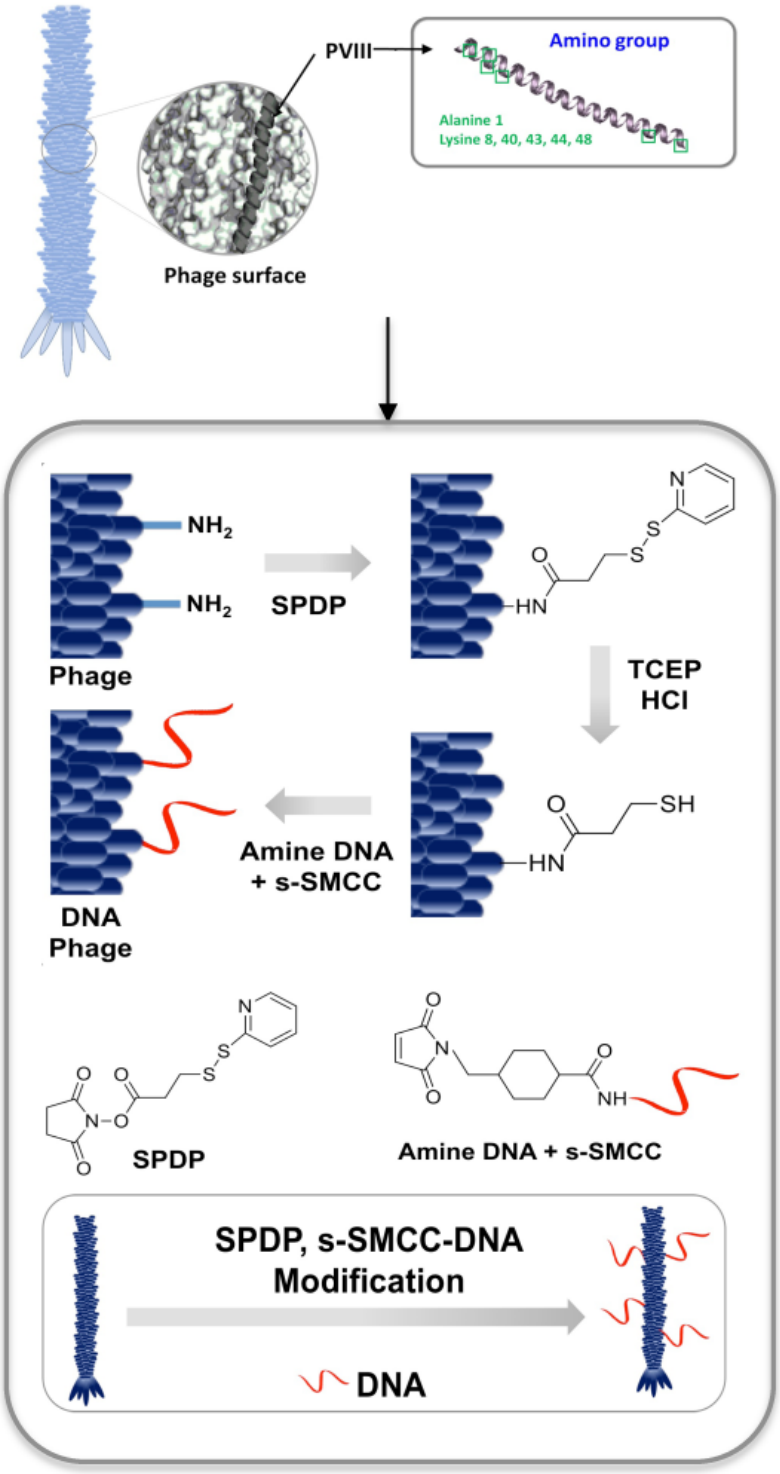

Figure 3.2 Synthesis of DNA-modified M13 Bacteriophage.

thus, we can greatly favor the reaction of the thiols with the maleimide-DNA. The resulting conjugate was characterized by matrix-assisted laser desportion ionization time-of-flight mass spectrometry (MALDI-TOF MS), UV-Vis spectroscopy, and gel electrophoresis. The conversion ratio of SPDP-modified pVIII to total pVIII was quantitatively measured by MALDI-TOF MS. This synthetic approach led to addition of approximately 1210 ± 85 SPDP groups per virus (Figure 3.2 a). After Coomassie staining SDS PAGE gels, densitometric analysis was used to quantify the ratio of DNA-conjugated to unfunctionalized pVIII.[19, 34] Using this approach, the phage-DNA conjugate prepared from 300 μM maleimide-modified DNA was determined to have 259 ± 19 DNAs per phage. (Figure 3.2 b, Table 3.1).

Table 3.1 The number of DNA-PVIIIs calculated by the densitometric method shown in Figure 3.2 b).

Maleimide DNA (μM)	DNA-P8 numbers
30	23
100	72
300	278

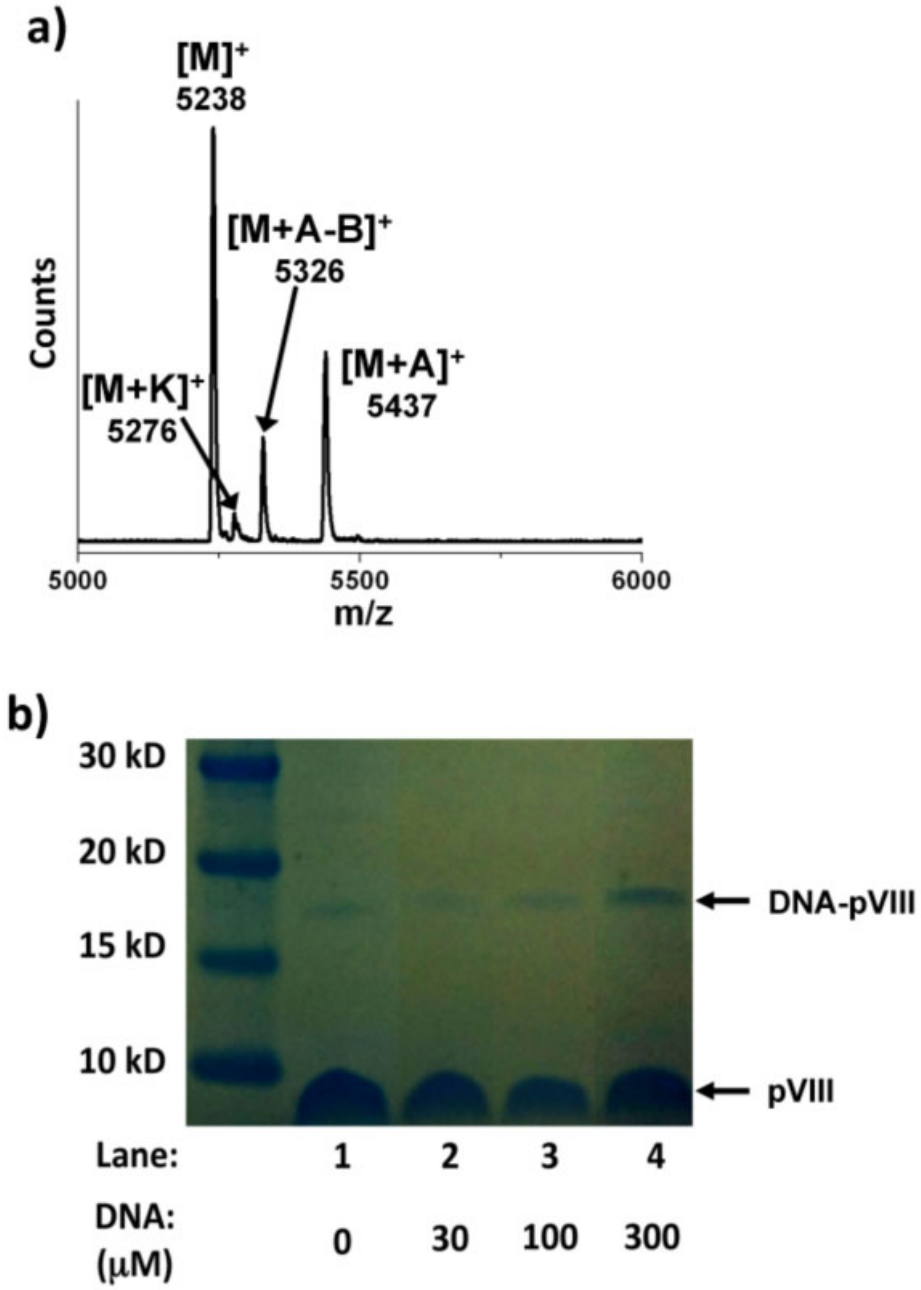

Figure 3.3 a) MALDI-TOF MS of unmodified pVIII ([M]+), pVIII + SPDP ([M+A]+), and pVIII + SPDP - pyridine 2-thione ([M+A-B]+). b) Engineered DNA-M13 bacteriophage analyzed by SDS-PAGE. Lane 1 corresponds to native M13 bacteriophage. Lanes 2-4 correspond to phage reacted with different amounts of s-SMCC derivatized DNA oligonucleotide (A_{30}). Reprinted with permission from *ACS Nano*, *Ju Hun Lee*, *Dylan W. Domaille*, *Jennifer N. Cha*, Vol. 6, page 5621-5626, **2012**. Copyright ©2012 American Chemical Society.

3.4 Test for preservation of DNA-phage binding after modification

Next, to determine if chemical modification of the phage altered or inhibited its ability to bind its specific protein target, the DNA-conjugated phage were tested for binding to anti-goat IgG through ELISA. As shown in Table 1, the DNA-conjugated phage showed similar binding affinities and specificities for anti-goat IgG as compared to unmodified bacteriophage (Table 3.2). Although the relative ELISA signals from the DNA-conjugated phage were slightly lower than native phage which could be attributed to the DNA on the phage inhibiting anti-M13 antibody binding, the modification of the phage did not significantly alter the ELISA signals. Control assays showed that the DNA-conjugated phage bound neither the incorrect antigen biotinylated amylase nor the strepatvidin surfaces, indicating that DNA conjugation also did not affect the specificity of the phage.

Table 3.2 Comparison of native and DNA-phage binding to anti-goat IgG (model antigen) from horse radish peroxidase-conjugated anti-M13 antibodies, after addition of ABTS. The UV absorbance values at 410 nm. anti-goat IgG was used as model antigen

	Pure phage + Antigen	Pure phage + streptavidin	DNA phage + Antigen	DNA phage + Strepavidin
UV Abs.	2.163	0.401	1.258	0.265

3.5 Diagnostic Results

To use the DNA-phage for both protein detection and identification, the A_{30}-DNA phage were incubated with varying concentrations of the model antigen, biotinylated anti-goat rabbit IgG, and captured using streptavidin-coated magnetic beads. Unbound phage were removed by washing with PBST (PBS with 0.1% Tween) (Figure 3.4). T_{15}-conjugated 10 nm Au nanoparticles (NPs) were then added to the magnetic bead pellets and vortexed to hybridize with the bound A_{30}-phage. After adding the DNA-Au NPs and removing the beads with a magnet, an immediate decrease in color was observed in the supernatant for samples containing antigen, indicating that some of the DNA-conjugated Au NPs had bound to the phage on the beads (Figure 3.5). With increasing amounts of antigen, more DNA-Au NPs bound to the magnetic beads, indicating that more phage bound to the beads at higher antigen amounts. Control assays using the incorrect antigen (biotinylated amylase, and biotinylated bovine serum albumin (BSA)), the absence of antigen, or the absence of phage showed no color changes upon addition of Au NPs (Figure 3.6).

In order to more precisely quantify the amount of antigen and to provide a method for identifying the specific antigen, the DNA-Au NPs were eluted back into solution, and the DNA sequences on the Au NPs were determined with DNA microarrays. To achieve this, the T_{15}-DNA Au NPs bound to the A30-phage were competitively eluted by adding excess T_{30} DNA, heating the solution and allowing it to cool. Though this process released the bound DNA-Au NPs at lower concentrations of antigen (25-100 femtomoles), at higher antigen concentrations heating alone was found to be insufficient to dissociate any of the T_{15}-Au NPs. It is possible that at higher antigen concentrations,

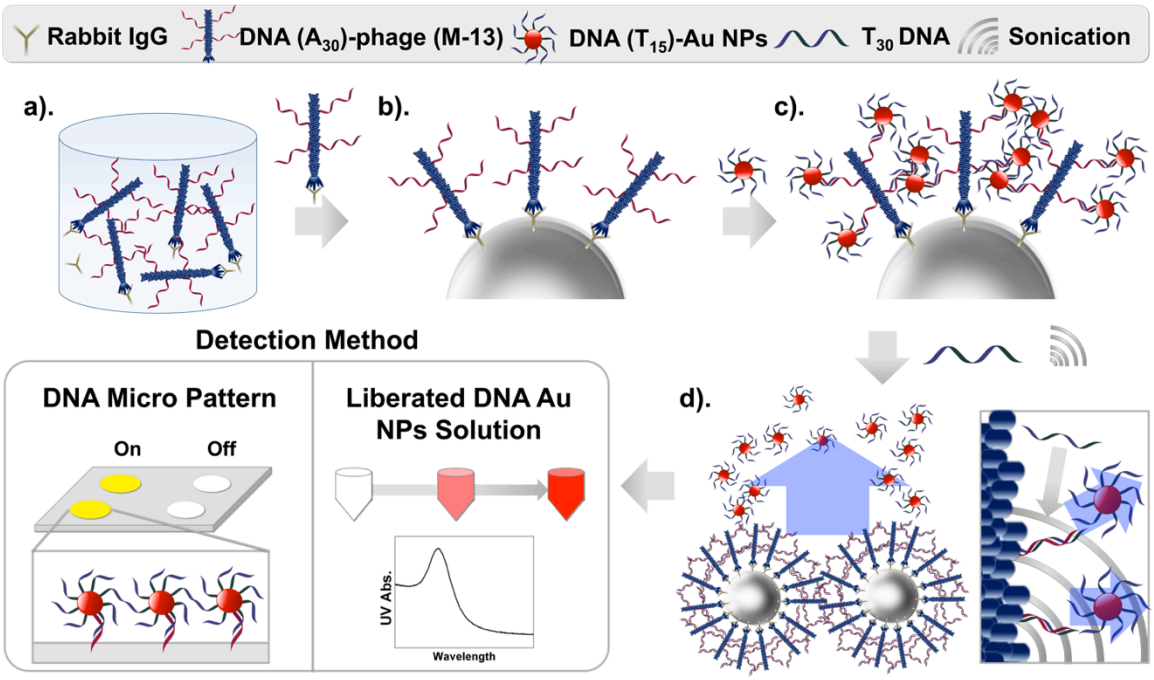

Figure 3.4 Sensor Design with DNA-phage (a) DNA-phage were reacted with the target antigen in the solution phase. (b) Complexes of DNA (A_{30})-phage and antigen were captured with magnetic beads. (c) DNA (T_{15})-Au NPs were hybridized with captured DNA (A_{30})-phage. (d) DNA (T_{15})-Au NPs were competitively eluted with T_{30} DNA and sonication. Liberated DNA-Au NPs were analyzed by UV-Vis spectroscopy values, and the sequence was identified with a DNA microarray. Reprinted with permission from *ACS Nano*, *Ju Hun Lee*, *Dylan W. Domaille*, *Jennifer N. Cha*, Vol. 6, page 5621-5626, **2012**. Copyright ©2012 American Chemical Society.

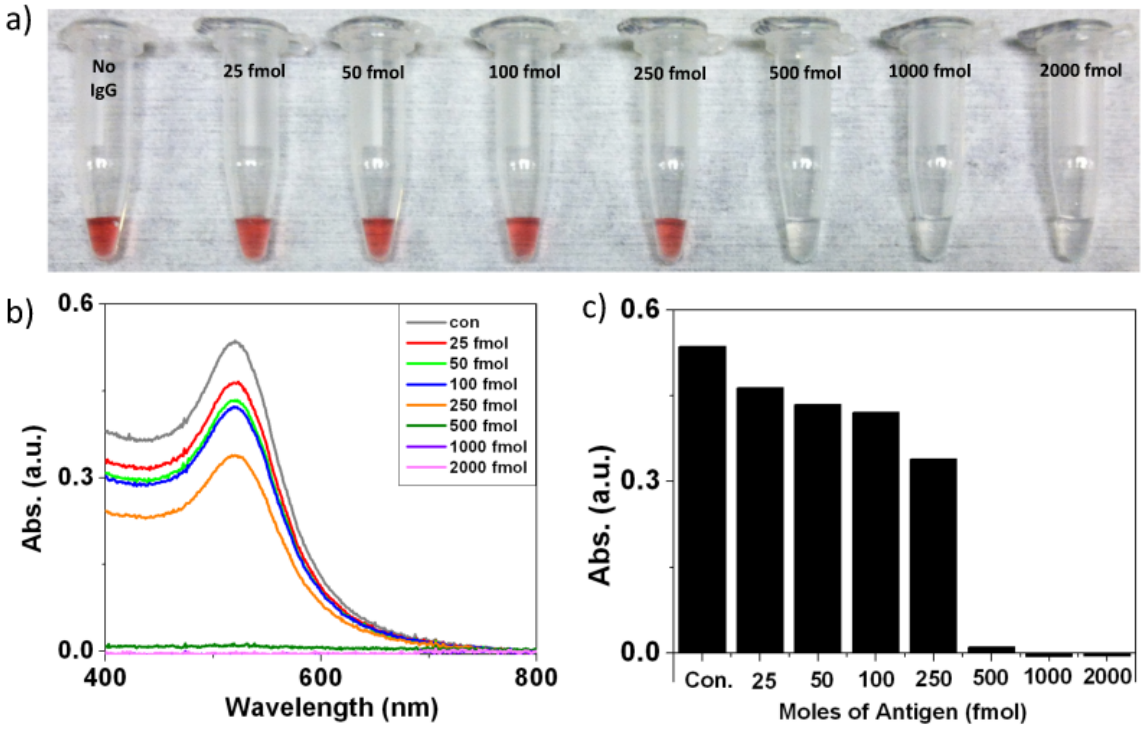

Figure 3.5 After conjugating DNA-Au NPs with DNA-phage on magnetic beads, decrease in color of the supernatant as an indicator for increased antigen concentration. (a) Images of supernatant. (b) UV/Vis spectra of (a). (c) UV absorption values at 520 nm as a function of the antigen concentration. Reprinted with permission from *ACS Nano*, *Ju Hun Lee*, *Dylan W. Domaille*, *Jennifer N. Cha*, Vol. 6, page 5621-5626, **2012**. Copyright ©2012 American Chemical Society.

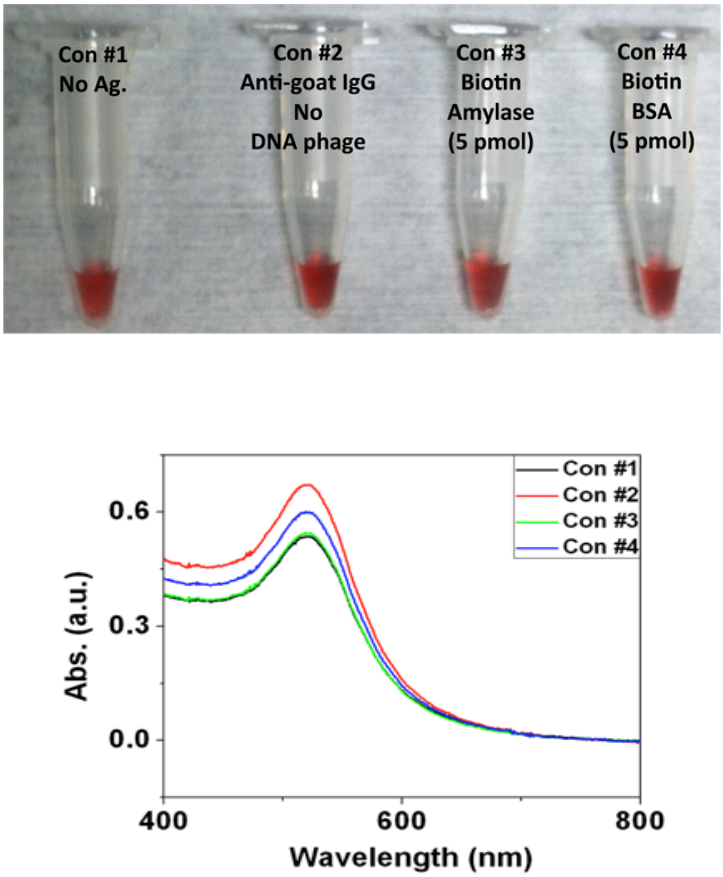

Figure 3.6 After conjugating DNA-Au NPs with DNA-phage on magnetic beads, control assay images of supernatant, and UV/Vis spectra. Con. #1: no antigen with DNA phage, Con. #2: 5 pmol of anti-goat IgG, no DNA phage, Con #3: 5 pmol of biotin Amylase with DNA phage, and Con. #4: 5 pmol of biotin BSA with DNA phage. Reprinted with permission from *ACS Nano*, *Ju Hun Lee*, *Dylan W. Domaille*, *Jennifer N. Cha*, Vol. 6, page 5621-5626, **2012**. Copyright ©2012 American Chemical Society.

the higher DNA-phage loading on the magnetic beads led to more DNA-Au NP binding, which interfered with the diffusion of either the competitive T_{30} strand and/or the liberated DNA-Au NPs. To circumvent these problems, the samples were sonicated briefly to increase the rate and extent of nanoparticle dissociation. With even very brief heating and sonication, in the presence of T_{30}, the DNA-Au NPs were easily dissociated from the phage at all antigen concentrations studied (Figure 3.7). UV-Vis measurements of the supernatants showed that increasing amounts of T15-Au NPs were eluted with increasing amounts of antigen, with a detection limit of 25 fmole antigen (Figure 3.8). Control assays using the incorrect antigen (biotinylated amylase, and biotinylated bovine serum albumin (BSA)), the absence of antigen, or the absence of phage showed almost no color of Au NPs as well as relatively weak or negligible UV-Vis signal in the liberated solutions (Figure 3.9). Alternatively, the UV-Vis absorption values were converted to moles of NPs, and this was used as a method to quantify the moles of antigen in solution (Figure 3.8 c)). The error bars in figure 3.8 c) correspond to the standard deviation of the assay from three independent preparations of the conjugate; thus, the variability inherent in the preparation of each batch is included in the uncertainty of each value.

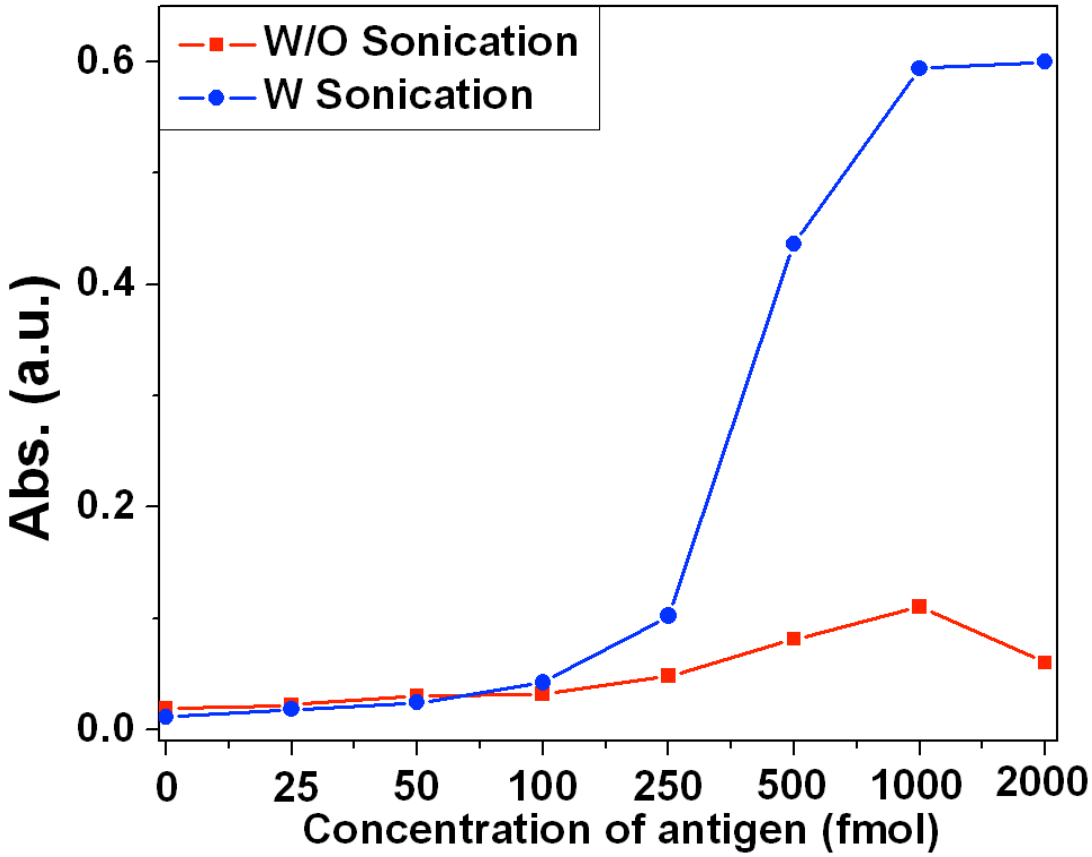

Figure 3.7 UV/Vis absorption value (at 520 nm) with (W) and without (W/O) sonication during assay. Reprinted with permission from *ACS Nano*, *Ju Hun Lee*, *Dylan W. Domaille*, *Jennifer N. Cha*, Vol. 6, page 5621-5626, **2012**. Copyright ©2012 American Chemical Society.

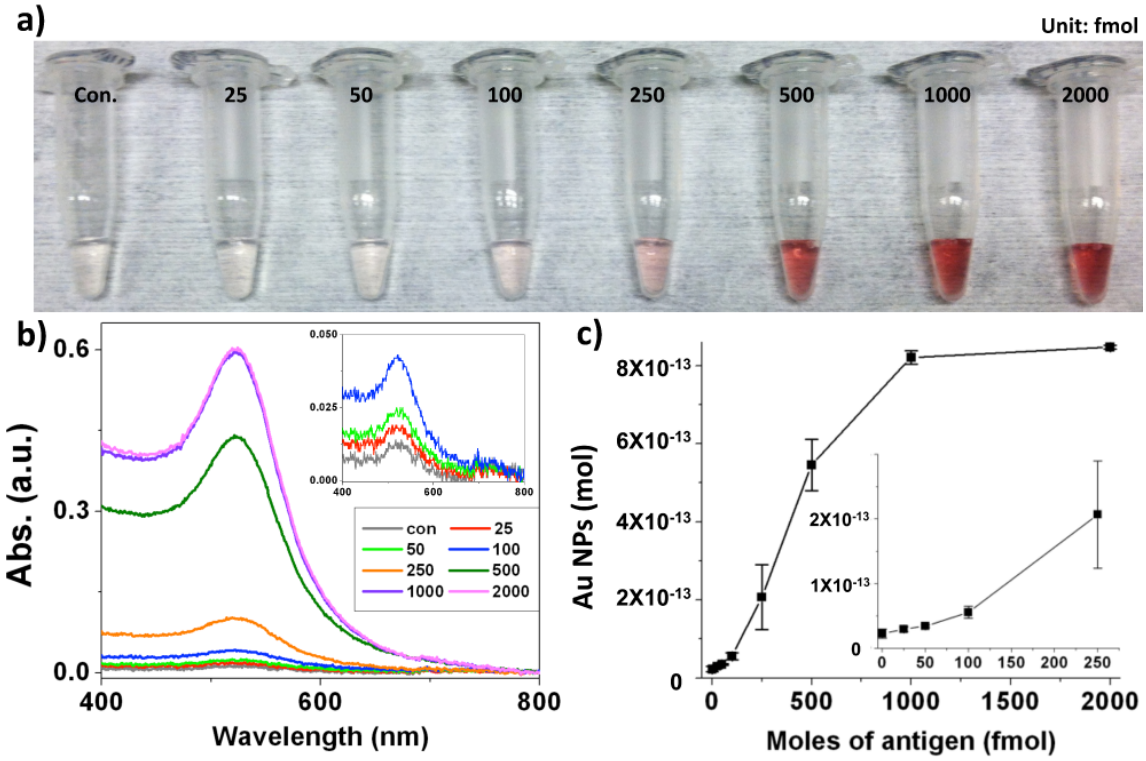

Figure 3.8 a) After NP liberation, the supernatant showed an increase in color with an increase in antigen. (b) UV-Vis spectra of liberated DNA-Au NPs. The inset shows UV-vis spectra of the lower antigen concentration regime. (c) Plot of total number of moles of liberated Au NPs *versus* antigen moles. Inset for lower amount of antigen. Error bars represent correspond to the standard deviation (n=3). Reprinted with permission from *ACS Nano*, *Ju Hun Lee*, *Dylan W. Domaille*, *Jennifer N. Cha*, Vol. 6, page 5621-5626, **2012**. Copyright ©2012 American Chemical Society.

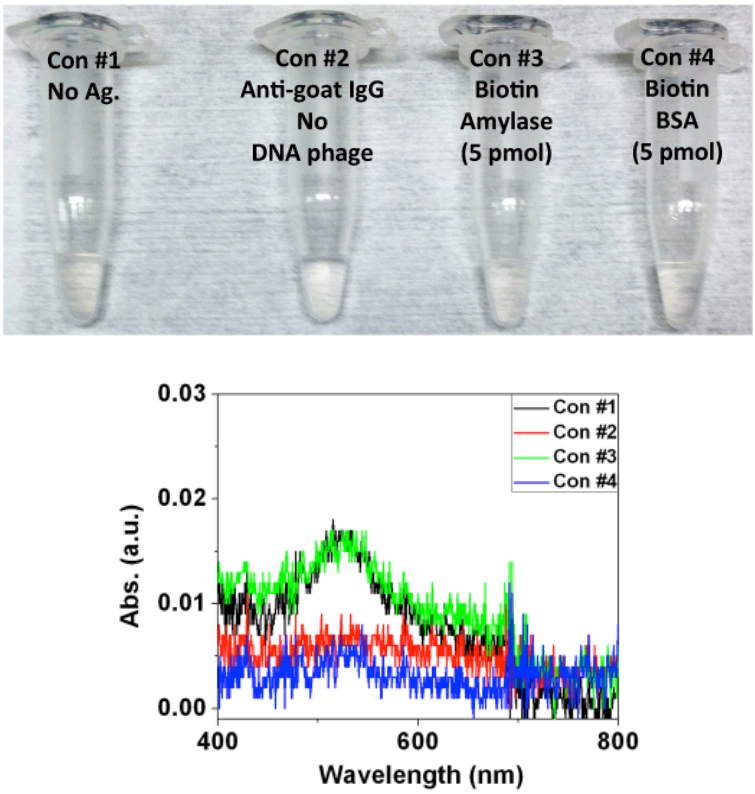

Figure 3.9 After NP liberation, the images of supernatant for control assay, and UV-Vis spectra of liberated DNA-Au NPs. Con. #1: no antigen with DNA phage, Con. #2: 5 pmol of anti-goat IgG, no DNA phage, Con #3: 5 pmol of biotin Amylase with DNA phage, and Con. #4: 5 pmol of biotin BSA with DNA phage. Reprinted with permission from *ACS Nano*, *Ju Hun Lee*, *Dylan W. Domaille*, *Jennifer N. Cha*, Vol. 6, page 5621-5626, **2012**. Copyright ©2012 American Chemical Society.

To identify the DNA sequence on the Au NPs and therefore the antigen, after competitive elution, excess T30 DNA was removed by microcentrifuge filtration. The filtered and concentrated DNA-Au NPs were then adsorbed to printed DNA microarrays, and after washing away excess nanoparticles with saline sodium citrate (SSC) buffer, the T_{15} -Au NPs were easily detected on printed arrays of A_{15} (Figure 3.10). Printed control arrays of T_{15} (Figure 3.10, Con. 1) showed no binding of the T_{15}-Au NPs, demonstrating the high binding specificity and validating the use of DNA microarrays to identify the DNA sequence and, therefore, the antigen in solution.

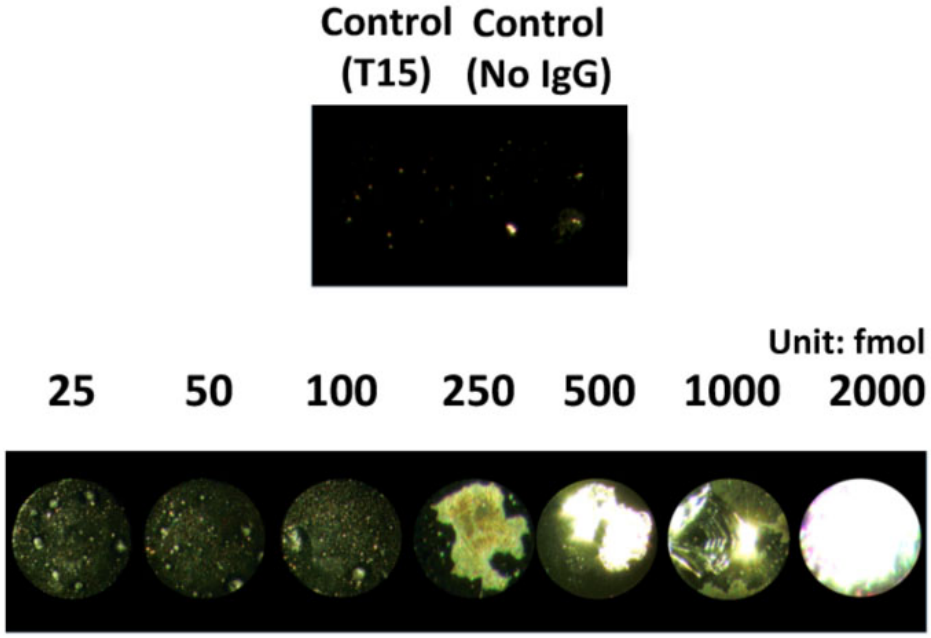

Figure 3.10 Dark field optical microscopy images of micropatterned DNA after hybridization with liberated DNA-Au NP. Reprinted with permission from *ACS Nano*, *Ju Hun Lee*, *Dylan W. Domaille*, *Jennifer N. Cha*, Vol. 6, page 5621-5626, **2012**. Copyright ©2012 American Chemical Society.

3.6 Materials and Experimental Sections

Unless otherwise note, all reagents were obtained from commercial sources and used without further purification. Water used in buffers or in reactions was deionized with a Milli-Q Advantage A-10 water purification system (MilliPore, USA). UV-vis spectra were acquired on a DU 730 spectrophotometer (Beckman Coulter, USA).

3.6.1 Phage Display

Commercial M13 bacteriophage libraries (New England Biolabs) were used for phage display screening. Phage libraries were reacted in solution with 10 pmol of the model antigen, biotinylated rabbit IgG (Sigma Aldrich), captured using streptavidin-coated magnetic Dynabeads, and washed with TBS and Tween-20 (TBST). Bound phage were eluted with 0.2 M glycine-HCl buffer (pH 2.2) with BSA and neutralized with 1 M Tris buffer (pH 9.1). Three rounds of screening were run, at which point individual phage plaques were subjected to DNA sequencing. After three rounds of screening, the consensus peptide sequence DHVRSSSISSLT was obtained. All DNA was purchased from Integrated DNA Technology (Iowa, USA).

3.6.2 DNA Conjugation of Phage

Amine-terminated oligonucleotides (A_{30}) were attached to the phage by first reacting the pVIII protein amine groups with N-succinimidyl 3-(2-pyridyldithio) propionate (SPDP, Thermo scientific). 200 μM SPDP was reacted with 1.5 mg/ml phage in pH 7.4 PBS at RT for 1 hr. Excess SPDP was removed by precipitating the phage with PEG/NaCl solution (20% w/v PEG/2.5 M NaCl). The SPDP-modified phage were next

reacted with excess tri(2-carboxyethyl)phosphine hydrochloride (TCEP-HCl, Thermo scientific) for 30 min to reduce the disulfide bridge. The reaction mixture was desalted twice. Concurrently and in separate vials, amine-terminated oligonucleotides in PBS (pH 7) were reacted with a 10-fold molar excess of sulfo-succinimidyl 4-[N-maleimido-methyl]cyclohexane-1-carboxylate (s-SMCC) at RT for 40 min, and the resulting maleimide-modified DNA was precipitated in ethanol and centrifuged to remove excess s-SMCC. Deprotected thiol-modified phage and maleimide-modified DNA were then reacted at RT in 1X PBS overnight. The DNA-modified phage were purified by centrifuge filtration..

3.6.3 MALDI-TOF for characterization of DNA modified phage

For characterization of SPDP modified phage, 2 μL of the SPDP phage solution (2 mg/mL) was denatured with 3 M guanidine chloride for 5 min at RT, purified with a Millipore C18-ZipTip, and characterized with a Bruker MALDI mass spectrometer. 2, 4, 6-trihydroxyacetophenone monohydrate:ammonium citrate solution (50 mg/mL:12.5 mg/mL in MeOH) was used as the matrix.

3.6.4 DNA Microarrays

Epoxy-coated glass substrates (Arrayit) were used to generate the DNA micro patterns. Amine-terminated DNA (75 μM of oligonucleotides with 25 v/v % Spotting Solution Plus) was printed on the epoxy glass substrate, immobilized for 1~2 hr in a humidified chamber, and baked at 60^{o}C for 30 min. The patterned glass substrates were used immediately or stored under dry and dark conditions at room temperature. The

printed micro A15-patterned glass was successively washed with 0.1% Triton X-100 for 5 min, DI water for 1 min, and blocked (12.5 mM ethanolamine, 0.025% SDS in 25 mM Tris, pH 9.0) at 50^{o}C for 15 min.

3.6.5 DNA-Phage-Based Protein Detection and Identification Assay

600 fmol of DNA-phage was reacted with varying amounts of biotinylated anti-goat IgG. The DNA-phage-antibody complexes were captured with streptavidin-coated magnetic beads (Dynabeads) and washed with 1X PBS containing Tween-20 (0.1%). DNA-conjugated (T_{15}) 10 nm Au NPs were reacted with the A_{30} DNA-phage on magnetic beads in 1X PBS. The supernatants were collected, and the absorption at 520 nm was monitored to determine how many DNA-Au NPs were bound. The bound 10 nm DNA-Au NPs were eluted by competitive elution with DNA (T_{30}) at 95 ^{o}C for 10 min. After heating and cooling, the samples were briefly sonicated. Liberated 10 nm DNA Au NPs were purified with a 100 K MWCO filter to remove remaining T_{30} and to concentrate the solutions. The 10 nm DNA Au NPs were adsorbed to DNA microarrays in 50 mM $MgCl_2$ for 1 h in a humidified chamber. After hybridization, the substrate was washed sequentially with 2X SSC with 0.1% SDS, 2X SSC, and 1X SSC.Carbon-coated copper mesh TEM grids (Electron Microscopy Sciences, Inc., USA) were glow discharged for 40 s at 20 mA to make hydrophilic surfaces, and then 1 μL of samples were dropped on the grid and allowed to air dry. Transmission electron microscope (TEM) images were acquired on a CM 100 TEM (Phillips, USA). For images of M13 bacteriophage, uranyl acetate negative staining methods were used.

3.7 Conclusion

In conclusion, we have demonstrated that M13 bacteriophage can be modified with multiple DNA oligonucleotides to generate a single bioanalytical platform that not only enables the facile and rapid detection of antigens in solution but also provides a system for protein identification. Because every virus is composed of thousands of the coat pVIII protein, none of which is responsible for binding the antigen, it is possible to chemically conjugate distinct moieties onto a single virus scaffold that play dual roles in protein sensing and identification. Interactions between the DNA-phage and DNA-Au NPs led to observation of immediate color changes, which can first be used optically or spectroscopically to detect the presence of an antigen in solution. In addition, the same DNA-phage platform can be used to identify the types of antigens in solution by competitively eluting the DNA-Au NPs from the phage and adsorbing the particles to printed DNA microarrays. Because each phage recognizes 1-2 antigens yet can bind to hundreds of DNA-Au NPs through the pendant DNA chains on the virus' pVIII proteins, these sensors are extremely sensitive, easy to use, can provide both protein detection and identification in an extremely high throughput manner, and are ultimately inexpensive to manufacture. Future work will involve studying the use of DNA-phage for multiplexing with clinically relevant biomarkers.

3.7 Acknowledgements

This chapter, in full, is a reprinted of the material as it appears in *ACS Nano*, *Ju Hun Lee*, *Dylan W. Domaille*, *Jennifer N. Cha*, Vol. 6, page 5621-5626, **2012**. Copyright ©2012 American Chemical Society. The dissertation author was the primary investigator and author of this paper.

3.9 References

1. Siegel, R.; Ward, E.; Brawley, O.; Jemal, A. Cancer Statistics, 2011, The Impact of Eliminating Socioeconomic and Racial Disparities on Premature Cancer Deaths. *CA Cancer J. Clin.* **2011**, 61, 212-236.

2. Torthill, I. E. Biosensors for Cancer Markers Diagnosis. *Semi. Cell Dev. Biol.* **2009**, 20, 55–62.

3. Peeling, R. W; Holmes, K. K.; Mabey, D; Ronald, A. Rapid Tests for Sexually Transmitted Infections (STIs): the Way Forward. *Sex. Transm. Infect.* **2006**, 82, v1-v6.

4. Xia, F.; Zuo, X.; Yang, R.; Xiao, Y.; Kang, D.; Vallée-Bélisleb, A.; Gong, X.; Yuen, J. D.; Hsu, B. B. Y.; Heeger, A. J. *et al.* Colorimetric Detection of DNA, Small Molecules, Proteins, and Ions Using Unmodified Gold Nanoparticles and Conjugated Polyelectrolytes. *Proc. Natl. Acad. Sci.* **2010**, 107, 10837-10841.

5. Martinez, A.W.; Phillips, S.T.; Butte, M. J.; Whitesides, G. M. Patterned Paper as a Platform for Inexpensive, Low-Volume, Portable Bioassays. *Angew. Chem. Int. Ed.* **2007**, 46, 1318-1320.

6. Martinez, A.W.; Phillips, S.T.; Whitesides, G.M.; Carrilho, E. Diagnostics for the Developing World: Microfluidic Paper-Based Analytical Devices. *Anal. Chem.* **2010**, 82, 3-10.

7. Rosi, N. L.; Mirkin, C. A. Nanostructures in Biodiagnostics. *Chem. Rev.* **2005**, 105, 1547-1562.

8. Hahm, J.; Lieber, C. M. Direct Ultrasensitive Electrical Detection of DNA and DNA Sequence Variations Using Nanowire Nanosensors. *Nano Lett.* **2004**, 4, 51-54.

9. Kim, D.; Daniel, W. L.; Mirkin, C. A. Microarray-Based Multiplexed Scanometric Immunoassay for Protein Cancer Markers Using Gold Nanoparticle Probes. *Anal. Chem.* **2009**, 81, 9183-9187.

10. Xiang, Y.; Xie, M.; Bash, R.; Chen, J. J. L.; Wang, J. Ultrasensitive Label-Free Aptamer- Based Electronic Detection. *Angew. Chem. Int. Ed.* **2007**, 119, 9212-9214.

11. Borisov, S. M.; Wolfbeis, O. S. Optical Biosensors, *Chem. Rev.* **2008,** 108, 423-461.

12. Medintz, I. L; Clapp, A. R.; Mattoussi, H.; Goldman, E. R.; Fisher, B.; Mauro, J. M. Self-Assembled Nanoscale Biosensors Based on Quantum Dot FRET Donors. *Nat. Mater.* **2003**, 2, 630-638.

13. Cui, Y.; Wei, Q.; Park, H.; Lieber, C. M. Nanowire Nanosensors for Highly Sensitive and Selective Detection of Biological and Chemical Species. *Science* **2001**, 293, 1289-1292

14. Mateu M. G. Virus Engineering: Functionalization and Stabilization. *Protein Eng. Des. Sel.* **2011**, 24, 53-63.

15. Yildiz, I.; Shukla, S.; Steinmetz, N. F. Applications of Viral Nanoparticles in Medicine. *Curr. Opin. Biotech.* **2011**, 22, 901-908.

16. Ngweniform, P.; Abbineni, G.; Cao, B.; Mao, C. Self-Assembly of Drug-Loaded Liposomes on Genetically Engineered Target-Recognizing M13 Phage: A Novel Nanocarrier for Targeted Drug Delivery. *Small* **2009**, 5, 1963-1969.

17. Mao, C.; Liu, A.; Cao, B. Virus-Based Chemical and Biological Sensing. *Angew. Chem. Int. Ed.* **2009**, 48, 6790-6810.

18. Yacoby, I.; Bar, H.; Benhar, I. Targeted Drug-Carrying Bacteriophages as Antibacterial Nanomedicines. *Antimicrob. Agents Chemother.* **2007**, 51, 2156-2163.

19. Tong, G. J.; Hsiao, S. C.; Carrico, Z. M.; Francis, M. B. Viral Capsid DNA Aptamer Conjugates as Multivalent Cell-Targeting Vehicles. *J. Am. Chem. Soc.* **2009**, 131, 11174–11178.

20. Robertson, K. L.; Soto, C. M.; Archer, M. J.; Odoemene, O.; Liu, J. L. Engineered T4 Viral Nanoparticles for Cellular Imaging and Flow Cytometry, *Bioconjugate Chem.* **2011**, 22, 595-604.

21. Li, K; Chen, Y.; Li, S.; Nguyen, H. G.; Niu, Z.; You, S.; Mello, C. M.; Lu, X.; Wang, Q. Chemical Modification of M13 Bacteriophage and Its Application in Cancer Cell Imaging. *Bioconjugate Chem.* **2010**, 21, 1369-1377.

22. Lee, J. H.; Cha, J. N. Amplified Protein Detection through Visible Plasmon Shifts in Gold Nanocrystal Solutions from Bacteriophage Platforms. *Anal. Chem.* **2011**, 83, 3516-3519.

23. Goldman, E. R.; Pazirandeh, M. P.; Mauro, J. M.; King, K. D.; Frey, J. C.; Anderson, G. P. Phage-displayed Peptides as Biosensor Reagents. *J. Mol. Recognit.* **2000**, 13, 382-387.

24. Petrenko, V. A.; Vodyanoy, V. J. Phage Display for Detection of Biological Threat Agents. *J. Microbiol. Meth.* **2003**, 53, 253-262.

25. Arter, J. A.; Taggart, D. K.; Mcintire, T. M.; Penner, R. M.; Weiss, G. A. Virus-PEDOT Nanowires for Biosensing. *Nano Lett.* **2010**, 10, 4858-4862.

26. Smith, G. P.; Petrenko, V. A. Phage Display. *Chem. Rev.* **1997**, 97, 391-410.

27. Barbas III, C. F.; Burton, D. R.; Scott, J. K.; Silverman, G. J. *In Phage Display. A Laboratory Manual*; Cold Spring Harbor Laboratory Press: New York, 2001; pp 1.1–16.

28. Kehoe, J. W.; Kay, B. K. Filamentous Phage Display in the New Millennium. *Chem. Rev.* **2005**, 105, 4056-4072.

29. Hemminga, M. A.; Vos, W. L.; Nazarov, P. V.; Koehorst, R. B. M.; Wolfs, C. J. A. M.; Spruijt, R. B.; Stopar. D. Viruses: Incredible Nanomachines. New Advances With Filamentous Phages. *Eur. Biophys. J*. **2010**, 39, 541–550.

30. Stoeva, S. I.; Lee, J.; Smith, J. E.; Rosen, S. T.; Mirkin, C. A. Multiplexed Detection of Protein Cancer Markers with Biobarcoded Nanoparticle Probes. *J. Am. Chem. Soc.* **2006**, 128, 8378-8379.

31. A. J. Haes, R. P. V. Duyne, *Anal. Bioanal. Chem.* **2004**, 379, 920-930.

32. K. A. Willets, R. P. V. Duyne. *Annu. Rev. Phys. Chem.* **2007**, 58, 267-297.

33. Geißler, D.; Charbonniere, L. J.; Ziessel, R. F.; Butlin, N. G.; Löhmannsröben, H.; Hildebrandt, N. Quantum Dot Biosensors for Ultrasensitive Multiplexed Diagnostics. *Angew. Chem. Int. Ed.* **2010**, 49, 1396-1401.

34. Bailey, R. C.; Kwong, G. A.; Radu, C. G.; Witte, O. N.; Heath, J. R. DNA-Encoded Antibody Libraries: A Unified Platform for Multiplexed Cell Sorting and Detection of Genes and Proteins. *J. Am. Chem. Soc.* **2007**, 129, 1959-1967.

35. Hermanson, G. T. *Bioconjugate Techniques 2nd Eds.*; Academic Press: San Diego, 2008; pp 183-184

CHAPTER 4: Chemically Modified DNA Phage via aldehyde/ hydrazine and Surface Enhanced Raman Spectroscopy Sensor with Raman Active Gold Silver Core Shell Nanoparticles

"Live as if you were to die tomorrow. Learn as if you were to live forever."

- Mahatma Gandhi

4.1 Introduction

New diagnostics systems that can sense for particular biomarkers remain in critical need for early stage disease detection and prevention.[1-3] For biomedical applications, the naturally existing M13 bacteriophage has shown promising use as materials for therapy and sensing. The phage are resistant to changed temperatures, high salt concentration, acidic pH, and chaotropic agents [4, 5] and they are non-toxic and do not cause an immune response in humans.[6] Phage are also easily producible in *E. coli* cultures, are compatible with phage display technologies, and possess unique biochemical structural features that make them ideal candidates for chemical or genetic modification.[7-9] Due to these characteristics, M13 viruses have been used as drug delivery carriers,[10, 11] scaffolds for in vitro and in vivo imaging,[4, 12-14] and biosensors.[5, 15-17] To this end, we have recently demonstrated that chemically modified DNA-M13 bacteriophage can be used as an all-in-one bioanalytical platform

that enables both facile and rapid detection of antigens in solution and provides modalities for protein identification.[18-20]

Due to their unique optical, electronic or magnetic properties, nanomaterials have been extensively studied for generating signals in biosensor applications.[1, 2, 21-29] Among the many different detection methods, sensing strategies based on Surface Enhanced Raman Spectroscopy (SERS) from metallic nanostructures has been a particularly promising approach. The Raman signal is greatly enhanced when molecules are brought near the surface of noble metals in a variety of morphologies; the largest effects are seen from plasmonic coupling arising from nanometer gap junctions.[30-39] In addition to being very sensitive, SERS can be used as a molecular fingerprinting technique due to the detailed spectrum consisting of narrow lines, which allows resolution of spectral features within the simultaneous detection of different probes,[33, 40] thus providing a means to identify and measure multiple biomarkers to increase diagnostic accuracy through multiplexed analysis.[41-43] Because SERS signal depends greatly on the distance between the molecule and the metal surface, control over the position of the nanoparticle and the Raman active dye is crucial for generating large, reproducible SERS signals.[44-47] To resolve problems arising from inconsistent enhancement factors and uncertainty in the SERS signal caused by structural variation, researchers have developed a new class of nanoscale SERS probes including DNA-tethered nanoparticles or Raman active dye embedded nanostructures.[44-47]

In this chapter, I report an advanced biosensor system that combines DNA-conjugated SERS-active Au@Ag core/shell nanoparticles with DNA-modified M13 bacteriophage. By combining the use of filamentous phage with DNA interactions, high

loadings of SERS particles can be captured to a single phage leading to exponential increases in Raman intensity. While SERS has been used for detection previously, amplifying SERS signals through specific biomolecular interactions and taking advantage of the large macromolecular structure of the antigen-binding agent have not been demonstrated. These detection systems exhibit a dramatic signal enhancement in the presence of a target protein and have high batch-to-batch reproducibility, leading to a rapid, reliable, and high-throughput biosensing system with a favorable cost-to-benefit ratio.

4.2 Theoretical background of Surface Enhanced Raman Spectroscopy

Since Van Duyne and Jeanmaire's and Albrecht and Creighton's initial discovery of Raman enhancement on rough silver electrodes,[32] surface enhanced Raman spectroscopy (SERS) has remarkably progressed and used for single molecule detection. Figure 4.1 represents a comparison in signal intensity from normal Raman spectroscopy versus the observed enhanced Raman spectroscopy at surfaces. In normal Raman spectroscopy, the total Stokes Raman signal I_{NRS} is proportional to σ^{R}_{free} (Raman cross section), $I(\nu_L)$ (excitation laser intensity), and N (number of molecules in the probed volume) (Figure 4.1, left).[32] Because Raman cross sections are extremely small such as 10^{-31} and 10^{-29} cm^2/molecule, at least $\sim 10^8$ molecules are necessary to generate a measurable normal Raman scattering signal. [32, 34] On the other hand, in SERS (Figure 1, right), the molecules are attached to metal nanostructures or aggregated metal. The surface-enhanced Stokes Raman signal I_{SERS} is proportional to σ^{R}_{ads} (Raman cross section of the adsorbed molecule), $I(\nu_L)$ (the excitation laser intensity) and N´ (number of molecules which are involved in the SERS process).[32] N´ can be smaller than the number of molecules in the probed volume N. As generally agreed, multiple factors were attributed for SERS enhancement and two effects have been considered key factors and are expressed in a formula (1)[34]:

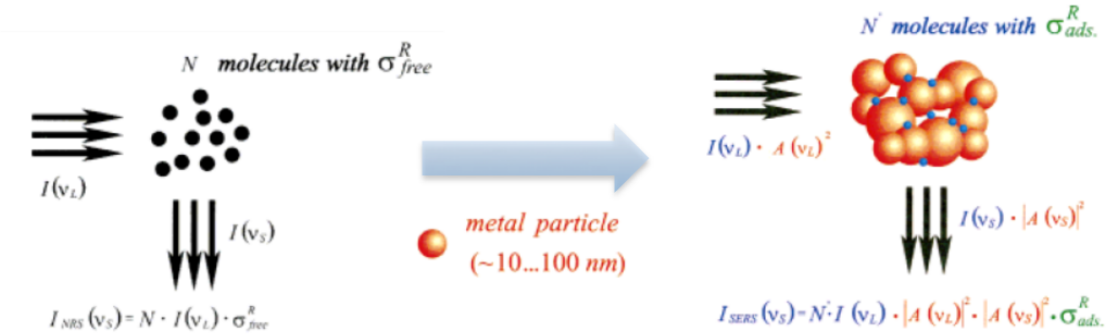

Figure 4.1 Comparison of "normal" (left) and surface enhanced (right) Raman scattering. In Figure 1a (left), the conversion of laser light I_L into Stokes scattered light I_{NRS} is proportional to the Raman cross section σ^R_{free}, the excitation laser intensity I_L, and the number of target molecules N in the probed volume. Figure 1b (right) displays a schematic of a SERS experiment. σ^R_{ads} describes the increased Raman cross section of the adsorbed molecule ("chemical" enhancement); $A(\nu_L)$ and $A(\nu_S)$ are the field enhancement factors at the laser and Stokes frequency, respectively; N´ is the number of molecules involved in the SERS process. Reprinted with permission from ref 32 (K. Kneipp et al *Chem. Rev.* **1999**, 99, 2957-2975). Copyright ©1999 American Chemical Society.

(1) The scattering occur in the enhanced local optical fields of near the metallic nanostructures or/and between the nanogap junction of nanostructures. (electromagnetic field enhancement)

(2) A molecule in contact with noble nanostructures exhibits a 'new Raman process' at a cross section larger than the normal Raman cross section of a free molecule. (chemical or electronic enhancement, first-layer effect).

$$P^{SERS}(\nu_s) = N' \sigma^{R}_{ads} |A(\nu_L)|^2 |A(\nu_S)|^2 I(\nu_L) \quad (1)$$

$A(\nu_L)$ and $A(\nu_S)$ indicate enhancement factors for the laser and for the Raman scattered field, respectively. σ^{R}_{ads} expresses an increased cross section of the new Raman process of the adsorbed molecule. N′ is the number of molecules which are involved in the SERS process and would be smaller than the number of molecules in the probed volume N. [34]

4.8.1 Electromagnetic Field Enhancement

$$E_M = E_0 + E_{sp} \quad (2)$$

If the radius of the noble metal nanostructure is small enough (radius/wavelength of light ≤ 0.05, Rayleigh limit), a molecule with distance 'd' from nanostructure is exposed to E_M

(formula (2)). In (2), E_0 expresses incoming field, E_{sp} represents the field of a dipole induced in the metal nano-sphere like equation (3).[34]

$$E_{sp} = r^3 \frac{\varepsilon - \varepsilon_0}{\varepsilon + 2\varepsilon_0} E_0 \frac{1}{(r+d)^3} \quad (3)$$

The field enhancement factor A(ν) indicates the ratio of the field at the position ('d' was the distance between a molecules and surface of nanostructures) of the molecule and the incoming field, and thus, would be expressed in formula (4).

$$A(\nu) = \frac{E_M(\nu)}{E_0(\nu)} \sim \frac{\varepsilon - \varepsilon_0}{\varepsilon + 2\varepsilon_0} \left(\frac{r}{r+d}\right)^3 \quad (4)$$

The enhancement factor (A(ν)) shows the maximum value when the real part of ε(ν) is $-2\varepsilon_0$. In addition, in order to induce strong electromagnetic enhancement, the imaginary part of the dielectric constant should be small, which indicates the condition about the resonant excitation of surface plasmons of the metal sphere.[34] Therefore, if the surface plasmons of the metal sphere are in resonance mode, the scattered Stokes or anti-Stokes field is enhanced. With the enhancement effect for the laser and the Stokes field, the electro-magnetic enhancement factor for the Stokes signal power $G(\nu_s)$ would be expressed as formula (5):

$$G_{em}(\nu_s) = |A(\nu_L)|^2 |A(\nu_s)|^2 \sim \left|\frac{\varepsilon(\nu_L)-\varepsilon_0}{\varepsilon(\nu_L)+2\varepsilon_0}\right|^2 \left|\frac{\varepsilon(\nu_s)-\varepsilon_0}{\varepsilon(\nu_s)+2\varepsilon_0}\right|^2 \left(\frac{r}{r+d}\right)^{12} \quad (5)$$

This equation was derived based on a very simple model, but includes the important variables to describe the relation between electromagnetic SERS enhancement and incident electromagnetic fields. In equation (5), the enhancement factor of SERS is proportional to the fourth power of the local field of the noble metal nanostructures, so when the excitation and the scattered fields are in resonance with the surface plasmons, the enhancement scales to the 10^5 in the case of small sphere. Moreover, the electromagnetic enhancement factor in SERS system strongly decreases with increased distance by the decrease of field of a dipole over the distance $(1/d)^3$ to the fourth power, resulting in $(1/d)^{12}$.[34]

4.8.2 Chemical or Electronic Enhancement

Several different mechanisms are considered as the origins of a chemical or electronic SERS enhancement effect. Chemical or electronic enhancements are called 'the first-layer effect' because the mechanisms require direct contact between molecule and surface of metal nanostructures. The first hypothesis about enhancement is caused by the formation of an adsorbate-surface complex through electronic coupling between molecule and metal, lead to an increased Raman cross section of the adsorbed molecules in the complex. Another hypotheses about the mechanism of electronic enhancement is that it is induced by a resonance Raman effect due to the shifted and broadened electronic levels in the adsorbed molecule.

(1) Raman resonant from the highest occupied molecular orbital (HOMO) to the lowest unoccupied molecular orbital (LUMO) within adsorbate (molecule)

(2) Raman resonant from HOMO in molecule to Fermi level of metal (between molecule and metal)

(3) Raman resonant from Fermi level of metal to LUMO in molecule (between molecule and metal)

In typical energy level of molecule-metal system, the energy levels of HOMO, and LUMO are approximately symmetric relative to the Fermi level of the metal, and three possible resonant Raman (electronic paths) would be occurred as lists above. In addition, depending on the shift of Fermi level, resonance conditions for paths (2), and (3) could be changed, called potential-dependent SERS enhancement.[34]

Another first-layer SERS effect is caused by dynamical charge transfer, which is assumed followed four steps:[34]

(1) photon annihilation, excitation of an electron into a hot-electron state.

(2) transfer of the hot electron into the LUMO of the molecule.

(3) transfer of the hot electron from the LUMO (with changed normal coordinates of some internal molecular vibrations) back to the metal.

(4) return of the electron to its initial state and Stokes photon creation.

4.3 Chemical Strategy to Modification of M13 Bacteriophage

This section, in part, is a reprint of the material as it appears in *Chem. Commun.*, 2013, 49, 1759-1761. *Dylan W Domaille, Ju Hun Lee*, *Jennifer N. Cha*. The dissertation author was the investigator and author of this paper. Reproduced from ref 20 with permission of The Royal Society of Chemistry.

Phage display against the model protein anti-goat rabbit immunoglobulin (IgG) provided M13 bacteriophage expressing five copies of the 12-mer peptide (DHVRSSSISSLT) sequence on the p3 proteins located on the end of the phage.[18] Previously, we reported the use of 1-ethyl-3-(3-dimethylaminopropyl)carbodiimide (EDC) and succinimidyl-3-(2-pyridyldithio)propionate (SPDP) /sulfosuccinimidyl-4-(N-maleimido-methyl)cyclohexane-1-carboxylate (s-SMCC) for conjugating DNA oligonucleotides to the p8 major capsid proteins on the virus.[18, 19] However, undesired intra- and inter-virus crosslinking and low DNA conjugation yields led us to use aldehyde-functionalized phage and hydrazine-terminated DNA instead. In doing so, we were able to take advantage of the high chemoselectivity of acyl hydrazone formation under mild conditions without considerably affecting the biological reactivity of the p3 proteins.[20, 48] The chemical strategy outlined in Figure 4.2. Benzylaldehyde groups were first introduced on the phage by reacting the nucleophilic amines (*i.e.*, N-terminus amine and lysine side-chains) of the p8 proteins with 4-formyl succinimidyl benzoate. Because the phage coat has 2700 copies of the p8 protein, a 50-amino acid peptide with three buried lysine residues and a solvent accessible N-terminus,

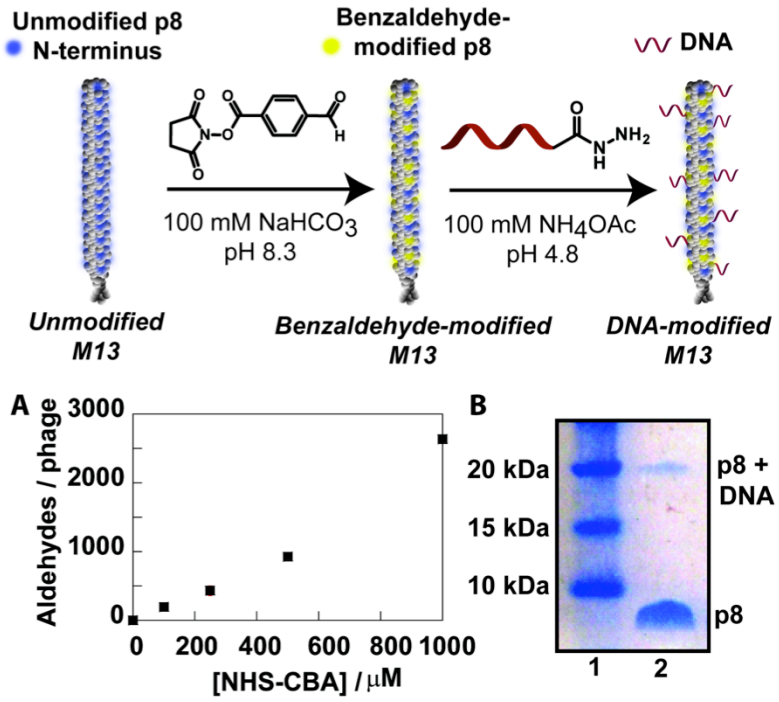

Figure 4.2 M13 bacteriophage is treated with 4-formyl succinimidyl benzoate (NHS-CBA) to install benzaldehyde groups on the phage coat p8 protein. Acyl hydrazide derivatized DNA is then reacted with the benzaldehyde-derivatized phage to conjugate DNA to the phage through hydrazone linkages. (A) Dose–response curve of the M13 bacteriophage with NHS-CBA. Shown are values for 0, 0.1, 0.25, 0.5, and 1.0 mM NHS-CBA. Error bars represent standard deviation (n = 3). (B) SDS-PAGE gel that shows the conjugation of 11.1 kDa DNA to the p8 protein. Reproduced from ref 20 with permission of The Royal Society of Chemistry.

the phage coat has several thousand nucleophilic amines that are readily conjugated to small-molecule NHS-esters. Previous work has established that the p8 N-terminus is preferentially targeted by NHS-esters because of its higher solvent accessibility and slightly lower pKa value compared to lysine side chains. Matrix-assisted laser desorption ionization time-of-flight (MALDI-TOF) mass spectrometry analysis indicated that the number of aldehydes per phage could be altered by varying the amount of NHS-ester in the reaction; between 200 and 2650 benzaldehyde moieties could be installed per phage with 0.1–1 mM NHS-CBA (Figure 4.2 a). Single p8 modifications were observed up to ca. 500 μM NHS-CBA, at which point double modifications began to occur. No chromatography was necessary to purify the phage-aldehyde as the modified viruses could simply be precipitated with PEG and NaCl. With the aldehyde-derivatized phage in hand, we next sought to conjugate the hydrazide-derivatized DNA to the phage coat whilemonitoring by sodium dodecyl sulfate polyacrylamide gel electrophoresis (SDS-PAGE). A brief screen of conditions revealed that 1.0 mg mL^{-1} phage-benzaldehyde in 100 mM NH4OAc buffer, pH 4.8, with 100 mM DNA for 24 h at room temperature provided excellent conjugation to the phage (Figure 4.2 b). Under these conditions, we were able to install several hundred DNA per M13 bacteriophage. Control experiments established that both the phage-aldehyde and hydrazide-derivatized DNA are necessary for DNA conjugation. The reaction required neither inorganic catalysts nor synthetically elaborate precursors, and the conditions were mild enough that the integrity of both the phage and the DNA is preserved. The degree of DNA incorporation depends on both the number of aldehydes on the phage and the concentration of DNA in the reaction. Fig. 2a shows that higher concentrations of DNA led to higher DNA loading on the phage. We

could also readily incorporate DNA that ranged in size from 3.2 kDa to 10.3 kDa (Figure 4.3b). A phage with ca. 800 aldehyde moieties could be heavily loaded with DNA, irrespective of DNA size. Densitometry indicated that between 460–675 DNA per phage could be incorporated under these conditions, which corresponds to 58–85% conversion of the phage-aldehydes to phage–DNA hydrazones (Figure 4.3c). Having established chemically conjugation method, for followed diagnosis experiments, we consistently observed and synthesized DNA-phage with 6.4 kDa DNA strands (MW: 6361 Da). The resulting DNA phage conjugates were characterized by densitometric, and showed that 315 ± 41 DNA strands could be conjugated to the M13 bacteriophage.

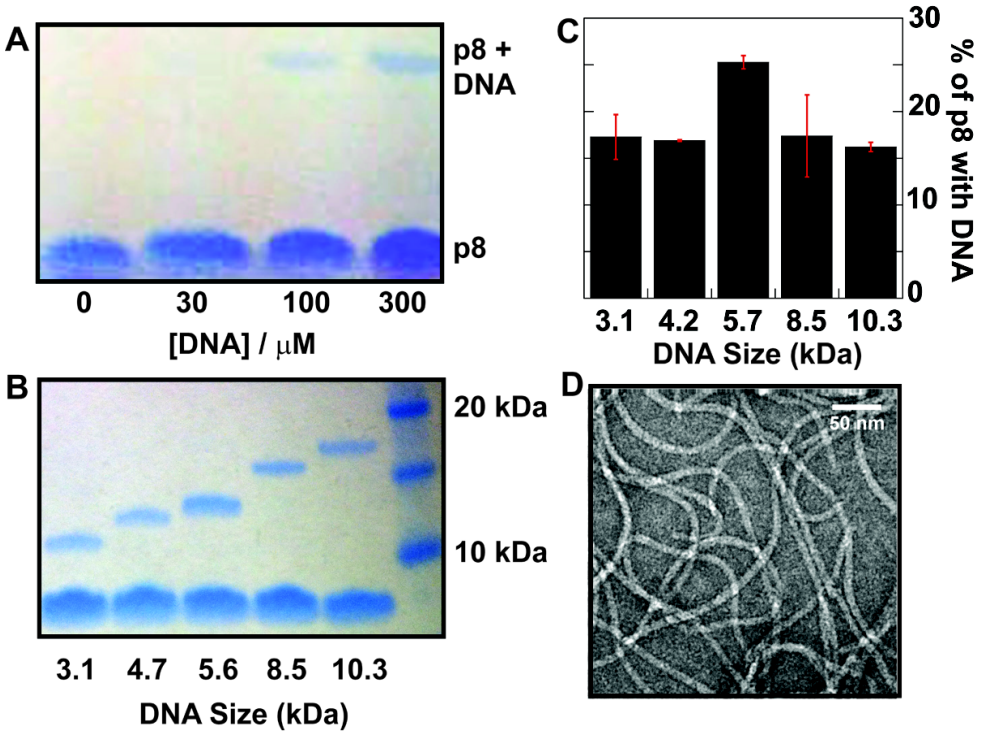

Figure 4.3 Analysis of the efficiency with which DNA is incorporated and verification that the phage is intact after DNA modification. (A) Effect of DNA concentration on DNA loading. The conjugation was carried out at 1.0 mg mL^{-1} phage aldehyde in 100 mM NH_4OAc, pH 4.8 buffer, with the indicated concentration of DNA for 24 h. (B) Conjugation of 3.1–10.3 kDa DNA. The same conditions were used as in (A), except that the DNA concentration was fixed at 100 mM. (C) Quantification of the DNA incorporation with respect to DNA size. Error bars represent standard deviation. (D) TEM image of the phage–DNA conjugate, which shows that the integrity of the phage is preserved. Scale bar is 50 nm. Reproduced from ref 20 with permission of The Royal Society of Chemistry.

4.4 Synthesis of Raman Active Gold Silver Core Shell Nanoparticles

Next, we attempted to bind SERS nanoparticles to the DNA-conjugated phage. In order to optimize the detection scheme, we first sought to produce DNA conjugated SERS particle probes that showed significant enhancement factor (EF) values. Recently, Lim *et al.* reported the synthesis of SERS active nanostuctures with narrow distributions of large EF values,[45] in which 20 nm gold nanoparticles were decorated with thiolated DNA labeled with Raman-active Cy3 dye. In order to increase the number of dyes per particle, we decided to alter their synthesis by directly conjugating the Raman-active molecules to the Au surface first, followed by addition of thiolated DNA strands. Thiolated Cy3 was prepared (Figure 4.4) and conjugated to 20 nm gold nanoparticles by reacting 300-fold molar excess of thiolated-Cy3 with the particles overnight. Next, the Cy3 20nm Au NPs were reacted with thiolated DNA by salt aging.[49] To measure the number of bound Cy3 to the Au NPs, the nanoparticles were reacted with DTT to liberate the Cy3 which was quantified by UV Vis absorbance. From this it was determined that the average number of Cy3 per particle was 225 ± 25. Next, to produce active SERS reporters the DNA-Cy3 conjugated Au nanocrystals were reacted with poly(N-vinylpyrrolidone) (PVP), sodium L-ascorbate, and silver nitrate to form a silver shell around each Au NP.[40, 50-53] As previously reported, 300 mM NaCl provided optimum uniform silver shells.[50, 51] In addition, because the exposed silver surfaces were later found to induce nonspecific binding, short DNA (T_{10}) strands were added to the DNA-Cy3-Au@Ag NPs to passivate the surface. While it usually is difficult modify the surface of silver nanoparticles with DNA due to their limited stability in salt concentration and

poor cooperative binding,[54] we were able to conjugate thiolated T_{10} to the DNA-Cy3-Au@Ag NPs through salt aging (Figure 4.5 a).

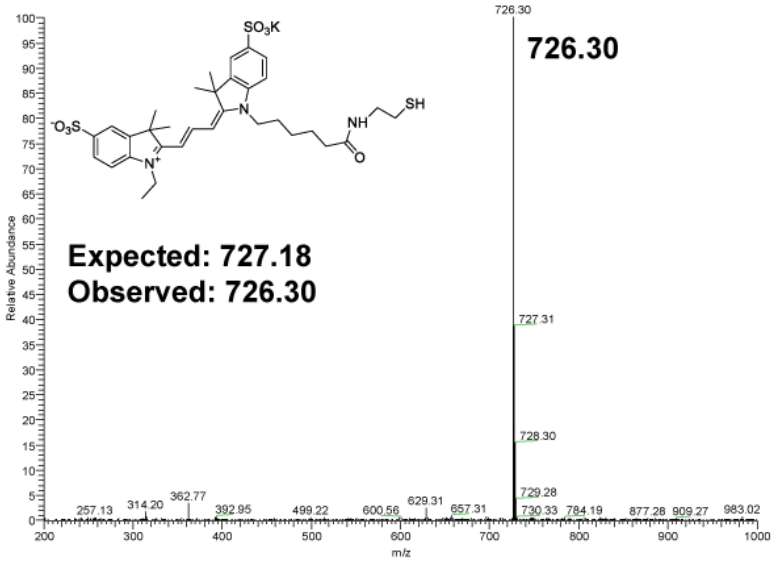

Figure 4.4 Electrospray ionization mass spectrometry (ESI MS) of thiolated Cy3. Reproduced from Adv. Func. Materials, *Ju Hun Lee*, *Phyllis F. Xu*, *Dylan W. Domaille*, *Chulmin Choi*, *Sungho Jin*, *Jennifer N. Cha*, *Submitted*.

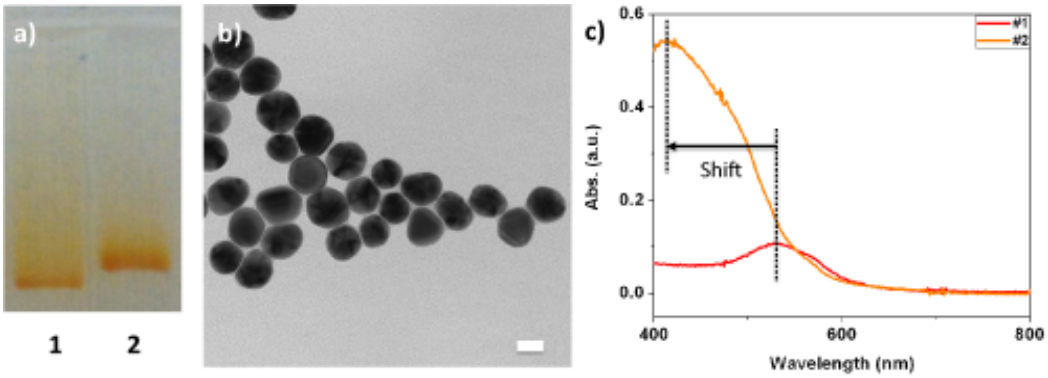

Figure 4.5 a) 1% agarose gel results after T_{10} passivattion on DNA-Au@Ag nanoparticles. 1) DNA-Au@Ag NPs, 2) T_{10} passivated DNA-Au@Ag NPs. (130 V constant, 30 min.). b) TEM images of T_{10}-passivated DNA-Cy3-Au@Ag NPs (scale bar = 20 nm), c) UV vis spectra of DNA-Cy3-Au NPs, and DNA-Cy3-Au@Ag NPs. #1: UV vis spectra of DNA-Cy3-Au NPs, #2: UV vis spectra of DNA-Cy3-Au@Ag NPs. The maximum absorbance peak was shifted from ~520 nm to ~410 nm. Reproduced from Adv. Func. Materials, *Ju Hun Lee*, *Phyllis F. Xu*, *Dylan W. Domaille*, *Chulmin Choi*, *Sungho Jin*, *Jennifer N. Cha*, *Submitted*.

4.5 Characteristics of Raman Active Nnaoparticles

The synthesized DNA-Cy3-Au@Ag NPs were characterized by transmission electron microscopy (TEM) and UV-Vis spectroscopy (Figure 4.5 b)). As shown in Figure 4.6, TEM imaging clearly showed the core gold nanoparticles with a uniform silver shell coating. The average shell layer thickness of the silver on the gold core nanoparticles was found to be 10 ± 2 nm (n = 50). The UV-Vis spectrum showed that the maximum plasmon band had shifted from ~520 nm to ~410 nm without any secondary surface plasmon resonance modes (Figure 4.5 c)), indicating that uniform silver shells were formed on the gold without any directional or asymmetric growth. We next measured the SERS response of the synthesized DNA-Cy3-Au@Ag NPs. To calibrate the Raman intensity as a function of the number of Au@Ag nanoparticles, as shown in Figure 4.7, we first photolithographically fabricated an array of Si pillars 4 μm in diameter and 1 μm in height to match the laser spot size of the micro-Raman. These micropatterned substrates were then made hydrophilic through UV-ozone treatment, and varying concentrations of the DNA-Cy3-Au@Ag nanoparticles were absorbed to the pillar arrays in 150 mM NaCl. After counting the number of nanoparticles on individual pillars in each sample by scanning electron microscopy (SEM), micro-Raman analysis was performed. For the Raman spectroscopy measurements, we measured the fingerprint peak region of Cy3 at 1580 cm^{-1} using laser excitations of 543.5 nm and 632.8 nm (He-Ne laser) (=130 μW, accumulation time: 30 sec) and the Raman intensity at 1580 cm^{-1} as a function of number of nanoparticles on the pillars was determined using both laser lines (Figure 4.8).

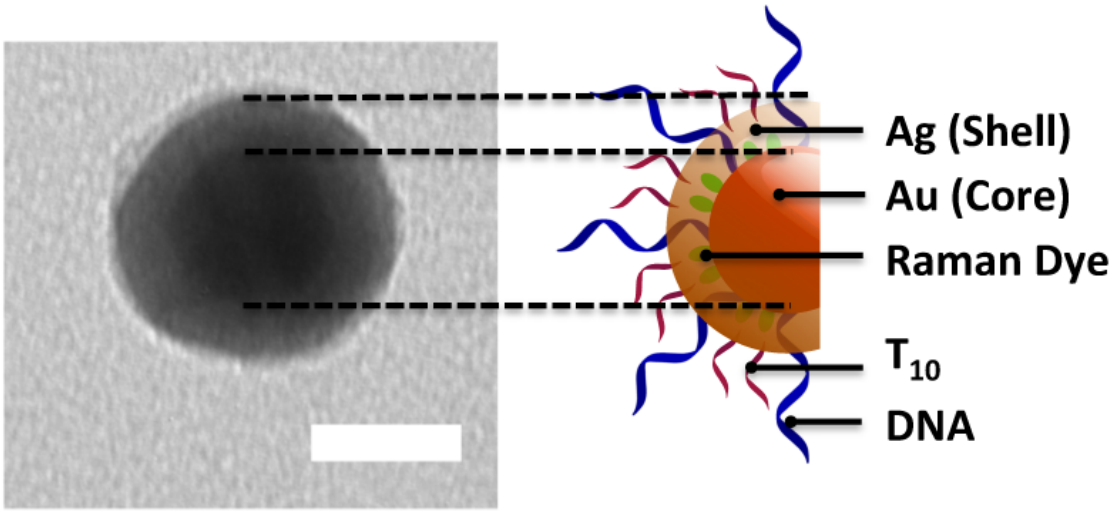

Figure 4.6 TEM image of T_{10} passivated DNA-Cy3-Au@Ag nanoparticles and nanoparticle schematic (Scale bar = 20 nm). Reproduced from Adv. Func. Materials, *Ju Hun Lee*, *Phyllis F. Xu*, *Dylan W. Domaille*, *Chulmin Choi*, *Sungho Jin*, *Jennifer N. Cha*, *Submitted*.

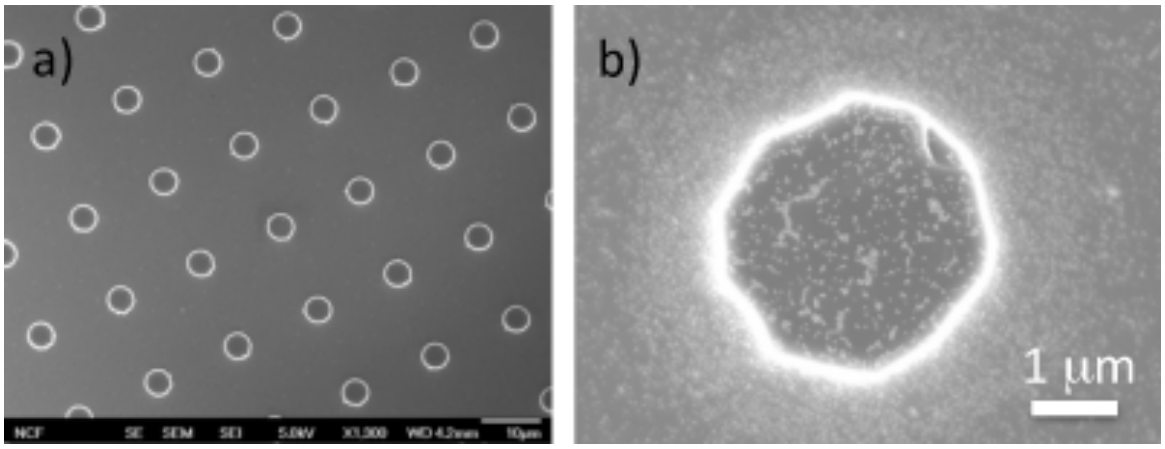

Figure 4.7 a) SEM image of silicon pillars, b) After absorbing of DNA-Cy3-Au@Ag nanoparticles on the pillars.

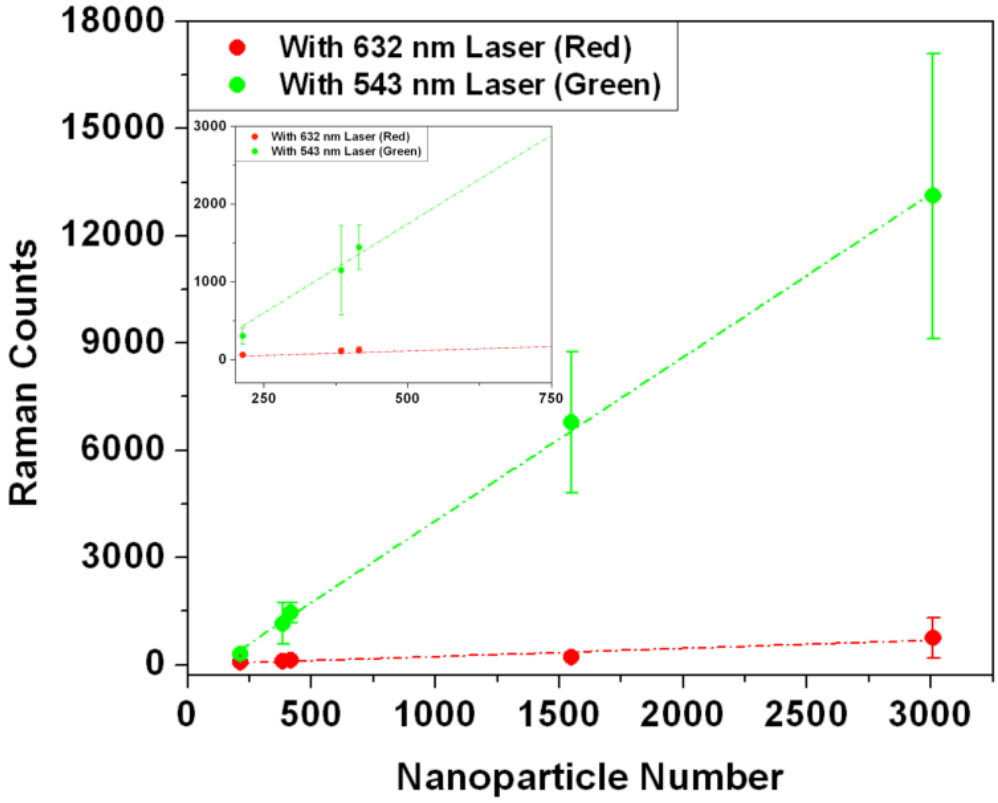

Figure 4.8 a) SERS signal of DNA-Cy3-Au@Ag nanoparticles as a function of nanoparticle number. The green line represents Raman intensities measured with the 543.5nm laser, red line represents Raman signals generated with the 632.8nm HeNe laser. The inset shows the Raman signals obtained from lower amounts of nanoparticles. Each dot corresponds to the mean count obtained of particles on five different Si pillars. The error bars represent standard deviations.SEM image of silicon pillars, b) After absorbing of DNA-Cy3-Au@Ag nanoparticles on the pillars. Reproduced from Adv. Func. Materials, *Ju Hun Lee*, *Phyllis F. Xu*, *Dylan W. Domaille*, *Chulmin Choi*, *Sungho Jin*, *Jennifer N. Cha*, *Submitted*.

The resulting SERS plot demonstrated a well-defined linear relationship between the Raman intensity and number of nanoparticles. Variations in Raman intensities could be attributed to inhomogeneous distribution of size and shape of the gold core nanoparticles, varying numbers of Cy3 per particle, and deviations in the silver shell thicknesses. The slope of the lines obtained from 543.5 nm excitation was 4.58 (R^2 = 0.9989) while the slope obtained from 632.8nm excitation was 0.23 (R^2 = 0.9013). This 20-fold signal enhancement seen with 534.5 nm excitation was partially attributed to the well-known resonance effect observed when excitation wavelengths are close to the maximum electronic absorption of Cy3 (excitation wavelength = 555 nm). For the Raman measurement of Cy3 alone, the probe excitation volume was approximated to be a cylinder with a radius of 2.0 μm and a height of 22.5 μm, resulting in 5.95×10^{10} molecules being measured (N_{bulk}). The Raman intensity of Cy3 solution (I_{bulk}) ($\lambda_{excitation\ max}$ = 555 nm) was determined by using 632.8 nm excitation laser in order to reduce fluorescence background. The calculated EF values of the DNA-Cy3-Au@Ag nanoparticles were compensated for the differences in SERS intensity from the two laser lines. To calculate N_{bulk}, the height (h) was calculated by followed equation (6),

$$\frac{h}{2r} = \frac{3.28 \times \eta}{NA} \qquad (6)$$

Because, Cy3 was dissolved into 26.8% DMSO, and deionized water. The η value (= refractive index of medium) was interpolated with the value in the reference paper. [55] To inhibit from the strong fluorescence background, 632.8 nm laser was employed for Cy3 solution during Raman measurement. The Raman experiment of Cy3 solution was carried out with the exactly same condition (Power: 130 μW, Accumulation time: 30 sec.)

as Raman calibration experiment with nanoparticles, and protein assay. Assuming the excitation volume as a cylinder, the radius (r) of laser beam was 2μm. According to equation, the number of dye in the excitation volume was 5.95×10^{10}. The enhancement factor EF was calculated using the following equation (7),

$$EF = \frac{I_{SERS} \times N_{bulk}}{I_{bulk} \times N_{cy3-NPs}} \times \frac{f^4_{bulk}}{f^4_{SERS}} \quad (7)$$

Assignments
I_{SERS}: Raman Intensity of the Cy3 in DNA-Cy3-Au@Ag nanopartilces
I_{bulk}: Raman Intensity from Cy3 solution (350 mM)
$N_{cy3\text{-}NPs}$: The number of Cy3 in DNA-Cy3-Au@Ag nanoparitlces
N_{bulk}: The number of Cy3 in solution
f_{bulk}: The frequencies of Raman excitation laser for Cy3 solution (632. 8 nm)
f_{SERS}: The frequencies of Raman excitation laser for DNA-Cy3-Au@Ag nanoparticles (543.5 nm)

The I_{SERS} value came from Raman intensity per nanoparticles in Figure 4.8. N_{SERS} was amounts of Cy3 per nanoparticles from DDT liberated experiments (225). To compensate for contribution of different lasers, the calculated values were scaled suing f^4 law. The corrected resulting enhancement factor (EF) of green laser (543.5nm) was 1.39×10^6, while the EF of red laser (632.8 nm) was 1.29×10^5. The SERS Enhancement Factor (EF) values of the Raman data were determined by normalizing the laser power (130 μW) and acquisition time for all samples measured.

4.6 Layer by Layer Deposition of Nanostructure on the DNA Phage

We next sought to determine if these DNA-phage and DNA-Cy3-Au@Ag NPs could be applied to protein detection and identification. First, the ability of the DNA-Cy3-Au@Ag nanoparticles to hybridize to the DNA-phage was evaluated by TEM after uranyl acetate negative staining (Figure 4. 9 a)). As a comparison, aldehyde-conjugated phage alone did not show any binding to the DNA-Cy3-Au@Ag nanoparticles, indicating that aldehyde itself could not induce nonspecific binding between the nanoparticles and the phage (Figure 4.9 b). Because DNA hybridization was used to couple the SERS nanoparticles to the phage, the number of SERS nanoparticle probes per phage could further be increased simply by adding in a second layer of DNA-Cy3-Au@Ag NPs (DNA2-Cy3-Au@Ag NPs) that were complementary to the first set of DNA-Cy3-Au@Ag NPs (DNA1-Cy3-Au@Ag NPs). DNA2-Cy3-Au@Ag NPs bound to the DNA1-Cy3-Au@Ag NPs on the DNA phage were also imaged by TEM after uranyl acetate negative staining, and as shown in Figure 4.10**,** the DNA2-Cy3-Au@Ag NPs formed a second layer successively along the first layer of bound nanoparticles.

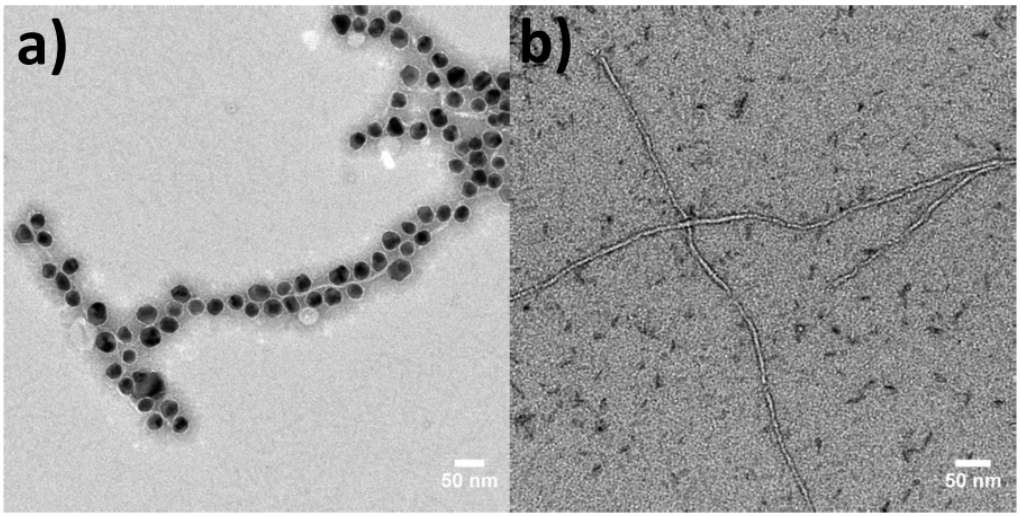

Figure 4.9 a) Uranyl acetate negative stained TEM images of DNA conjugated phage after reaction with DNA Cy3-Au@Ag nanoparticles. b) Uranyl acetate negative stained TEM images of aldehyde conjugated phage after reaction with DNA-Cy3-Au@Ag nanoparticles. Reproduced from Adv. Func. Materials, *Ju Hun Lee*, *Phyllis F. Xu*, *Dylan W. Domaille*, *Chulmin Choi*, *Sungho Jin*, *Jennifer N. Cha*, *Submitted*.

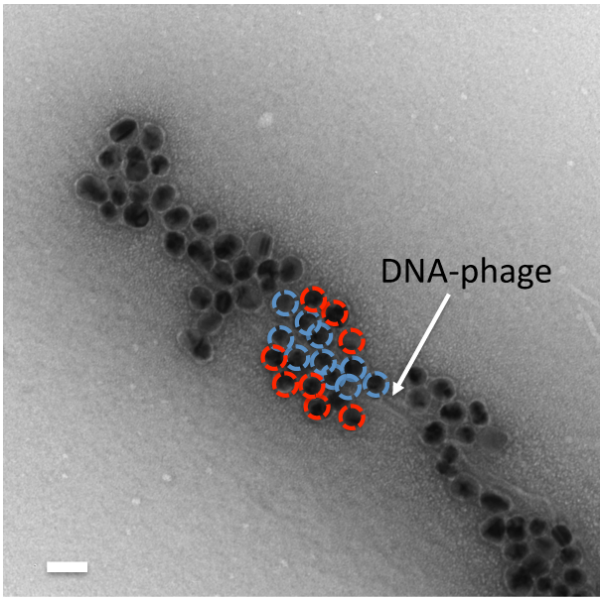

Figure 4.10 Uranyl acetate negative stained TEM image of DNA phage after successive reactions with DNA1-Au@Ag NPs and DNA2-Au@Ag NPs. The white arrow indicates the DNA phage, the blue circles represent DNA1-Au@Ag NPs and the red circles represent the DNA2-Au@Ag NPsCy3-Au@Ag NPs (Scale bar: 50 nm). Reproduced from Adv. Func. Materials, *Ju Hun Lee*, *Phyllis F. Xu*, *Dylan W. Domaille*, *Chulmin Choi*, *Sungho Jin*, *Jennifer N. Cha*, *Submitted*.

4.7 Diagnostic Results

While SERS has been used for biosensing, increasing the number of SERS reporters bound to a single detection agent (antibody, aptamer, phage) in a label-specific manner have not been previously shown. Because of the extremely high surface area associated with a single bacteriophage and its ability to bind multiple SERS probes in response to 1-2 antigens, it was envisioned that the M13 viruses would provide much higher gains in SERS signals as opposed to antibodies, for example. To investigate this possibility, we developed the following assay outlined in Figure 4.11. First, varying amounts of the model antigen, biotinylated antigoat rabbit IgG were captured to 1 μm streptavidin-coated silica beads. Antigen-bound silica microparticles were then blocked with BSA followed by addition of DNA-conjugated phage. Unbound phage were removed by centrifuge washing the beads three times with buffer. DNA1-Cy3-Au@Ag nanoparticles were next added to the silica bead pellets and vortexed to hybridize with the DNA-phage in sodium citrate buffer (150 mM NaCl, 15 mM sodium citrate, 0.025 % Tween, pH 7.0). Unbound DNA1-Cy3-Au@Ag NPs were thoroughly removed by stringent washing with buffer followed by filtration through a 0.22 μm filter to remove any small nanoparticle aggregates. For further SERS amplification, DNA2-Cy3-Au@Ag NPs were added next, followed by washing and filtration to remove unbound particles and aggregates. To prepare samples for Raman spectroscopy, small volumes of the washed and diluted bead solutions were adsorbed to UVO-treated Si substrates, rinsed in buffer, and dried in air. Individual silica beads were then directly measured for Raman analysis.

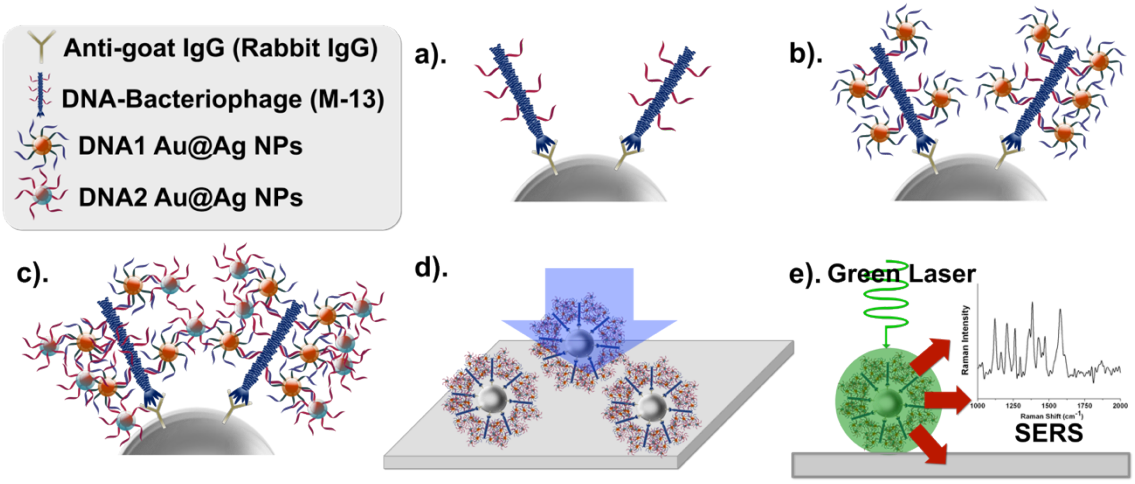

Figure 4.11 Quantitative SERS sensor design with DNA-phage: (a) Antigen was captured by streptavidin-coated silica microbeads followed by the addition of DNA phage (b) DNA1-Cy3-Au@Ag NPs were next hybridized with the bound DNA-phage (c) DNA2-Cy3-Au@Ag NPs were sequentially added to the bead and hybridized with DNA1-Cy3-Au@Ag NPs (d) The NP-phage-antigen conjugated silica beads were dried on UVO-treated Si surfaces (e) Individual silica beads were measured by Raman spectroscopy.

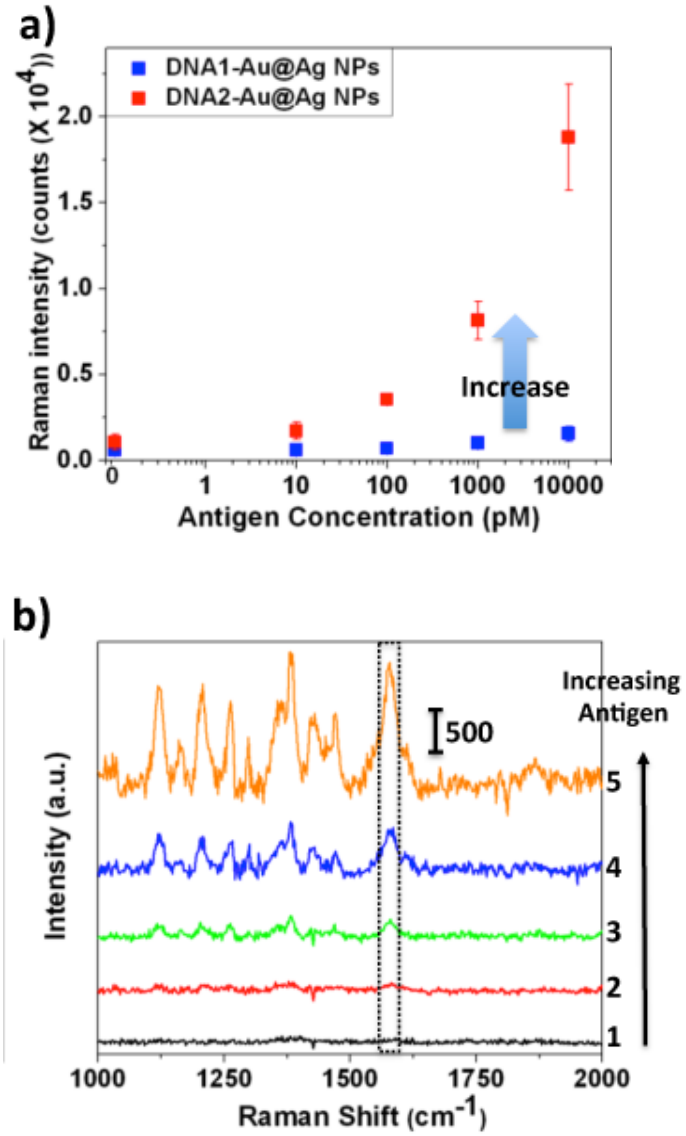

Figure 4.12 a) Plot of SERS intensities at 1580 cm^{-1} (fingerprint peak of Cy3) as a function of antigen concentration. Each data point represents the sum of Raman intensities measured from nine individual silicon microbeads. Blue dots (DNA1-Au@Ag NPs) represent Raman intensities measured after conjugation with DNA1-Au@Ag NPs. Red dots represent intensities measured after the addition of DNA2-Au@Ag NPs. The error bars represent standard deviations obtained from three separate sensing assays**.** b) Representative SERS spectra obtained with varying amounts of antigen after conjugation with DNA2-Au@Ag nanoparticles (1: control (no antigen), 2: 10 pM (5 fmol), 3: 100 pM (50 fmol), 4: 1 nM (500 fmol), 5: 10 nM (5 pmol)). Dotted box indicates the fingerprint peak (1580 cm^{-1}) of Cy3. Reproduced from Adv. Func. Materials, *Ju Hun Lee*, *Phyllis F. Xu*, *Dylan W. Domaille*, *Chulmin Choi*, *Sungho Jin*, *Jennifer N. Cha*, *Submitted*.

The silica bead showed only a weak Raman peak around 2050 cm^{-1}, which was easily resolved from the 1580 cm^{-1} fingerprint peak region of Cy3. The assays were run under the same conditions as used previously to determine the EF values for the DNA-Cy3-Au@Ag NPs (power: 130 μW, accumulation time: 30 sec., 543.5 nm HeNe laser). As shown in Figure 4.12, there was a distinct increase in Raman intensity with increasing antigen after adding just the first layer DNA1-Cy3-Au@Ag NPs and control samples showed virtually no signal. However, all of the Raman signals except for the zero antigen control case could also be significantly enhanced by the addition of the SERS active DNA2-Cy3-Au@Ag NPs. With increasing amounts of antigen, there was an exponential increase in signal after the addition of DNA2-Cy3- Au@Ag NPs. A hypothesis for the exponential increase in signal is that at low concentrations the phage would lie more parallel to the silica bead surface, while at higher antigen concentrations and higher amounts of phage bound, the phage would be forced to orient more perpendicular to the particle surface such as in a brush layer (Figure 4.13). The greater exposed surface area per phage would lead to greater Au@Ag NP binding and since each bound NP still has multiple strands of exposed, accessible, and unhybridized DNA, leading to amplified SERS signals (Figure 4.13). Through this approach, the addition of DNA2-Cy3-Au@Ag NPs caused around 2-12 fold enhancement in Raman than what could be achieved with just DNA1-Cy3-Au@Ag NPs, and concentrations as low as 5 fmol (10 pM) could be more easily detected above background (Figure 4.12).

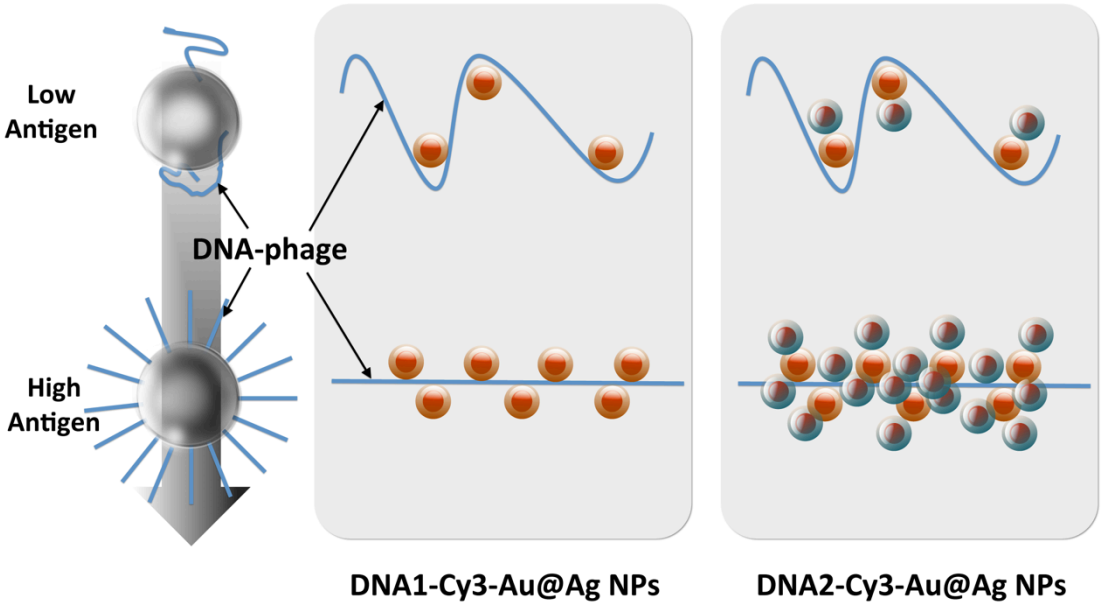

Figure 4.13 Proposed DNA-nanoparticle arrangement on DNA-phage in low and high amounts of antigen. Reproduced from Adv. Func. Materials, *Ju Hun Lee*, *Phyllis F. Xu*, *Dylan W. Domaille*, *Chulmin Choi*, *Sungho Jin*, *Jennifer N. Cha*, *Submitted*.

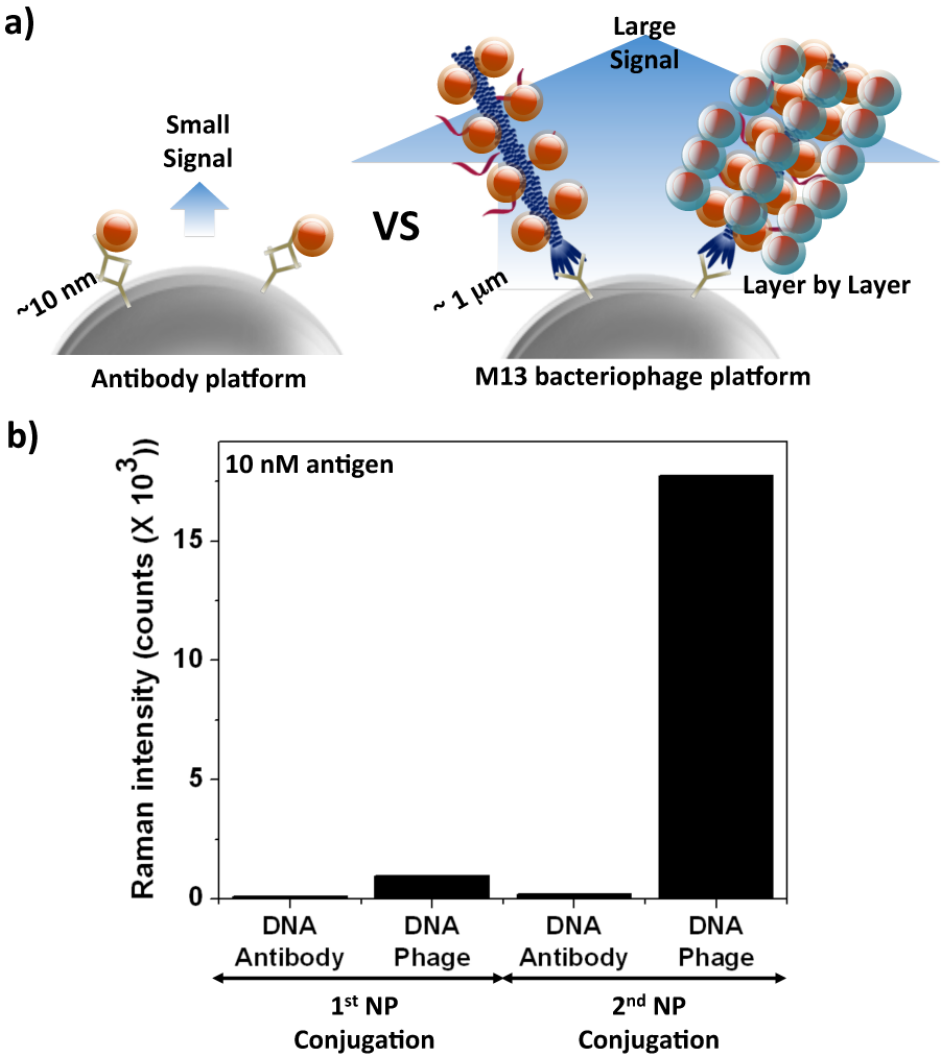

Figure 4.14 a) Schematic comparing antibody versus M13 bacteriophage amplifiable for SERS biosensing. b) Raman intensities obtained from DNA-antibody versus DNA-phage after first and second SERS NP reaction. The intensity values were obtained at 1580 cm^{-1} (fingerprint peak of Cy3). Each data point represents the sum of Raman intensities measured from nine individual silicon microbeads. The resulting values of Raman intensity were calibrated by subtracting background signals of no antigen.roposed DNA-nanoparticle arrangement on DNA-phage in low and high amounts of antigen. Reproduced from Adv. Func. Materials, *Ju Hun Lee*, *Phyllis F. Xu*, *Dylan W. Domaille*, *Chulmin Choi*, *Sungho Jin*, *Jennifer N. Cha*, *Submitted*.

Since it was hypothesized that the extremely large surface area of each phage body (1 μm x 6nm) led to significant gains in SERS, we decided to run comparison assays with DNA conjugated antibodies instead of phage, as shown in Figure 4.14. For this, using the same hydrazone chemistry as was used to produce DNA conjugated phage, DNA-conjugated goat IgG that would bind the anti-goat IgG was synthesized. The DNA strands on goat IgG were exactly the same sequence as those on the DNA-phage. To determine if chemical modification of the antibody could inhibit its ability to bind its protein target, FITC-labeled DNA-conjugated goat IgG was tested for binding to antigoat IgG by fluorescence microscopy. As shown in Figure 4.15, chemical modification of the goat IgG did not inhibit it from binding antigoat IgG. Next, using the same working concentrations as those used in the phage assay, we reacted the DNA-conjugated goat IgG with different amounts of the antigen antigoat IgG captured onto the silica microbeads. After removing unbound DNA conjugated antibody, we reacted the beads with the SERS active DNA1-Cy3-Au@Ag NPs. As before with the DNA-phage, we further reacted with DNA2-Cy3-Au@Ag NPs to see if any signals could be further amplified. As shown in Figure 4.14 b), with the DNA-antibody sensor system, very low SERS signals could be obtained as compared with the DNA-phage platform. In the case of 10 nM of antigen, even after conjugation with DNA1-Cy3-Au@Ag NPs and DNA2-Cy3-Au@Ag NPs, little increase was seen; the sensitivity of the DNA-antibody system was in high pM regime.

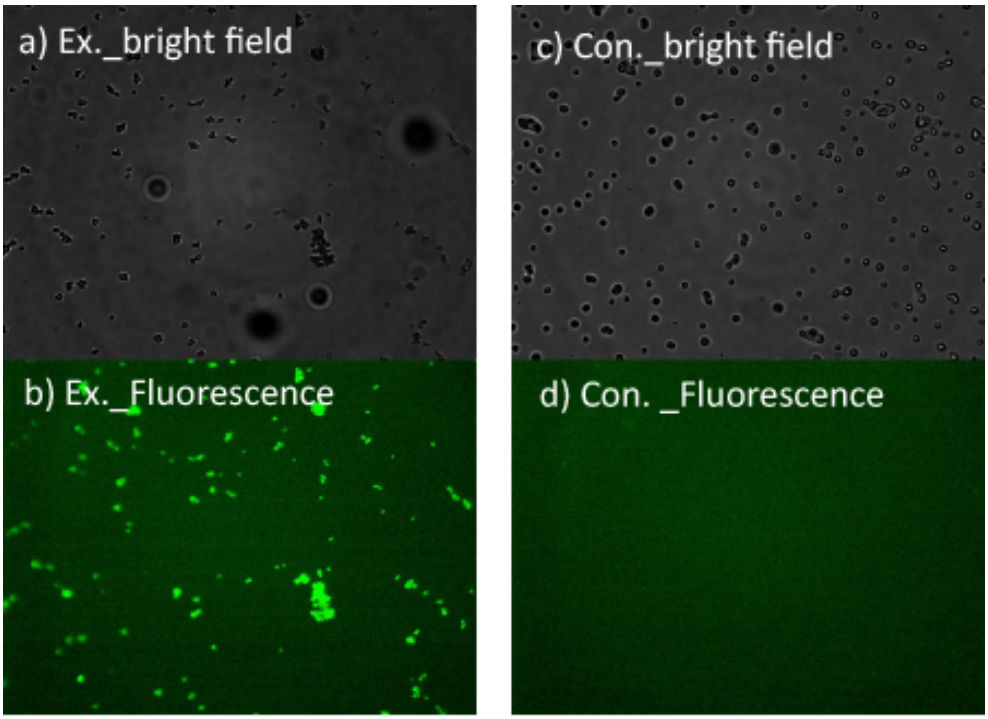

Figure 4.15 Bright field and fluorescence images of DNA and FITC conjugated goat IgG binding to anti-goat IgG. a and b) Bright field and fluorescence image of DNA-FITC-goat IgG reacted with biotinylated antigoat IgG on streptavidin coated silica beads), c and d) bright field and fluorescence image of DNA-FITC-goat IgG reacted with streptavidin coated beads. Silica beads for all samples were blocked with bovine serum albumin before reaction with DNA-FITC-goat IgG. All images were taken with X40 objective lense, 3.5 second accumulation time. Reproduced from Adv. Func. Materials, *Ju Hun Lee*, *Phyllis F. Xu*, *Dylan W. Domaille*, *Chulmin Choi*, *Sungho Jin*, *Jennifer N. Cha*, *Submitted*.

Through quantitative comparisons, the DNA-phage system was calculated to show nearly a 75-fold increase in Raman intensity over that of the DNA-antibody system. This dramatic increase in SERS signal demonstrates that the high surface area of filamentous bacteriophage provides significant advantages in terms of sensitivity over that of other systems, such as antibodies. The large differences in SERS signal between the DNA-phage and that of DNA-antibody provides the possibility of running single microbead analysis for multiplexed protein analysis.

4.8 Materials and Experimental Sections

Unless otherwise note, all reagents were obtained from commercial sources and used without further purification. Water used in buffers or in reactions was deionized with a Milli-Q Advantage A-10 water purification system (MilliPore, USA). UV-vis spectra were acquired on a DU 730 spectrophotometer (Beckman Coulter, USA).

4.8.1 DNA Sequences

All DNA was purchased from Integrated DNA Technology (Iowa, USA).

(1) DNA-phage: 5'-I linker–TTTTTGTGCGCAAAGAGTTT -3'

(2) DNA1-Cy3-Au@Ag nanoparticles: 5'-C6-Thiol-AAAAAAAAAA-PEG_{18}-AA-ACTCTTTGCGCAC -3'

(3) Capping DNA for DNA-Cy3 Au@Ag nanoparticle: 5'-C6-Thiol-TTTTTTTTTT-3'

(4) 2nd DNA-Cy3-Au@Ag nanoparticles: 5' - C6-Thiol-AAAAAAAAAA-PEG_{18}-G-TGCG-CAAAGAGTTT-3'

4.8.2 Synthesis, purification, and characterization of thiolated Cy3

Sulfo-N-hydroxysuccinimide Cy3 (s-NHS Cy3, 500 mg) (GE Healthcare, USA) was dissolved in DMSO (200 μL) and a solution of cysteamine hydrochloride (6.52 mmol) in pH 8.1 50 mM $NaHCO_3$ buffer (130 μL) was added. The reaction was allowed to proceed overnight at room temperature, at which point the crude reaction mixture was purified by preparatory thin layer chromatography plate (prep TLC) with CH_2Cl_2:MeOH (1:1). The pink bands were collected, eluted with a mixture of ethanol:methanol (9:1),

and identified by electrospray ionization mass spectrometry (ESI-MS). The mass of product was observed 726.30 m/z by ESI-MS (expected mass: 727.18) (LCQdeca mass spectrometer with electrospray ionization source, Thermo, USA). The final thiolated Cy3 was dissolved in DMSO and stored at 4 ^{o}C.

4.8.3 Synthesis of DNA-Cy3 Au@Ag Nanoparticles

2 mL of 20 nm citrate-coated gold nanoparticles (Ted Pella, USA) was conjugated with 300 fold molar access of previously prepared thiolated Cy3 (7.23 μL of 274 μM) for overnight at room temperature. Concurrently and in separate vial, 7 nmol of thiolated DNA in phosphate buffer (PB, 170 mM final concentration, pH 8.0) was treated with dithiothreitol (DTT, 50 mM final concentration) for 1 hour. DTT-treated thiolated DNA was purified by NAP-5 column (GE Healthcare, USA). Thiolated DNA was then conjugated to the Cy3-20nm gold nanoparticles by sequentially increasing the NaCl concentration up to 300 mM in the presence of sodium dodecyl sulfate (SDS, 0.1 %). After 16 h at room temperature, the DNA-Cy3 gold nanoparticles were purified three times by centrifugation at 15500 RPM. Next, polyvinylpyrrolidone (PVP, 40k, 0.25 % final concentration), (+)-sodium L-ascorbate (15 mM final concentration), and silver nitrate (0.15 mM final concentration) was sequentially added to a solution of DNA-Cy3 20 nm gold nanoparticles (0.5 nM final concentration in dd-H_2O). The solution was adjusted to 300 mM NaCl and 10 mM phosphate buffer, and the reaction was allowed to react for 3 hours with stirring (1150 RPM). The sample was centrifuged at 15500 RPM, and the supernatant was separated from the pellet of DNA-Cy3-Au@Ag nanoparticles. To protect against non-specific binding during the assay, DNA-Cy3-Au@Ag

nanoparticles were conjugated to thiolated T_{10} DNA in the same manner as described above.

4.8.4 Raman Measurements

A home-built micro-Raman system was used for all Raman measurements, based on an Olympus microscope (BX51TRF) with a 50x objective lens (NPlanFL BD, NA 0.8). The signal was spectrally dispersed and detected with a spectrometer with 600 g/mm grating and LN2-cooled CCD (Princeton Instruments SP2500i). Green (543.5 nm) and red (632.8 nm) HeNe laser lines were used for excitation, with an edge filter (Semrock) for filtering the laser line.

4.8.5 TEM Sampling and Imaging

Carbon-coated copper mesh TEM grids (Electron Microscopy Sciences, Inc., USA) were glow discharged for 40 s at 20 mA to make hydrophilic surfaces, and then 1 μL of samples were dropped on the grid and allowed to air dry. Transmission electron microscope (TEM) images were acquired on a CM 100 TEM (Phillips, USA). For images of M13 bacteriophage, uranyl acetate negative staining methods were used.

4.8.6 DNA-Phage and DNA Cy3-Ag@Au NPs-Based Protein Detection and Identification Assay

1 μm streptavidin coated silica micro particles (15 μL of 10 mg/mL, Bangs Lab. Inc, USA) were reacted with varying amounts of biotinylated anti-goat IgG (model antigen) in 1 × PBS containing 0.025 % Tween (0.025 % PBST). The antibody-

conjugated silica micro particles were blocked with blocking buffer (0.025 % PBST, 5 mg/mL of BSA) for 2 h. Blocked antibody-silica micro particles were collected by centrifuge at 2000 g and washed three times (0.025 % PBST, 1 mg/mL of BSA). 750 fmol of DNA-phage was then incubated with the silica micro particles (0.1 % PBST, 1 mg/mL of BSA), and after 1 h incubation, the solution was removed and the silica microparticles were washed three times (0.1 % PBST, 1 mg/mL of BSA). Phage-bound antibody silica micro particles were then conjugated with DNA-Cy3-Au@Ag nanoparticles (10 μL of 10 nM) in 0.025 % SSCT (150 mM NaCl, 15 mM citrate, and 0.025% Tween, pH 7.0), and after 45 min, the DNA1-Cy3-Au@Ag NP-bound silica micro particles were centrifuged at 1000 g, and the supernatant was discarded. The centrifugation purification was repeated. The solution of DNA1-Cy3-Au@Ag NPs were filtered using a 0.22 μm filter (polyvinylidene fluoride (PVDF) membrane, Millipore, USA), and washed with 0.025 % SSCT twice. The particles were dispersed in 250 μL 0.025 % SSCT, and 1 μL of the solution was diluted 10-fold and adsorbed to UVO-treated hydrophilic Si substrate for Raman measurement. The remaining solution of DNA1-Cy3-Au@Ag NPs bound micro particles was reacted with complementary DNA2-Cy3-Au@Ag NPs (10 μL of 10 nM) for 45 min. And washing, Raman samples were prepared as described above. Micro Raman measurements were carried out with separated single silica micro particles with 130 μW, 30 sec accumulation time.

4.9 Conclusion

We have demonstrated a novel phage-SERS sensing platform as a highly sensitive, facile, and rapid antigen detection system. As a first step, DNA-conjugated metal core-shell nanoparticles were successfully synthesized containing high loadings of Raman active dyes. These SERS-active particles were then used in conjunction with DNA-conjugated M13 bacteriophage to yield protein sensing agents with sensitive Raman detection limits. Additional layers of SERS nanoparticles were also deposited on a single phage via a layer-by-layer approach, leading to exponential gains in Raman intensities compared with single particle layers. These favorable sensitivities could not be achieved when using antibodies in place of phage, indicating that the large surface area of bacteriophage provide a mode for enhanced detection over that of other systems. While it was difficult to obtain more than two successive layers of nanoparticles, by tuning the number of DNA per particle and using non-competitive DNA sequences for layer-by-layer assembly, it should be possible to increase the sensitivity of these phage sensors further. Finally, since each SERS particle may contain a specific dye, and phage may be loaded with specific DNA sequences, it will be possible to extend this for multiplexed analysis in future studies.

4.10 Acknowledgements

This chapter, in part, is a reprinted with permission from Adv. Func. Materials, *Ju Hun Lee*, *Phyllis F. Xu*, *Dylan W. Domaille*, *Chulmin Choi*, *Sungho Jin*, *Jennifer N. Cha*, *Submitted*. The dissertation author was the primary investigator and author of this paper.

4.11 References

1. Bohunicky, B.; Mousa, S. A. Biosensors: The new wave in cancer diagnosis. *Nanotechnol. Sci. Appl.* **2011**, 4, 1-10.

2. Brambilla, D.; Droumaguet, B. L.; Nicolas, J.; Hashemi, S. H.; Wu, L.; Moghimi, S. M.; Couvreur, P.; Andrieux, K. Nanotechnologies for Alzheimer's Disease: Diagnosis, Therapy, and Safety Issues. *Nanomedicine: Nanotechnol., Biol. Med.* **2011**, 7, 521-540.

3. Shariat, S. F.; Scherr, D. S.; Gupta, A.; Bianco, F. J. Jr.; Karakiewicz, P. I.; Zeltser, I. S.; Samadi, D. B.; Akhavan, A. Emerging Biomarkers for Prostate Cancer Diagnosis, Staging, and Prognosis. *Arch. Esp. Urol.* **2011**, 64, 681-694.

4. Souza, G. R.; Christianson, D. R.; Staquicini, F. I.; Ozawa, M. G.; Snyder, E. Y.; Sidman, R. L.; Miller, J .H.; Arap, W.; Pasqualini, R. Networks of Gold Nanoparticles and Bacteriophage as Biological Sensors and Cell-Targeting Agents. *Proc. Natl. Acad. Sci. U. S. A.* **2006**, 103, 1215-1220.

5. Mao, C.; Liu, A.; Cao, B. Virus-Based Chemical and Biological Sensing. *Angew. Chem., Int. Ed.* **2009**, 48, 6790-6810.

6. Krag, D. N.; Shukla, G. S.; Shen, G.; Pero, S.; Ashikaga, T.; Fuller, S.; Weaver, D. L.; Burdette-Radoux, S.; Thomas, C. Selection of Tumor-Binding Ligands in Cancer Patients with Phage Display Libraries. *Cancer Res.* **2006**, 66, 7724-7733.

7. Smith, G. P.; Petrenko, V. A. Phage Display. *Chem. Rev.* **1997**, 97, 391-410.

8. Barbas III, C. F.; Burton, D. R.; Scott, J .K.; Silverman, G. J. *In Phage Display. A Laboratory Manual*; Cold Spring Harbor Laboratory Press: New York, 2001; pp 1.1–16.

9. Kehoe, J. W.; Kay, B. K. Filamentous Phage Display in the New Millennium. *Chem. Rev.* **2005**, 105, 4056-4072.

10. Yacoby, I.; Bar, H.; Benhar, I. Targeted Drug-Carrying Bacteriophages as Antibacterial Nanomedicines. *Agents and Chemother.* **2007**, 51, 2156-2163.

11. Ngweniform, P.; Abbineni, G.; Cao, B.; Mao, S. Self-Assembly of Drug-Loaded Liposomes on Genetically Engineered Target-Recognizing M13 Phage: A Novel Nanocarrier for Targeted Drug Delivery. *Small* **2009**, 5, 1963-1969.

12. Li, K.; Chen, Y.; Li, S.; Nguyen, H. G.; Niu, Z.; You, S.; Mello, C. M.; Lu, X.; Wang, Q. Chemical Modification of M13 Bacteriophage and Its Application in Cancer Cell Imaging. *Bioconjugate Chem.* **2010**, 21, 1369-1377.

13. Carrico, Z. M.; Farkas, M. E.; Zhou, Y.; Hsiao, S. C.; Marks, J .D.; Chokhawal, H.; Clark, D. S.; Francis, M. B. N-Terminal Labeling of Filamentous Phage to Create Cancer ncer Marker Imaging Agents. *ACS nano* **2012**, 6, 6675-6680.

14. Yi, H.; Ghosh, D.; Ham, M.; Qi, J.; Barone, P. W.; Strano, M. S.; Belcher, A. M. M13 Phage-Functionalized Single-Walled Carbon Nanotubes As Nanoprobes for Second Near-Infrared Window Fluorescence Imaging of Targeted Tumors. *Nano Lett.* **2012**, 12, 1176-1183.

15. Goldman, E. R.; Pazirandeh, M. P.; Mauro, J. M.; King, K. D.; Frey, J. C.; Anderson, G. P. Phage-Displayed Peptides as Biosensor Reagents. *J. Mol. Recognit.* **2000**, 13, 382-387.

16. Petrenko, V. A.; Vodyanoy, V. J. Phage Display for Detection of Biological Threat Agents. *J. Microbiol. Methods* **2003**, 53, 253-262.

17. Arter, J. A.; Taggart, D. K.; Mcintire, T. M.; Penner, R. M.; Weiss, G. A. Virus-PEDOT Nanowires for Biosensing. *Nano Lett.* **2010**, 10, 4858-4862.

18. Lee, J .H.; Cha, J. N. Amplified Protein Detection through Visible Plasmon Shifts in Gold Nanocrystal Solutions from Bacteriophage Platforms. *Anal. Chem.* **2011**, 83, 3516-3519.

19. Lee J. H.; Domaille, D. W.; Cha. J. N. Amplified Protein Detection and Identification through DNA-Conjugated M13 Bacteriophage. *ACS nano* **2012**, 6, 5621-5626.

20. Domaille, D. W.; Lee, J .H.; Cha. J. N. High Density DNA Loading on the M13 Bacteriophage Provides Access to Colorimetric and Fluorescent Protein Microarray Biosensors. *Chem. Commun.* **2013**, 49, 1759-1761.

21. Torthill, I. E. Biosensors for Cancer Markers Diagnosis. *Semin. Cell Dev. Biol.* **2009**, 20, 55–62.

22. Kawasaki, E. S.; Player, A. Nanotechnology, Nanomedicine, and the Development of New, Effective Therapies for Cancer. *Nanomedicine: Nanotechnol., Biol. Med.* **2005**, 1, 101-109.

23. Chen, J.; Miao, N.; He, N.; Wu, X.; Li, S. Nanotechnology and Biosensors. *Biotechnol. Adv.* **2004**, 22, 505-518.

24. Rosi, N. L.; Mirkin, C. A. Nanostructures in Biodiagnostics. *Chem. Rev.* **2005**, 105, 1547-1562.

25. Hahm, J.; Lieber, C. M. Direct Ultrasensitive Electrical Detection of DNA and DNA Sequence Variations Using Nanowire Nanosensors. *Nano Lett.* 2004, 4, 51-54.

26. Kim, D.; Daniel, W. L.; Mirkin, C. A. Microarray-Based Multiplexed Scanometric Immunoassay for Protein Cancer Markers Using Gold Nanoparticle Probes. *Anal. Chem.* **2009**, 81, 9183-9187.

27. Medintz, I. L.; Clapp, A. R.; Mattoussi, H.; Goldman, E. R.; Fisher, B.; Mauro, J. M. Self-Assembled Nanoscale Biosensors Based on Quantum Dot FRET Donors. *Nat. Mater.* **2003**, 2, 630-638.

28. Cui, Y.; Wei, Q.; Park, H.; Lieber, C. M. Nanowire Nanosensors for Highly Sensitive and Selective Detection of Biological and Chemical Species. *Science* **2001**, 293, 1289-1292.

29. Xia, F.; Zuo, X.; Yang, R.; Xiao, Y.; Kang, D.; Vallée-Bélisle, A.; Gong, X.; Yuen, J. D.; Hsu, B. B. Y.; Heeger, A. J. *et al* Colorimetric Detection of DNA, Small Molecules, Proteins, and Ions Using Unmodified Gold Nanoparticles and Conjugated Polyelectrolytes. *Proc. Natl. Acad. Sci. U. S. A.* **2010**, 107, 10837-10841.

30. Kneipp, K.; Wang, Y.; Kneipp, H.; Perelman, L. T.; Itzkan, I.; Dasari, R. R.; Feld, M. S. Single Molecule Detection Using Surface-Enhanced Raman Scattering (SERS). *Phys. Rev. Lett.* **1997**, 78, 1667-1670.

31. Nie, S.; Emory, S. R. Probing Single Molecules and Single Nanoparticles by Surface-Enhanced Raman Scattering. *Science* **1997**, 275, 1102-1006.

32. Kneipp, K.; Kneipp, H.; Itzkan, I.; Dasari, R. R.; Feld, M. S. Ultrasensitive Chemical Analysis by Raman Spectroscopy. *Chem. Rev.* **1999**, 99, 2957-2975.

33. Cao, Y. C.; Jin, R.; Mirkin, C. A. Nanoparticles with Raman Spectroscopic Fingerprints for DNA and RNA Detection. *Science* **2002**, 297, 1536-1540.

34. Kneipp, K.; Kneipp, H.; Itzkan, I.; Dasari, R. R.; Feld, M. S. Surface-Enhanced Raman Scattering and Biophysics. *J. Phys.: Condens. Matter* **2002**, 14, R597-R624.

35. Dieringer, J. A.; Lettan II, R. B.; Scheidt, K. A.; Van Duyne, R. P. A Frequency Domain Existence Proof of Single-Molecule Surface-Enhanced Raman Spectroscopy. *J. Am. Chem. Soc.* **2007**, 129, 16249-16256.

36. Hossain, M. K.; Kitahama, Y.; Huang, G. G.; Han, X.; Ozaki, Y. Surface-Enhanced Raman Scattering: Realization of Localized Surface Plasmon Resonance Using Unique Substrates and Methods. *Anal. Bioanal. Chem.* **2009**, 394, 1747-1760.

37. Stevenson, R.; Ingram, A.; Leung, H.; McMillan, D. C.; Graham, D. Quantitative SERRS Immunoassay for the Detection of Human PSA. *Analyst* **2009**, 134, 842-844.

38. Guarrotxena, N.; Bazan, G. C. Antibody-Functionalized SERS Tags with Improved Sensitivity. *Chem. Commun.* **2011**, 47, 8784-8786.

39. Kasera, S.; Biedermann, F.; Baumberg, J. J.; Scherman, O. A.; Mahajan, S. Quantitative SERS Using the Sequestration of Small Molecules Inside Precise Plasmonic Nanoconstructs. *Nano Lett.* **2012**, 12, 5924-5928.

40. Stokes, R. J.; Macaskill, A.; Lundahl, P. J.; Smith, E.; Faulds, K.; Graham, D. Quantitative Enhanced Raman Scattering of Labeled DNA from Gold and Silver Nanoparticles. *Small* **2007**, 3, 1593-1601.

41. Stoeva, S. I.; Lee, J.; Smith, J. E.; Rosen, S. T.; Mirkin, C. A. Multiplexed Detection of Protein Cancer Markers with Biobarcoded Nanoparticle Probes. *J. Am. Chem. Soc.* **2006**, 128, 8378-8379.

42. Bailey, R. C.; Kwong, G. A.; Radu, C. G.; Witte, O. N.; Heath, J. R. DNA-Encoded Antibody Libraries: A Unified Platform for Multiplexed Cell Sorting and Detection of Genes and Proteins. *J. Am. Chem. Soc.* **2007**, 129, 1959-1967.

43. Geißler, D.; Charbonniere, L. J.; Ziessel, R. F.; Butlin, N. G.; Löhmannsröben, H.; Hildebrandt, N. Quantum Dot Biosensors for Ultrasensitive Multiplexed Diagnostics. *Angew. Chem., Int. Ed.* **2010**, 49, 1396-1401.

44. Lim, D.; Jeon, K.; Kim, H. M.; Nam, J.; Suh, Y. D. Nanogap-Engineerable Raman-Active Nanodumbbells for Single-Molecule Detection. *Nat. Mater.* **2010**, 9, 60-67.

45. Lim, D.; Jeon, K.; Hwang, J.; Kim, H.; Kwon, S.; Suh, Y. D.; Nam, J. Highly Uniform and Reproducible Surface-Enhanced Raman Scattering from DNA-Tailorable Nanoparticles with 1-nm Interior Gap. *Nat. Nanotechnol.* **2011**, 6, 452-460.

46. Lee, J.; Nam, J.; Jeon, K.; Lim, D.; Kim, H.; Kwon, S.; Lee, H.; Suh, Y. D. Tuning and Maximizing the Single-Molecule Surface-Enhanced Raman Scattering from DNA-Tethered Nanodumbbells. *ACS nano* **2012**, 6, 9574-9584.

47. Fang, Y.; Seong, N-H.; Dlott, D. D. Measurement of the Distribution of Site Enhancements in Surface-Enhanced Raman Scattering. *Science* **2008**, 321, 388-392.

48. Dirksen, A.; Dawson, P. E. Rapid Oxime and Hydrazone Ligations with Aromatic Aldehydes for Biomolecular Labeling. *Bioconjugate Chem.* **2008**, 19, 2543-2548.

49. Hurst, S. J.; Lytton-Jean, A. K. R.; Mirkin, C. A. Maximizing DNA Loading on a Range of Gold Nanoparticle Sizes. *Anal. Chem.* **2006**, 78, 8313-8318.

50. Lim, D. –K.; Kim, I. –J.; Nam, J. M. DNA-embedded Au/Ag Core–Shell Nanoparticles. *Chem. Commun.* **2008**, 42, 5312-5314.

51. Lee, J. H.; Kim, G. –H.; Nam, J. –M. Directional Synthesis and Assembly of Bimetallic Nanosnowmen with DNA. *J. Am. Chem. Soc.* **2012**, 134, 5456-5459.

52. McFarland, A. D.; Young, M. A.; Dieringer, J. A.; Van Duyne, R. P. Wavelength-Scanned Surface-Enhanced Raman Excitation Spectroscopy. *J. Phys. Chem. B* **2005**, 109, 11279-11285.

53. Zhang, Z.; Zhao, B.; Hu, L. J. PVP Protective Mechanism of Ultrafine Silver Powder Synthesized by Chemical Reduction Processes. *J. Solid State Chem.* **1996**, 121, 105-110.

54. Lee, J.; Lytton-Jean, A. K. R.; Hurst, S. J.; Mirkin, C. A. Silver Nanoparticle Oligonucleotide Conjugates Based on DNA with Triple Cyclic Disulfide Moieties. *Nano Lett.* **2007**, 7, 2112-2115.

55. R. G. Lebel, D. A. I. Goring, Density, viscosity, refractive index, and hygroscopicity of mixtures of water and dimethyl sulfoxide. *J. Chem. Eng. Data* **1962**, 7, 100.

CHAPTER 5: Future directions

In this dissertation, we have demonstrated the use of M13 bacteriophage as novel biomaterials for engineering highly sensitive, facile, and rapid antigen detection systems. Having shown their promise as diagnostics with one model antigen, we will next study the use of M13 bacteriophage to sense for clinically relevant proteins, specifically biomarkers related to cancer. Due to the complex pathogenesis of cancer,[1] one of the best scenario for cancer patients is the ability to detect cancer at very early stages, which can lead to substantial improvements in survival rates and disease monitoring. Cytokines, which are small signaling molecules used for cell signaling have been used as biomarkers for detecting particular types of cancer. We believe that our novel M13 bacteriophage based nano-biosensing system can be utilized for cytokine detection and identification with high sensitivity and accuracy. As discussed previously, a single M13 bacteriophage has a surface area of ~18,700 nm^2 surface area which is in 150 fold excess than a typical antibody (~125 nm^2). This high surface area of the virus also provides abundant amine nucleophiles for chemical modification with DNA or other moieties.

In order to achieve the cytokine detection with M13 bacteriophage, I will use phage that are fused with protein domains (ZZ domains) that bind specifically to the Fc regions of immunoglobulins (IgG). For this, a portion of the staphylococcal protein A will be inserted into the phage genome to produce ZZ domain expressing phage (FZZ phage).[2] The divalent ZZ protein (K_{aff}: 3.3×10^8) is able to bind human IgG with tenfold higher affinity as compared to monovalent Z protein (K_{aff}: 2.0×10^7).[3] As shown in Figure 5.1, the ZZ domain will be expressed on the p3 coat protein of the phage.

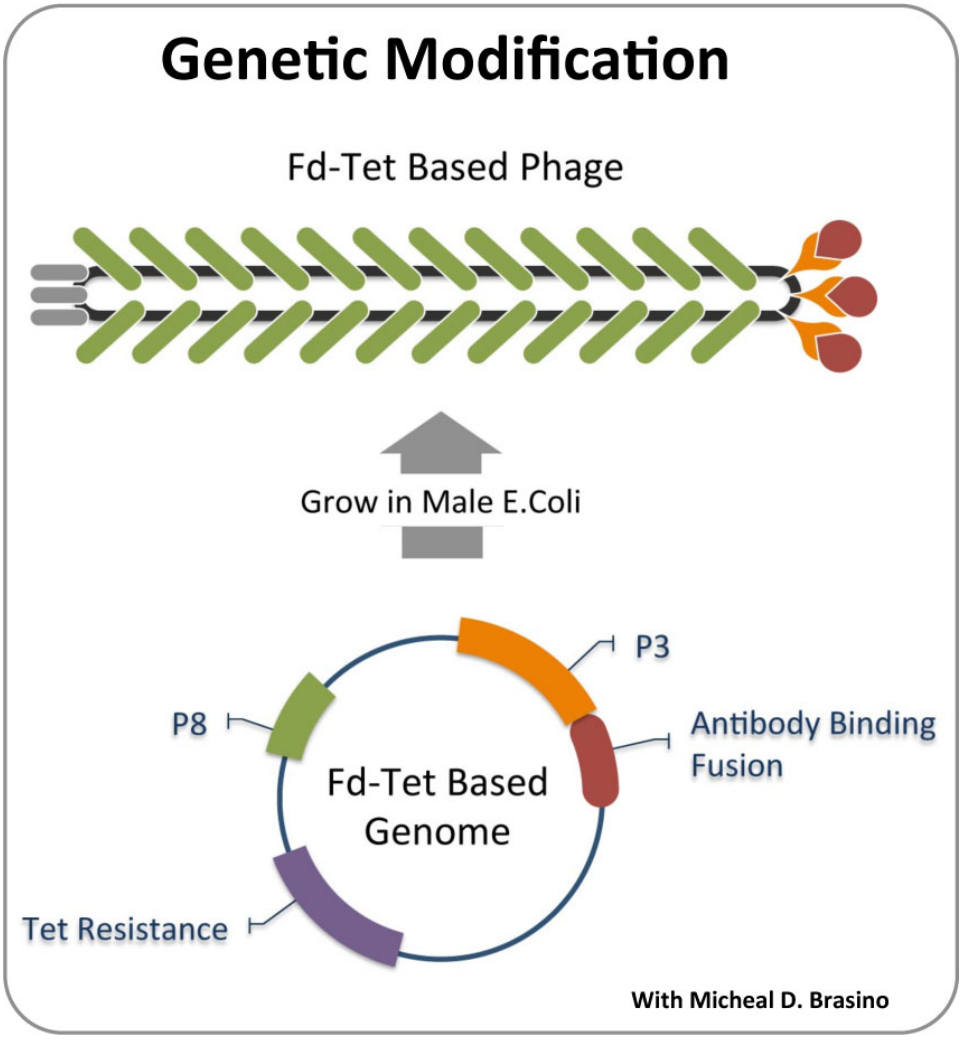

Figure 5.1 Schematic of genetic modification of ZZ domain fused M13 bacteriophage.

Specifically, the DNA fragment carrying the ZZ domain will be cloned into a digested tetracycline resistant filamentous phage (Fd-Tet based) vector. After cloning, ZZ domain fused M13 bacteriophage (FZZ phage) will be produced in *Escherichia Coli* (E-coli). The resulting FZZ phage will express ZZ domains on all 5 copies of the p3 minor coat protein.[4, 5]. As shown in Figure 5.2, the FZZ phage will be complexed with antibodies that recognize various different cytokines (*e.g.* TNF-a, INF-g, and IL-2) which will then be applied for multiplexed protein detection. These genetically engineered phage-antibodies will allow us to detect and quantify multiple types of cytokines at once which will improve disease diagnosis. [6-12]

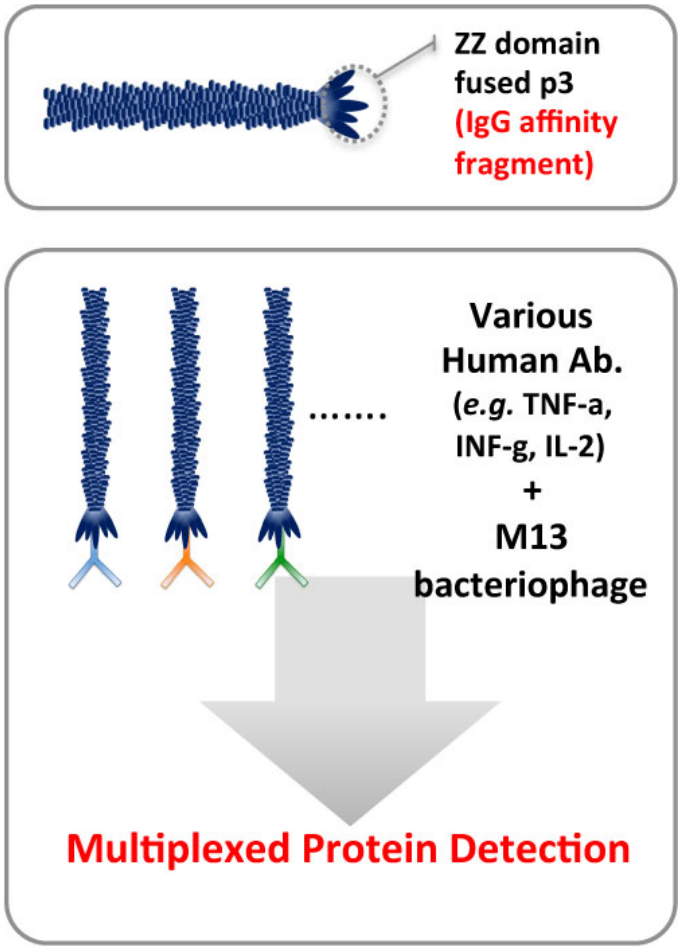

Figure 5.2 Schematic of multiplexed protein detection with complexes of various antibody and M13 bacteriophage.

5.1 References

1. Choi, Y.; Kwak, J, Park, J. W. Nanotechnology for Early cancer Detection, Sensors 2010, 10, 428-455.

2. Chen, C.; Huang, Q.; Jiang, S.; Pan, X.; Hua, Z. Immobilized Protein ZZ, an affinity tool fro immunoglobulin isolation and immunological experimentation. *Biotechnol. Appl. Biochem.* **2006**, 45, 87-92.

3. Nilsson, J.; Nilsson, P.; Williams, Y.; Pettersson, L.; Uhlén, M.; Nygren, P. Competitive Elution of Protein A Fusion Proteins Allows Specific Recovery under Mild Conditions. *Eur. J. Biochem.* **1994**, 224, 103-108.

4. Yacoby, I.; Bar, H.; Benhar, I. Targeted Drug-Carrying Bacteriophages as Antibacterial Nanomedicines. *Agents and Chemother.* **2007**, 51, 2156-2163.

5. Bar, H.; Ycoby, I.; Benhar, I. Killing cancer cells by targeted drug-carrying phage nanomedicines. BMC Biotechnol. 2008, 8, 37-51.

6. Torthill, I. E. Biosensors for Cancer Markers Diagnosis. *Semin. Cell Dev. Biol.* **2009**, 20, 55–62.

7. Mikolajczyk, S. D.; Song, Y.; Wong, J. R.; Matson, R. S.; Rittenhouse, H. G. Are Multiple Markers the Future of Prostate Cancer Diagnostics, *Clin. Biochem.* **2004**, 37, 519-528.

8. Rhodes, D. R.; Sanda, M. G.; Otte, A. P.; Chinnaiyan, A. N.; Rubin, M. A. Multiplex Biomarker Approach for Determining Risk of Prostate-Specific Antigen–Defined Recurrence of Prostate Cancer. *J. Natl. Cancer Inst.* **2003**, 95, 661-668.

9. Madu, C. O.; Lu, M. Y. Novel Diagnostic Biomarkers for Prostate Cancer, *J. Cancer* **2010**, 1, 150-177.

10. Kingsmore, S. F. Multiplexed Protein Measurement: Technologies and Applications of Protein and Antibody Arrays. *Nat. Rev. Drug Discov.* **2006**, 5, 310-320.

11. Stoeva, S. I.; Lee, J.; Smith, J. E. Rosen, S. T.; Mirkin, C. A. Multiplexed Detection of Protein Cancer Markers with biobarcoded Nanoparticles Probes. *J. Am. Chem. Soc.* **2006**, 128, 8378-8379.

12. Fan, R.; Vermesh, O.; Stivastava, A.; Yen, B. K. H.; Qin, L.; Ahmad, H.; Kwong, G. A. Liu, C.; Gould, K.; Hood, L.; Heath, J. R. Integrated Barcode Chips for rapid, Multiplexed Analysis of proteins in microliter quantities of blood. *Nat. Biotech.* **2008**, 26, 1373-1378.